POLYPYRROLE AND COMPOSITE ELECTRODES FOR ELECTROCHEMICAL SUPERCAPACITORS

By
CHAO SHI, B. Sc.

A Thesis
Submitted to the School of Graduate Studies
In Partial Fulfillment of the Requirements
For the Degree
Master of Applied Science

McMaster University
© Copyright by Chao Shi, August 2010

MASTER OF APPLIED SCIENCE (2010) McMaster University

(Materials Science and Engineering) Hamilton, Ontario

TITLE: Polypyrrole and Composite Electrodes for Electrochemical Supercapacitors

AUTHOR: Chao Shi, B.Sc. (Central South University, China)

SUPERVISOR: Dr. Igor Zhitomirsky

NUMBER OF PAGES: XV, 116

Chao Shi
Materials Science and Engineering

Abstract

Electrochemical supercapacitors (ES) have become an attractive technology in electrical energy storage devices and found many applications in a number of areas. The development of ES requires fabrication of advanced electrodes with novel materials and new techniques. Conducting polymer polypyrrole (PPy) has been found to be a promising electrode for ES due to its high pseudo capacitance and good elctrical conductivity. The polypyrrole based composite electrode with multiwall carbon nanotubes (MWCNTs) has been proved to enhance the electrochemical performance of ES.

Anodic electrochemical deposition of polypyrrole film and composite with MWCNTs has been successfully achieved on a stainless steel substrates in aqueous solutions. Novel additives, such as tiron (4,5-dihydroxy-1,3-benzenedisulfonic acid disodium salt) and sodium salicylate have been employed for the electro-synthesis of PPy. The role of additives in the electrodeposition process have been discussed. The electrochemical properties of PPy and PPy/MWCNT composite have been investigated and compared by using different characterization techniques.

The results showed that good quality PPy film and PPy/MWCNT composite can be obtained on stainless steel without anodic dissolution of anode using novel additives in aqueous solutions. The PPy films provided corrosion protection for stainless steel in aqueous solutions. High electrochemical performance of PPy film was achieved, the electrochemical behavior of PPy electrodes was significantly enhanced when MWCNTs were incorporated into the film matrix. Hence, investigations in this work indicated that

PPy and PPy/MWCNT composite deposited on the stainless steel substrates are promising electrode materials for ES.

Acknowledgement

I hereby sincerely acknowledge the support of many people without whom I would never have been able to complete this thesis.

First, I am greatly indebted to my supervisor, Dr. Igor Zhitomirsky, who has gone beyond a mere thesis supervisor by providing me with intellectual challenges, constant encouragements, and an appropriate research environment.

I would like to thank Jun Li, who have introduced me to the electrochemical supercapacitors in the beginning of my research.

I would also thank all my group mates in the lab, Yaohui Wang, Kangming Wu, Yingying Li, Rong Ma, Feng Sun and Deepark Komarappa, for their friendship and for rescuing me whenever I needed help.

Last but not least, my many thanks to my love family. I gratefully thank my wife, Xin Pang, for her unconditional trust and love in me, and for giving me valuable instructions through the whole journey of my studies. Extra special thanks to my sweet kids: my son Samuel and my daughter Claire, their love gives me great support and encourage me to the successes in my life and work.

I am very thankful for the financial support from the Natural Science and Engineering Research Council of Canada (NSERC).

Table of Contents

Abstract I

Acknowledgement III

Table of Contents IV

List of Figurers IX

1 Introduction 1

2 Literature Review 3

2.1 Energy Storage Devices 3

2.2 Applications of Electrochemical Supercapacitors 6

2.3 Energy Storage Mechanism of Electrochemical Supercapacitors 8

2.3.1 Electrochemical Double Layer Supercapacitors 8

2.3.2 Pseudo-Supercapacitors 11

2.3.3 Hybrid Supercapacitors 12

2.4 Materials for Electrodes of Supercapacitors 13

2.4.1 High Specific Surface Area Materials 13

2.4.2 Redox Pseudo-Capacitive Materials 19

2.4.2.1 Oxide Materials 19

2.4.2.2 Conducting Polymers 22

2.4.3 Composite Materials 23

2.5 Electrolytes 25

2.5.1 Aqueous Electrolytes 26

2.5.2 Organic Electrolytes 27

2.5.3 Ionic liquids 28

2.6 Fabrication of Conducting Polymers Electrodes 28

2.6.1 Properties of Conducting Polymers 29

2.6.2 Fabrication methods 34

2.6.3 Synthesis of PPy and PPy Based Composites 35

2.6.3.1 Chemical Method 36

2.6.3.2 Electrochemical Method 38

3 Objective 44

4 Approach and methodology 45

4.1 Approach 45

4.2 Methodology 45

4.2.1 Dissolution and Passivation 45

4.2.2 Novel Additives 46

5 Experimental Procedures 49

5.1 Materials Preparation....49

5.2 Equipment Set-up....49

5.3 Electropolymerization of PPy Film....49

5.4 Co-Deposition of PPy/MWCNT Composite....50

5.5 Characterization....51

5.5.1 Morphology Characterization....51

5.5.2 Electrochemical Characterization....51

6 Results and Discussion....55

6.1 Electropolymerization of PPy from Aqueous Salicylate Solutions....55

6.1.1 Electrochemical Behavior of Stainless Steel in Aqueous Salicylate Medium 55

6.1.2 Electropolymerization of PPy from Aqueous Salicylate Solutions....57

6.1.2.1 Cyclic Voltammogram Electropolymerization of PPy....57

6.1.2.2 Galvanostatic Electropolymerization of PPy....59

6.1.3 Characterization of PPy Film Deposited Using Sodium Salicylate....61

6.1.3.1 Deposit Mass and Morphology Characterization....61

6.1.3.2 Redox Reaction Properties....65

6.1.3.3 Capacitance of PPy Doped with Sodium Salicylate....66

6.1.4 Corrosion Performance of PPy Coated Stainless Steel....67

6.1.4.1 Open Circuit Potential Measurement 67

6.1.4.2 Potentiodynamic Polarization 68

6.2 Electropolymerization of PPy from Aqueous Tiron Solution 69

6.2.1 Electrochemical behavior of stainless steel in aqueous tiron medium 69

6.2.2 Electropolymerization of PPy from aqueous tiron solution 73

6.2.2.1 Galvanostatic Electropolymerization of PPy 73

6.2.3 Characterizations of PPy Film Prepared Using Tiron 75

6.2.3.1 Deposit Mass and Morphology Characterization 75

6.2.3.2 Redox Reaction Properties 79

6.2.3.3 Capacitance of PPy Doped with Tiron 81

6.2.3.3.1 Effect of Scan Rates on Capacitance of PPy/tiron Film 81

6.2.3.3.2 Effect of Concentration of Tiron on Capacitance of PPy/tiron Film 82

6.2.3.3.3 Effect of pH on Capacitance of PPy/tiron Film 83

6.2.3.3.4 Effect of Specific Mass on Capacitance of PPy/tiron Film 84

6.3 PPy/MWCNT Composite 85

6.3.1 Electro-Co-Deposition of PPy/MWCNT in The Presence of Tiron 85

6.3.1.1 The Role of Tiron in Electro-Co-Deposition 85

6.3.1.2 Deposition Mass 87

6.3.1.3 Morphology Characterization of PPy/MWCNT Composite. 88

6.3.2 Electrochemical behavior of PPy/MWCNT composite 90

6.3.2.1 Electroactivity of PPy/MWCNT Composite 90

6.3.2.2 Specific Capacitance of PPy/MWCNT 92

6.3.2.3 Electrochemical Impedance Spectra 95

6.3.2.4 Cycle Life Test 101

7 Conclusions 104

List of Figures

Figure 2-1 Ragone plot of various energy storage devices [10].....5

Figure 2-2 Schematic diagram of Electrochemical Double Layer [22].....9

Figure 2-3 Schematic diagram of an EDLC construction [23].....10

Figure 2-4 Normalized capacitance as a function of the pore size of CDC as well as the structure of ethyl-methylimmidazolium (EMI) and bis (trifluoromethane-sulfonyl) imide (TFSI) ions [31].....14

Figure 2-5 Schematic network for the pore size of an activated carbon grain [32].....15

Figure 2-6 Schematic of (A) SWCNT and (B) MWCNT [54].....18

Figure 2-7 Schematic diagram of charging/discharging process for CP electrodes. (a) p-type and (b) n-type [8].....23

Figure 2-8 SEM image of PPy/CNTs composite [78].....24

Figure 2-9 PPy/intercalated layered MnO_2 nanocomposite [79].....25

Figure 2-10 Chemical structure of common conducting polymers [91].....29

Figure 2-11 Non-degenerate ground state configurations and charge carrier defects of PPy [96].....31

Figure 2-12 SEM of PPy film surface at (a) oxidized and (b) reduced state [105].....34

Figure 2-13 Mechanism of chemical oxidative polymerization of pyrrole [113].....38

Figure 2-14 Overall electro-polymerization reaction of PPy [126].....39

Figure 2-15 CV of PPy films deposited with different methods in 0.1 M phosphate buffered saline (PBS) solution, E vs. Ag/AgCl [136].....43

Figure 4-1 Chemical structure of (a) sodium salicylate and (b) tiron 46

Figure 4-2 Chelate complexes formed with Fe^{2+} by (a) sodium salicylate and (b) tiron ..47

Figure 5-1 Scheme of PPy film preparation on SSt.....50

Figure 5-2 Scheme of PPy/MWCNT composite fabrication process.....51

Figure 5-3 Equivalent circuit of the PPy-electrolyte system [144] 53

Figure 6-1 Cyclic voltammogram of the stainless steel recorded in 0.15 M sodium salicylate aqueous neutral solution at a scan rate of 20 mV s^{-1} 56

Figure 6-2 Cyclic voltammogram of the stainless steel surface recorded in 0.15 M sodium nitrate aqueous neutral solution at a scan rate of 20 mV s^{-1} 57

Figure 6-3 Cyclic voltammogram of 1^{st}, 2^{nd}, 3^{rd} and 10^{th} scans during the electropolymerization on stainless steel from solution containing 0.2 M pyrrole and 0.15 M sodium salicylate. Scan rate: 20 mV s^{-1}. 58

Figure 6-4 Galvanostatic behavior for deposition of 0.1 M pyrrole on stainless steel at a current density of 1 mA cm^{-2} in the presence of 0.15 M (a) sodium salicylate and (b) sodium nitrate. 60

Figure 6-5 PPy/sodium salicylate film mass versus deposition time at 1 mA cm^{-2} 61

Figure 6-6 SEM images of cross section for the PPy/sodium salicylate film shown at (a) low magnification and (b) high magnification. 62

Figure 6-7 SEM image of surface for PPy/sodium salicylate on stainless steel shown at a (a) low magnification and (b) high magnification. 63

Figure 6-8 SEM images for the PPy/sodium salicylate film on a stainless steel wire. Inset is the surface image in the circle area at high magnification.....64

Figure 6-9 CV for the film deposited from the 0.1 M pyrrole solution containing 0.15 M sodium salicylate on a stainless steel foil at scan rate of (a) 2, (b) 5 and (c) 10 mV s^{-1}. Film Mass: 207 μg cm^{-2} 65

Figure 6-10 SC versus scan rates for the films deposited from the solution containing sodium salicylate on a stainless steel foil with a film mass of (a) 165, (b) 373, (c) 658 μg cm^{-2} 66

Figure 6-11 Open circuit potential–time curve recorded for (a) bare stainless steel and (b) PPy coated stainless steel in aqueous 0.5 M NaCl solution. 67

Figure 6-12 Potentiodynamic polarization curves for (a) bare stainless steel and (b) PPy coated stainless steel recorded in a 0.5 M Na_2SO_4 solution 68

Figure 6-13 Cyclic voltammogram of the stainless steel surface recorded in 0.15 M tiron aqueous neutral solution at a scan rate of 20 mV s^{-1} 70

Figure 6-14 Cyclic voltammogram of the stainless steel surface recorded at a scan rate of 20 mVs^{-1} in a 0.15 M, 0.01M and 0.005M tiron aqueous neutral solution 71

Figure 6-15 Cyclic voltammogram of the stainless steel surface recorded at a scan rate of 20 mV s^{-1}, 10 mV s^{-1} and 5 mV s^{-1} in a 0.005 M tiron aqueous neutral solution 71

Figure 6-16 Cyclic voltammogram of the stainless steel surface recorded in a 0.15 M Na_2SO_4 aqueous neutral solution at a scan rate of 20 mV s^{-1} 72

Figure 6-17 Galvanostatic behavior of PPy deposit on stainless steel from a 0.05 M pyrrole solution in the presence of 0.005 M (1) pTS-Na and (2) tiron at a current density of 1 mA cm^{-2}. Inset shows the chemical structure of (a) pTS-Na and (b) tiron. 74

Figure 6-18 PPy/tiron film mass versus deposition time at 1 mA cm^{-2} 75

Figure 6-19 PPy/tiron film obtained at a constant current of 1 mA cm^{-2} with deposition time (a) 6 min and (b) 18 min on silicon wafer 76

Figure 6-20 SEM image of surface of PPy/tiron on stainless steel shown at a (a) low magnification and (b) high magnification 78

Figure 6-21 SEM images for the PPy/tiron film on a stainless steel wire. Inset is the cross-section image in a rectangle frame at a high magnification 79

Figure 6-22 CV for the film deposited from the 0.1 M pyrrole solution containing 0.005 M tiron on a stainless steel foil in 0.5 M Na_2SO_4 electrolyte at scan rate of (a) 2, (b) 5 and (c) 10 mV s-1. Film mass: 213 μg cm^{-2} 80

Figure 6-23 SC versus scan rate for the films deposited from the 0.1 M pyrrole solution containing 0.005 M tiron on a stainless steel foil in 0.5 M Na_2SO_4 electrolyte with the film mass of 213 μg cm^{-2} 81

Figure 6-24 Plot of SC versus concentration of tiron at different scan rates. PPy films were obtained on stainless steel from 0.05M solutions containing tiron. Film mass: 140 μ g cm^{-2}. 82

Figure 6-25 Plot of SC versus scan rate for the films deposited from 0.05M pyrrole solutions containing 0.005M tiron on a stainless steel at the pH values of 1, 3, 5, 7. Film mass: 145 μg cm^{-2} 84

Figure 6-26 Plot of SC versus specific mass on a stainless steel at different scan rates. PPy films were obtained from 0.05 M pyrrole solutions containing 0.005 M tiron 85

Figure 6-27 Photo of 0.4 g L^{-1} MWCNT suspension in the presence of 5 mM tiron 87

Figure 6-28 Deposit mass versus deposition time at a current of 1 mA cm^{-2} for the composite from 0.1 M pyrrole solution containing 5 mM tiron and 0.4 g L^{-1} MWCNTs.88

Figure 6-29 SEM image of the films prepared on stainless steel foil at a current of 1 mA cm^{-2} from 0.1M pyrrole solution containing 5mM tiron and 0.4g L^{-1} MWCNTs. Inset is the surface at low magnification. The dashed circle is the area shown at higher magnification 89

Figure 6-30 CV data at a scan rate of 100 mV s^{-1} for the 160 μg cm^{-2} films prepared at a current density of 1 mA cm^{-2} from 0.1 M pyrrole solution containing 5 mM tiron(a) without MWCNTs and (b) containing 0.4 g L^{-1} MWCNTs 90

Figure 6-31 CV data at a scan rate of (a) 200, (b) 300, (c) 400, (d) 500 mV s^{-1} for the 160 μg cm^{-2} films prepared at a current density of 1 mA cm^{-2} from 0.1 M pyrrole solution containing 5 mM tiron and 0.4 g L^{-1} MWCNTs 92

Figure 6-32 SC versus scan rate for the 160 μg cm^{-2} films prepared at a current density of 1 mA cm^{-2} from 0.1 M pyrrole solutions containing 5 mM tiron: (a) without MWCNTs and (b) containing 0.4 g L^{-1} MWCNTs 94

Figure 6-33 SCs measured at a scan rate of 5 mV s^{-1} versus film mass for the films prepared at a current density of 1 mA cm^{-2} from 0.1 M pyrrole solution s containing 5 mM tiron: (a) without MWCNTs and (b) containing 0.4 g L^{-1} MWCNTs 95

Figure 6-34 Nyquist plots for the 160 μg cm^{-2} films prepared at a current density of 1 mA cm^{-2} from 0.1 M pyrrole solution s containing 5 mM tiron: (a) without MWCNTs and (b) containing 0.4 g L^{-1} MWCNTs. Inset is the enlarged region at high-frequency 96

Figure 6-35 Equivalent circuit model for pure PPy and PPy/MWCNT composite electrode in a 0.5 M Na_2SO_4 electrolyte 98

Figure 6-36 Modified equivalent circuit model for pure PPy and PPy/MWCNT electrode in a 0.5 M Na_2SO_4 electrolyte 99

Figure 6-37 Nyquist plot of PPy and PPy/MWCNT composite recorded at OCP. Experimental (circle) and theoretical (solid line). EIS data fitting results according to the EEC model 100

Figure 6-38 CV of the PPy/MWCNT film recorded in the (a)1^{st} and (b)1000^{th} potential cycle at a scan rate of 50 mV s^{-1} in 0.5M Na_2SO_4 electrolyte solution. Inset is CV of the PPy film in the 1^{st} and 1000^{th} potential cycle under same test condition. Film mass:183μg cm^{-2} 101

Figure 6-39 SC at a scan rate of 50 mV s^{-1} versus cycle number for the 220 μg cm^{-2} films prepared at a current density of 1 mA cm^{-2} from 0.1 M pyrrole solutions containing 5 mM Tiron (a) without MWCNTs and (b) containing 0.4 g L^{-1} MWCNTs 103

List of Tables

Table 2-1 Comparison of the properties of conventional capacitor, batteries and ES [12].6

Table 2-2 EDLC and Pseudocapacitance compared [26] 12

Table 2-3 Properties of various electrolytes [32] 26

Table 2-4 Conductivity and doping type of some conducting polymers [92] 30

Table 2-5 Comparison of chemical and electrochemical polymerization [119]. 36

Table 2-6 List of dopant anions and their electrolyte sources [92]. 41

1 Introduction

The Electrochemical Supercapacitor (ES) has been investigated as an advanced energy storage technology. The combination of batteries and capacitors make unique electrochemical energy storage devices with high power density and high energy density. The key part of an ES is the electrode. The materials for electrodes and the storage mechanism have been studied, including high surface area carbon, transition metal oxides and conducting polymers.

Polypyrrole (PPy) is one of the most promising conductive polymers to be used as electrode materials due to the high pseudocapacitance, low cost and easy fabrication. Electrochemical polymerization is an attractive method for the fabrication of PPy films. In this method, the PPy deposits can be obtained on the anode in a facile way from solutions containing pyrrole and dopants. One of the major challenges for the electrochemical polymerization of pyrrole is to form adherent PPy coatings on reactive metal substrates, because the dissolution of the metal occurs prior to the coating formation. Another important parameter affecting the deposition yield, physical characteristics, and morphology of PPy is the nature of anionic dopant. Sodium salicylate and 4, 5-dihydroxy-1, 3-benzenedisulfonic acid disodium salt (tiron) are promising anionic dopants for the fabrication of PPy films and composites. PPy films were deposited on stainless steel substrates in the presence of tiron and sodium salicylate and investigated for application in electrochemical supercapacitors.

The interest in PPy for application in electrochemical supercapacitors (ES) is attributed to the high specific capacitance of this material. The possibility of depositing

PPy on stainless steel substrates is important for practical applications of PPy films in ES, using low-cost stainless steel current collectors. The important task is to avoid anodic dissolution of the substrates and reduce contact resistance, since a high contact resistance can result in a low capacitance.

However, the electrochemical performance of PPy film degrades due to its swelling and shrinkage during the cycling process. To overcome this poor stability problem, multiwalled carbon nanotubes were incorporated into the polymer matrix. The fabrication of PPy films containing multi-walled carbon nanotubes (MWCNTs) was performed on stainless steel substrates using additive tiron as dopants and surfactant. In order to investigate the deposition mechanism, the results obtained for tiron molecules containing OH groups were compared with the molecules without OH groups. The results presented below showed that tiron can be used for the dispersion, charging and anodic co-deposition of MWCNTs. The PPy/MWCNT composite films showed improved capacitive behavior compared to the pure PPy films.

2 Literature Review

2.1 Energy Storage Devices

The world is observing the decreasing availability of fossil fuels and the increasing energy consumption accompanied by global warming due to the accumulation of CO_2 emission [1]. Further, the pollutants which are serious health hazards to mankind have been identified as coming out of the use of fossil fuels. Although, many efforts have been focused on renewable power, such as the sun, wind, and water, or even the nuclear source, they still have many limitations mainly related to reliability and sustainability [2-4]. As a result, energy storage systems play an important role in storing or retrieving electrical energy to meet the increasing demands. The performance of energy systems can be improved by developing advanced materials [5].

Conventional capacitors, batteries, fuel cells and electrochemical supercapacitors (ES) have different charge storage mechanisms. Conventional capacitors are based on the charge accumulation which is achieved electrostatically on the electrode plates separated by dielectric or vacuum. The charge/discharge process is highly reversible and non-Faradaic. Batteries are based on the chemical reaction between the electrode and electrolyte, the charging process is Faradaic with phase change [6]. Fuel cells generate ions or electrons during the reduction of oxidant or oxidation of fuel through internal electrolyte, directly converting energy from chemical form to electrical one [7]. ES are

based on the electrosorption or redox reaction which occurs at the electrodes through Faradaic or non-Faradaic process [8].

There are two important parameters for describing the behavior of energy storage devices: the energy density and the power density. Energy density is the energy stored per unit mass and is proportional to voltage squared. It can be calculated by:

$$W = \frac{1}{2} C V^2 \qquad (2\text{-}1)$$

where, C is the specific capacitance. V is the voltage. Power density is the amount of energy delivered per unit mass. It can be defined as:

$$P = iV \qquad (2\text{-}2)$$

where, i is the current. The maximum power delivery can be derived from the simple series circuit [9]:

$$P_{max} = \frac{1}{4R_s} V_i^2 \qquad (2\text{-}3)$$

where, R_s is the equivalent series resistance (ESR), V_i is the initial voltage.

The Ragone plot [10], as shown in Figure 2-1, is currently employed to characterize the different types of energy storage devices. It indicates that batteries and fuel cells show very high energy density (about 10-1000 Wh kg^{-1}), they can store a large amount of energy but take a long time to discharge or recharge due to their low power delivery. Conventional solid state and electrolytic capacitors have high power density (up to 10^7 W kg^{-1}); however, they suffer very low energy stored to meet requirement of long duration. Either case is not able to meet the needs of today's power technology.

The ES combines the energy storage properties of batteries or fuel cells with the power charge/discharge characteristics of conventional capacitors. ES can store hundreds or thousands of times more charge over the conventional capacitors due to their much larger surface area. They are able to hold a very high charge which can be released in a controlled manner. Hence, an ideal supercapacitor should have high power, high energy density, long shelf and cycle life (> 10^5 cycles), high efficiency (90 - 95% or higher), processability, friendliness to environment and relatively low cost [3,11]. In Table 2-1, the differences of properties for different energy storage devices are summarized [12].

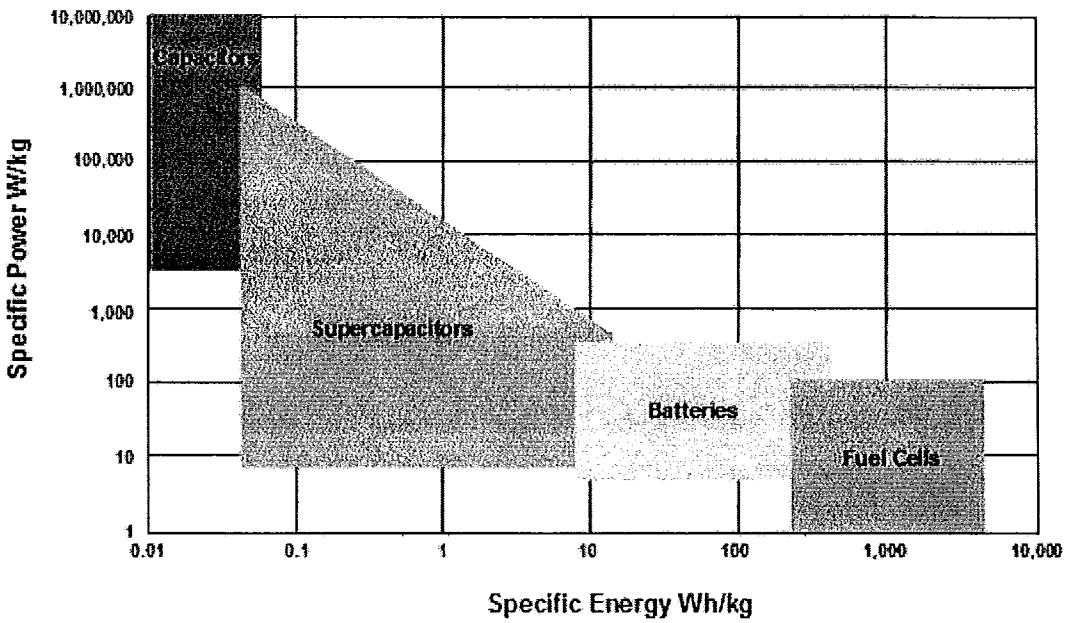

Figure 2-1 Ragone plot of various energy storage devices [10].

Table 2-1 Comparison of the properties of conventional capacitor, batteries and ES [12]

Items	Supercapacitor	Battery	Capacitor
Charge time	1-30 s	1-5 hr	10^{-3}-10^{-6} s
Discharge time	1-30 s	0.3-3 hr	10^{-3}-10^{-6} s
Energy density ($Wh\ kg^{-1}$)	1-10	10-100	<0.1
Power density ($W\ kg^{-1}$)	<10,000	<1000	<100,000
Efficiency of Charge/discharge	0.85-0.98	0.7-0.85	>0.95
Cycle life	$>10^5$	1000	$>10^5$

2.2 Applications of Electrochemical Supercapacitors

ES are also named "supercapacitors", "power cache" or "gold capacitors". They have many advantages as new energy storage devices. They are called "supercapacitors" [13] because of the use of extremely high capacitance materials as electrodes. They can be widely used as energy storage devices in many fields such as small portable electronics, transportation and industrial equipment. In the application of electric vehicles (EVs) and hybrid electric vehicles (HEVs) [14, 15], supercapacitors can supply pulse power for batteries or fuel cells in engine starting, acceleration, and also can store energy during braking within a short time. The stored energy can be reused when the vehicle starts moving again. In particular, supercapacitors may also replace or be combined with

batteries as the electric power source of EVs or HEVs due to their high power delivery or uptake and relatively high energy stored [16]. An obvious advantage for using supercapacitors is to reduce the size of batteries and keep a combustion engine working at an optimized condition, hence the vehicle efficiency can be improved and cycle life of the primary source can also be enhanced.

Supercapacitors have another promising application in portable electric devices due to their small size with the capability of longer cycle life and the ability of fast charge/discharge [17, 18]. The new applications of supercapacitors have been seen in digital camera flash, mobile phones, uninterruptible power back up for computers, laptops and smart cards. It is also believed that supercapacitors can be utilized for Micro or Nano Electro Mechanical systems (MEMs or NEMs) which have attracted attention for potential applications in micro sensors and actuators [19].

In addition, supercapacitors have advantages for application in the relatively wide temperature range of -30° C to +60° C. It is in this regard that ES exceed batteries, which show good performance only in relatively narrow temperature range [20].

Despite the advantages of ES discussed above, compared to other energy storage devices, ES are currently prevented from being commercially used in long duration applications mainly due to their high capital cost. The requirement of high energy stored also limit the use of ES. Hence, discovering new materials for fabricating electrodes of ES to reduce the cost and increase energy density are the urgent issues for the future research work [5].

2.3 Energy Storage Mechanism of Electrochemical Supercapacitors

Although Becker [21] proposed the concept of ES in his first patent in 1957, ES have gained low attention until recently because of low energy storage and relatively high cost compared to batteries. However, with the development of new materials and the progress of design for fabricating electrodes of ES, higher energy density have become obtainable during the last 10 years. Based on the charge storage mechanism as well as the active materials used, the ES can be classified in three types: Electrochemical Double layer supercapacitors (EDLCs), Faradaic pseudo capacitors or redox capacitors, and hybrid electrochemical capacitors [12].

2.3.1 Electrochemical Double Layer Supercapacitors

EDLCs are electrochemical capacitors which store the electric energy directly in the double layer, also named Helmholtz Layer (Figure 2-2 (a)). The concept of double layer has been further extended in the Gouy–Chapman model and later in the 'Stern model' (Figure 2-2 (b) and (c)) [22].

Charge separation occurs on polarization at the interfaces between the solid electrode materials surface and the liquid electrolyte solution in the mini pores inside the electrode. The surface charge generated from surface dissociation, ion adsorption and crystal lattice [12]. The capacitance arises from an EDLC analogous to a parallel plate capacitor which can be described as double layer capacitance:

$$C_{dl} = \frac{\varepsilon_r \varepsilon_0 A}{d} \qquad (2\text{-}4)$$

where; ε_r is the relative dielectric constant in the double layer. ε_0 is the permittivity of free space. d represents the effective thickness of the double layer with surface area A. Compared to a conventional capacitor, the thickness for a EDLC is in the order of 5-10 Å which is much smaller than the distance between the plates of a electrolytic or dielectric capacitor.

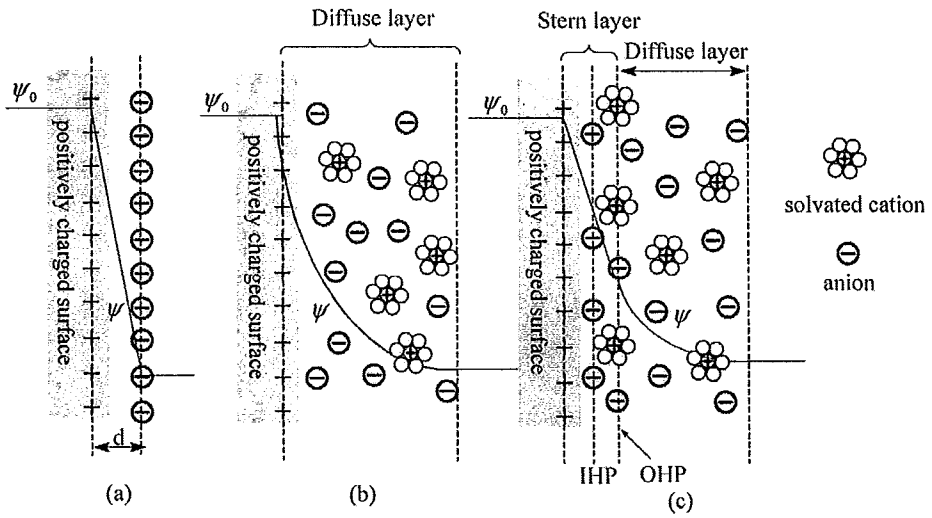

Figure 2-2 Schematic diagram of Electrochemical Double Layer [22]

The corresponding electric field in the electrochemical DL is as high as 10^6 V cm^{-1}. Because the charge storage is largely electrostatic in nature, there is no charge transfer across the interface (non-Faradiac); hence, highly reversible charging/discharging and very long cycle life are achievable. Further, in order to achieve a higher capacitance, the electrode surface area can be additionally increased by using porous materials such as carbon with an extremely large internal effective surface (typically > 1000 m^2 g^{-1}). Therefore, compared to conventional capacitors where the total capacitance is typically in

the μF or pF range, the combination of high accessible specific surface area and atomic scale of charge separation in EDLCs result in very high capacitance (typically in the range of several F) and increasing amount of charge (electric energy). A schematic diagram [23], shown in Figure 2-3, exhibits the simple construction of an EDLC. Such a complete cell system can be considered as two capacitors (each electrode/electrolyte interface represents a capacitor) in series. Hence, for a symmetrical capacitor, the cell capacitance (C_{Cell}) can be written as [10]:

$$\frac{1}{C_{Cell}} = \frac{1}{C_1} + \frac{1}{C_2} \qquad (2\text{-}5)$$

Where C_1 and C_2 represent the capacitance of the two similar electrodes.

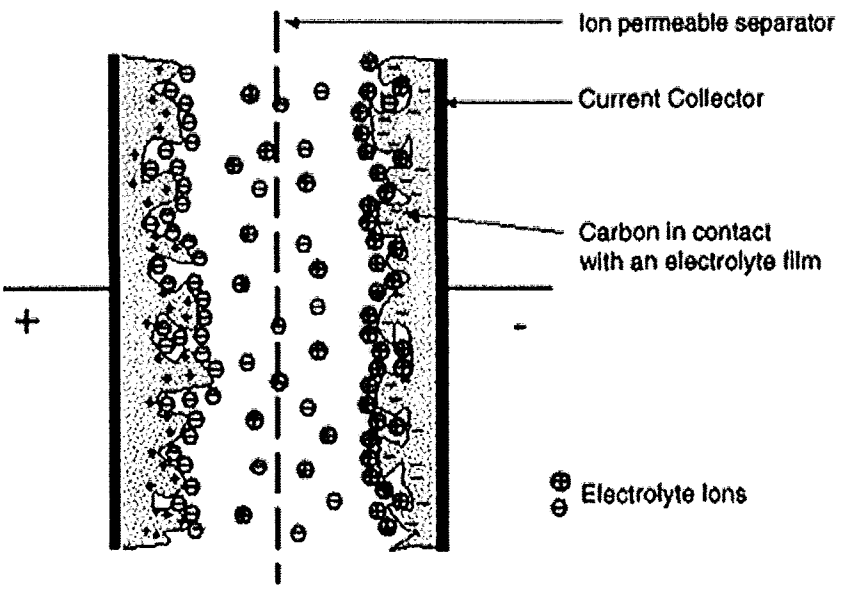

Figure 2-3 Schematic diagram of an EDLC construction [23]

2.3.2 Pseudo-Supercapacitors

The second type of ES is the so called pseudocapacitor. Pseudocapacitance (C_ϕ) arises in cases where, for thermodynamic reasons, the passage of charge, q, originated from Faradaic charge transfer at the surface or in the bulk near the surface of the solid electrode material, is a function of potential V. The derivative dq / dV corresponds to a Faradaic capacitance (pseudocapacitance) [24],

$$C_j = dq/dV \qquad (2\text{-}6)$$

Three types of charge transfer processes associated with pseudocapacitance have been proposed [24, 25], including surface adsorption of ions from the electrolyte, redox reactions and doping /dedoping of active conducting polymers. The first two processes are highly dependent on the surface area of the electrode material while the third process is a bulk process. The third process is less dependent on the surface area although the electrodes require micro-pores for ion transfer [17]. The last two redox reaction processes exhibit reversible charge/discharge behavior in cyclic voltammetry and also show substantially larger (10−100 times) capacitance than those for carbon double layer systems [8].

It should be noted that the two different storage mechanisms, usually co-exist in the supercapacitor system. Generally, one of the storage mechanisms dominate in the system, the other one is relatively small (ca. 2% to 5%). To distinguish between these two systems, a comparison of EDLC and pseudocapacitance is shown in Table 2-2 [26].

Table 2-2 EDLC and pseudocapacitance compared [26]

	Double-layer capacitance	**Pseudocapacitance**
1	Non-faradaic	Involves faradaic process(es)
2	20–50 μF cm^{-2}	2000 μF cm^{-2} for single-state process; 200–500 F cm^{-2} for multi-state, overlapping processes
3	C fairly constant with potential, except through the point of zero charge (p.z.c.)	C fairly constant with potential for RuO_2; for single-state process, exhibits marked maximum
4	Highly reversible charging/discharging	Can exhibit several maxima for overlapping, multi-state processes, as for H at Pt
5	Has restricted voltage range (contrast non-electrochemical electrostatic capacitor)	Quite reversible but has intrinsic electrode-kinetic rate limitation determined by R_f
6	Exhibits mirror-image voltammogram	Has restricted voltage range; exhibits mirror-image voltammogram;

2.3.3 Hybrid Supercapacitors

The use of DL capacitance and pseudocapacitance materials for different electrodes in asymmetrical configuration resulted in hybrid type electrochemical capacitors. The hybrid supercapacitors (HS) have gained attention in recent years [27-29]. Hybrid supercapacitors possess increased specific energy compared to electrochemical capacitors containing two similar electrodes, because of a larger voltage window. The principle of the HS design is to use a DL capacitance electrode combined with a

pseudocapacitance electrode. The two electrodes are charged in different modes: one is electrostatically charged-discharged, while the other is pseudo capacitive; it undergoes a Faradaic process, which starts at defined electrode potentials and gives rise to a pseudocapacitance. In HS, the increase in both the working voltage and the specific energy were achieved. The higher maximum operating voltage (V_{max}) and the lower equivalent series resistance (ESR) were additional beneficial factors, which allowed significant improvement in the overall performance of the supercapacitors for the HEV and EV applications.

2.4 Materials for Electrodes of Supercapacitors

ES can be classified by several criteria, i.e., electrode materials used, the electrolyte, or the cell design. With respect to electrode materials used, three types of ES are distinguished as follows: high specific area materials, redox pseudo-capacitive materials and composite materials.

2.4.1 High Specific Surface Area Materials

Typically, carbon-based materials in various forms (powders, fibers, aerogels, sheets, monoliths, tubes, etc.) have been extensively utilized to fabricate electrodes of EDLC mainly due to their very high specific surface area (SSA), good electrical conductivity, high chemical stability, easy processability, relatively low cost and wide temperature range of stability [12]. In a review article, Pandolfo et al. [30] stated that the enhanced double layer capacitance is also determined by other important aspects, such as

wettability, electrochemical stability, nature of electrolyte and open porosity. In particular, a recent study of relation between the ion size and pore size for an EDLC done by Largeot et al. [31] showed that the pore size of carbon-derived carbide (CDC) leading to the maximum double-layer capacitance is very close to the ion size. In this work, ethyl-methylimmidazolium (EMI) and bis (trifluoromethane-sulfonyl) imide (TFSI) ionic liquids were used; both larger and smaller pores lead to a significant drop in capacitance as shown in Figure 2-4.

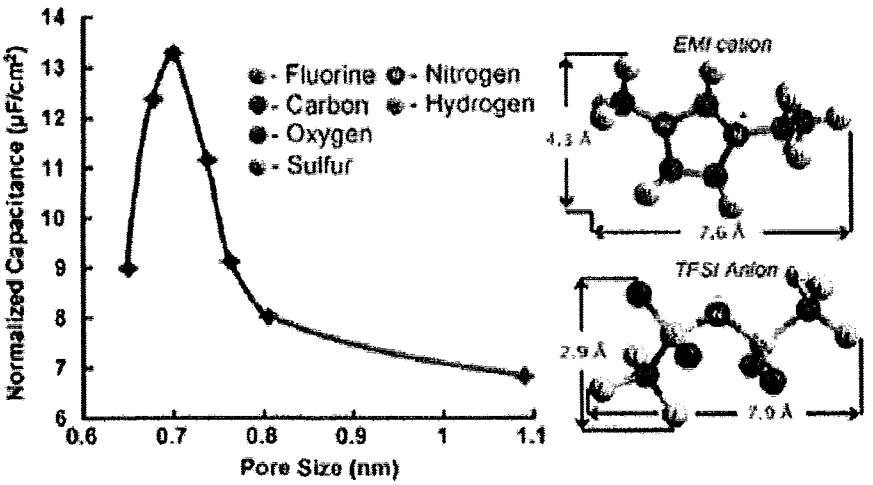

Figure 2-4 Normalized capacitance as a function of the pore size of CDC as well as the structure of ethyl-methylimmidazolium (EMI) and bis (trifluoromethane-sulfonyl) imide (TFSI) ions [31]

Activated carbon is especially attractive as an electrode for EDLC because of its high surface area, low cost and commercial availability. Activated carbon is derived from carbon-rich organic precursors such as wood, coal, pitch by heat treatment in inert atmosphere followed by selective oxidation process in water, CO_2, or KOH, named activation, to obtain the high SSA and pore volumes [5]. After activation, three types

pore size [5] (micropores (ϕ<2nm), mesopores (ϕ2-50nm), macrospores (ϕ>50nm), shown in Figure 2-5 [32], can be reached in carbon grains.

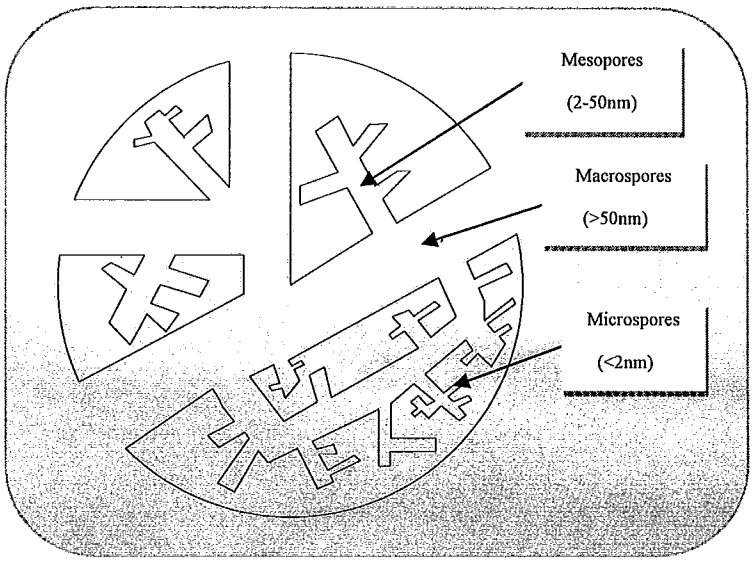

Figure 2-5 Schematic network for the pore size of an activated carbon grain [32]

Theoretically, the higher the SSA of AC, the higher the specific capacitance should be achieved. Macrospores negligibly contribute to the SSA whilst mesopores contribute to SSA and provide wider transport pores for ion diffusion [30]. Zhou et al. [33] concluded that the specific capacitance increases when SSA and mesoporosity of the activated carbon electrode increases. Micropores have a high surface-area volume ratio. For example, the high SSA 1000-2500 m^2 g^{-1} as measured by BET method has been reported for activated carbon cloth (ACC) [34]. However, it is not always true that high SSA results in high capacitance. In some cases, it was reported that high specific capacitance (ca. 300 F g^{-1}) was obtained with low surface area carbon fiber (< 1 m^2 g^{-1}) using a proprietary activation process, and the higher capacitance was related to surface

functional groups [35]. Although SSA is a primary parameter for the performance of EDLC, the pore size, pore size distribution (PSD), pore geometry and structure, and surface functionality can also influence the electrochemical behavior to a great extent [36-41]. It was also concluded that the pore structure of an AC electrode in different electrolytes influences the EDLC capacitive behavior. The earlier work demonstrated that the capacitance of AC is higher in aqueous electrolytes than in organic electrolytes [41].

Carbon aerogels are considered as promising materials for ES due to their advantages of high porosity (over 50%, with pore diameter under 100 nm, very high surface areas (400–1000 m^2g^{-1}), good electrical conductivity, and the possibility of the fabrication of binder-free porous structure [42-44]. Carbon aerogels can be prepared by the pyrolysis of organic aerogels based on resorcinol-formaldehyde (RF) or phenol-furfural (PF) precursors through sol-gel process in which particle sizes, pore shape and density can be controlled [45, 46]. The performance and structure of aerogels for ES strongly depends on the molar resorcinol to catalyst (R/C) ratio. The particle size increased and the BET surface area decreased with the increase of R/C ratio. The high capacitance of 183.6 F g^{-1}, the low resistance (0.3Ω) and the small leakage current (0.17mA) were achieved with R/C ratio of 1500 [47]. Capacitance values up to 104 F g^{-1} and 77 F cm^{-3} have been achieved in the 1.0 M H_2SO_4 electrolyte using mixed cresol resorcinol-formaldehyde (CRF) carbon aerogels. The capacitance was strongly correlated with mesopores surface area rather than the BET surface area [48]. Capacitance increased almost linearly with the BET surface area [49]. However, further investigations revealed that although a large increase of BET surface area in the range of 650~2500 m^2 g^{-1} was

achieved by thermal activation, the accompanying increase of capacitance was relatively small. The capacitance also decreased from 18μF cm^{-2} of activated sample to 8μF cm^{-2} of inactivated sample, and this was attributed to an increase of inaccessible pores volume after activation[30].

Glassy carbons (GC) are produced by the thermal degradation of polymers resins such as phenolic resins or furfuryl alcohol. The physical properties of GC are found to be dependent on the maximum temperature during the heat treatment process. After activation, the isolated porosity of GC can be opened to achieve a high SSA. Thermal activation provided more accessible porosity than electrochemical oxidation process. It was found that thermal oxidation creates an active film on GC whose growth and thickness are probably controlled by diffusion of the oxidant into the film. It was found that the internal volumetric surface area decreases upon activation, whereas the volumetric electrochemical double layer capacitance increases and this effect is correlated with the opening, the growth and the coalescence of the pores [50, 51]. The properties of low electrical resistance, high accessible SSA after activation and easy processability make GC a good candidate for electrodes of ES.

Carbon nanotubes (CNTs) are produced by the catalytic decomposition of certain hydrocarbons .The nanoscale tubular morphology is an important characteristic of CNTs which are classified into two forms: multi-walled CNTs (MWNTs) and single-walled CNTs (SWNTs) [52,53]. Schematic representations of a SWNT and MWNT are shown in Figure 2-6 [54].

CNTs have attracted great attention owing to their unique pore structure characteristics, such as high strength, good electrical conductivity, good electrolyte accessibility, good chemical and thermal stability which are important for ES electrode applications.

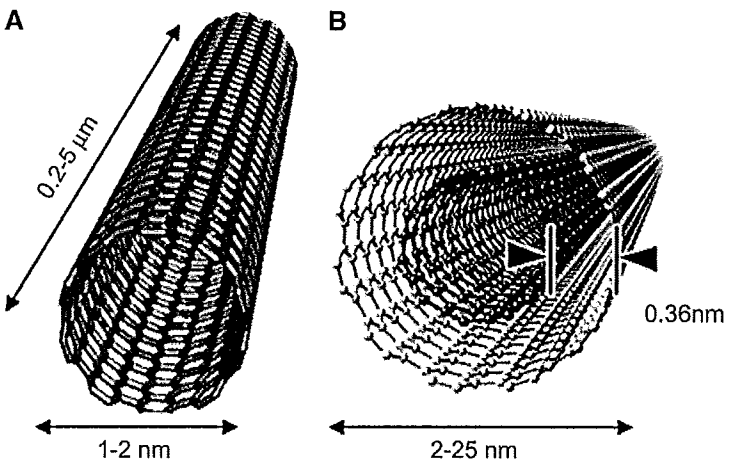

Figure 2-6 Schematic of (A) SWCNT and (B) MWCNT [54]

Generally, CNTs have relatively small SSA (<500 $m^2 g^{-1}$) compared to ACs (1000-3500 $m^2 g^{-1}$). For purified CNTs, the specific capacitance is typically in the range of 15 to 80 F g^{-1}. However, specific capacitance ca. 130 Fg^{-1} was achieved by oxidative (acid) treatment because the surface texture of CNTs was modified and additional surface functionality was introduced [55, 56]. In order to improve capacitance of CNTs, chemical activation with potassium hydroxide was reported [57]. The activated CNTs had 3 times higher BET specific surface area and 1.5 times higher pore volume than the normal CNTs. The electrochemical capacitance of the activated CNTs was 2 times that of the normal CNTs. It is noteworthy to mention that an aligned CNT array electrode possesses higher C_{sp}, lower ESR, and better rate capability than the entangled CNT electrode in the ionic

electrolyte and organic electrolyte. The reason for that is entangled CNTs are less efficient in facilitating fast ionic transport compared to aligned CNTs because an aligned CNT electrode possesses larger pore size as well as more regular pore structure and conductive paths [58, 59].

2.4.2 Redox Pseudo-Capacitive Materials

Metal oxides, nitrides and conducting polymers have been extensively studied in the past decades because they process pseudo-capacitive behavior. Because of the fast, reversible redox reactions occurring at the surface of these active materials, their specific pseudo-capacitance is larger than DL capacitance of carbon materials

2.4.2.1 Oxide Materials

Transition metal oxides such as RuO_2, IrO_2, NiO, MnO_2, Fe_3O_4, V_2O_5 etc. have various valence states. They have gained growing interest in the preparation of electrodes with pseudo capacitive properties. Their high specific capacitance and very low resistance are suitable for supercapacitor applications.

Among these materials, RuO_2 is a promising electrode material because of its high rate capacity, high conductivity, good electrochemical reversibility, long cycle life as well as very high capacitance [60-65]. The pseudo-capacitive behavior of RuO_2 is characterized by a fast reversible electron transfer together with an electro-adsorption of protons on the surface of RuO_2 particles according to the redox action: $RuO_2+xH^++xe^- \leftrightarrow RuO_{2-x}(OH)_x$, where, $0 \leq x \leq 2$, Ru oxidation states can change from (II) to (IV) [5]. Kim

et al. [65] reported that the specific capacitance of hydrous ruthenium oxide is dependent on the annealing conditions. The change in the number of active reaction sites, the electron and proton conductivity were responsible for the specific capacitance change of hydrous ruthenium oxide during annealing. Pristine $RuO_2 \cdot xH_2O$ and vapor-grown carbon fiber (VGCF)/$RuO_2 \cdot xH_2O$ nanocomposite have been prepared by a thermal decomposition method, the specific capacitances of pristine $RuO_2 \cdot xH_2O$ and its composite are 410 and 1017 F g^{-1}, respectively. Such a high performance of nanocomposite is believed to the highly open morphology of the composite material and to the highly electronically conducting support by incorporated carbon fiber [62].

However, the rarity of ruthenium in the earth's crust and hence the high market price of RuO_2 limits applications mostly in military and aerospace [24]. Less expensive oxides such as manganese oxide are more attractive for pseudocapacitors. The low cost and environmental friendliness as well as high electrochemical capacitance are the salient advantages of MnO_2. The charge storage mechanism of MnO_2 was proposed to be surface adsorption of electrolyte cations (M^+=K^+, Na^+, Li^+...) on MnO_2 as well as protons intercalation. The pseudocapacitance of $MnO_2 \cdot H_2O$ is attributed to the redox transitions of interfacial oxycation species in various oxidation states. These redox transitions of hydrous manganese oxides include the transitions between Mn(III)/Mn(II), Mn(IV)/Mn(III) and Mn(VI)/Mn(IV) within the potential window of water decomposition. This can be described in the reaction: $(MnO_2)_{surface}+xM^+ + yH^+ + (x+y)e^- \leftrightarrow (MnOOM_x)_{surface}\ H_y$. [66]. Cyclic voltammetry (CV) exhibits the fast, reversible redox behavior of MnO_2. The methods used for the fabrication of manganese oxide electrodes

can be electrochemical deposition [67], precipitation method [68] or sol–gel route [69]. Different types of crystal structures of MnO_2 were reported, including hexagonal ε-MnO_2, defective rock salt MnO_2 and defective antifluorite MnO_2 [70]. Yuan et al. [71] prepared mesoporous MnO_2 with an adsorption average pore diameter of 9.7 nm, mesoporous volume of 0.58 cm^3, and BET surface area of 239 m^2 by means of organic-aqueous interfacial method without any surfactants or organometallic precursors. The SC of ca. 285 F g^{-1} and 220 Fg^{-1} were obtained for the mesoporous MnO_2 at a scan rate of 2 mVs^{-1} and 100 mVs^{-1}, respectively. The attenuation of the capacitance for ca. 21% after 1000 continuous charging/discharging cycles suggested the good electrochemical stability. The effect of heat treatment and binder material used on capacitive property of MnO_2 was studied [68], the best capacitive performance was obtained with the material treated at 200°C, the highest specific capacitance (267 F g^{-1}) was obtained with an electrode containing 70% of MnO_x, 15% of carbon black, 10% of graphite fibres.

Magnetite (Fe_3O_4) is another recently discovered inexpensive electrode material. The electrochemical properties of Fe_3O_4 are attributed to a different capacitance mechanism compared to that of either RuO_2 or MnO_2. The capacitive behavior of Fe_3O_4 was investigated in sodium sulfite and sodium sulfate electrolytes [72]. The results indicated that the capacitive behavior was very sensitive to the nature of electrolyte anion species. The capacitive current of Fe_3O_4 electrode originated from the combination of EDLC and pseudo capacitance in Na_2SO_3 (aq), whilst the current was contributed to the entire EDLC in Na_2SO_4 (aq), and in KOH (aq). The relatively low capacitance observed was due to low electronic conductivity of the electrode material.

2.4.2.2 Conducting Polymers

Conducting polymers (CPs) represent a promising class of materials for use in ES and have been extensively studied in the last decade. Typical examples of CPs are PPy, Polyaniline (PAn), Poly (3,4-ethyelenedioxythiophene) (PEDOT), Polythiophene (PTh), and Poly (p-phenylene vinylene) (PPV). CPs possesses π-conjugated polymer chains in the backbone and the delocalized conjugated polymer structure can be highly electrical conductive after redox process, also named doping (oxidation) and dedoping process (reduction). Two types of charging process are classified: p-type and n-type, as shown in Figure 2-7 [8]. It was reported that p-dopable polymers are more stable against degradation than n-dopable polymers [73]; hence, investigations dealing with p-dopable polymers are more promising. Compared to carbon–based electrode materials, CPs have a relatively high specific capacitance, low ESR and good electrical conductivity in the charged states, whilst compared to RuO2, CPs have a relatively low materials cost and more environmental friendliness. The pseudocapacitance of CPs arises due to the fast and reversible redox reaction processes. The charging in CP films takes place not only on the surface, but also throughout the bulk volume, offering the opportunity to achieve high levels of specific capacitance. The values reported for CPs, for example, PANI can reach value of 1600 F g^{-1} when the thin film is electrodeposited on a porous carbon substrate [74]. Many factors affected the capacitance of CP films such as the nature of monomers, the electrolyte, the pH value of solution, the substrate, the deposition condition, etc. In particular, dopants (counter ions) influence the morphology, microstructure, electrochemical and mechanical properties of CP films [75,76].

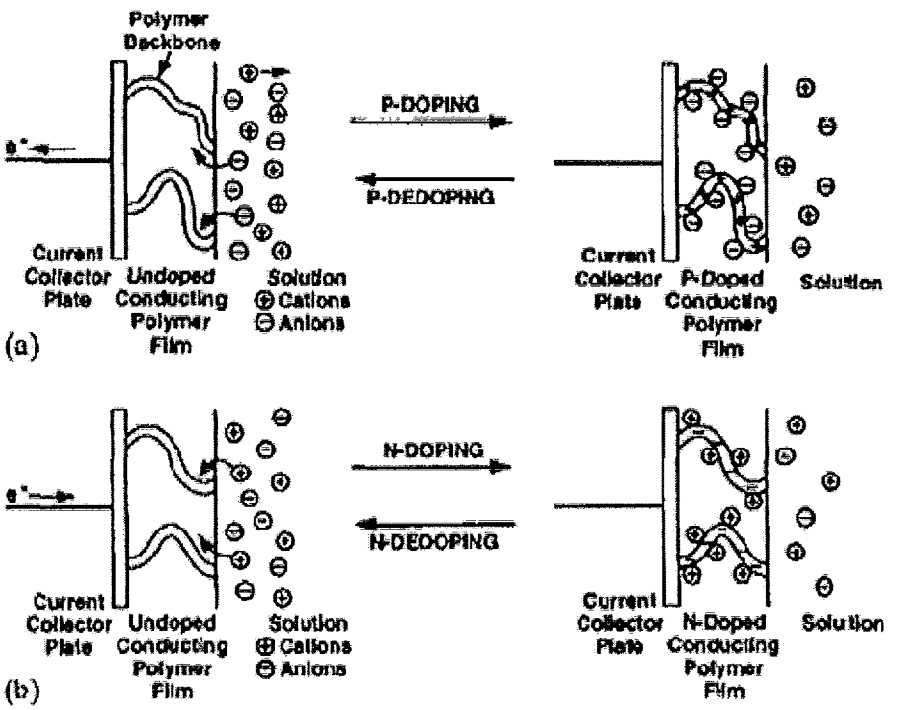

Figure 2-7 Schematic diagram of charging/discharging process for CP electrodes. (a) p-type and (b) n-type [8]

However, the main drawback of CPs for application as supercapacitor electrodes comes from their poor stability during cycling. Due to their volumetric changes in the doping/dedoping process, swelling, shrinkage, cracks or breaking of CP films may occur, resulting in the reduction of mechanical and electrochemical properties. The working potential range of the CP electrode is limited by the degradation caused by over-oxidation.

2.4.3 Composite Materials

Composite electrodes integrate two or more pure materials (CPs and metal oxides or carbons) within the same electrode. The strategy for material integration is to utilize the advantages of different materials in the composite electrode. Carbon –based materials

facilitate DL charge storage with high surface area, so that they are able to increase the contact between the deposited pseudo capacitive materials and electrolyte whilst redox materials also can increase the capacitance of the composite electrode. Further, carbon materials such as CNTs exhibit high mechanical strength properties, when combined with CPs, the composite CNT/CP structures are reinforced, which can significantly reduce the degradation of CP films [77,78]. In the study of Du [78] et al., the CNTs were used as the reinforcing material to overcome the PPy swelling and shrinkage during the doping-undoping process. The results showed that PPy was coated on the surface of the CNTs; The SEM image of PPy/MWCNT is shown in Figure 2-8. The electrochemical capacitance was 154.5 F g^{-1}, which was about 6 times that of pure PPy (ca. 25 F g^{-1}).

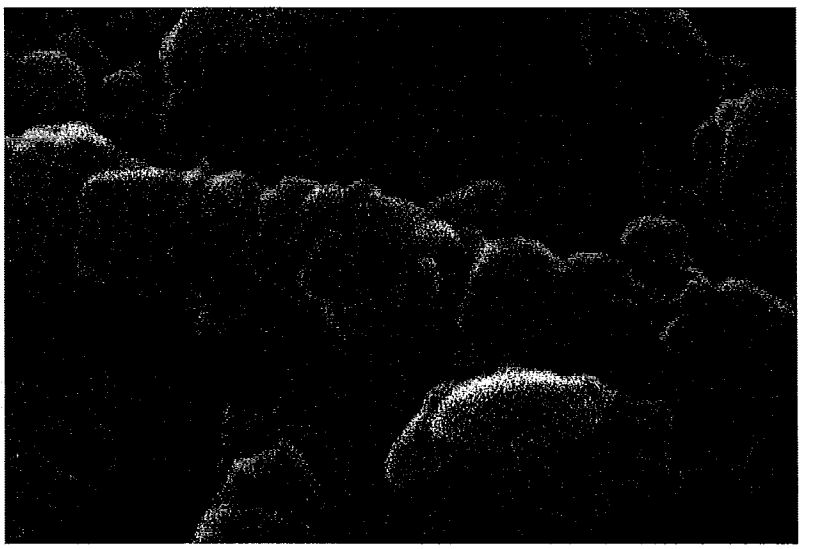

Figure 2-8 SEM image of PPy/CNTs composite [78]

Metal oxide with CP composite was also studied by Zhang et al. [79]. MnO_2/PPy composites were successfully synthesized, as shown in Figure 2-9. It was found that the conductivity of MnO_2/PPy composite increased by 5 orders of magnitude compared to

that of pristine MnO_2. The capacitance of the composite was also increased compared with that of the pristine MnO_2. These experiments have demonstrated that composite electrodes are able to achieve higher capacitances than either a pure CNT or pure polymer or metal oxide -based electrode.

It was suggested that entangled mat structure of composite can be more accessible to the electrolyte, resulting a three-dimensional distribution of charge. Moreover, the structural integrity of the entangled mat limited the mechanical stress caused by the insertion and rejection of ions in the deposited polymer film. Therefore, these composites have been shown to achieve improved cycling stability comparable to that of EDLCs.

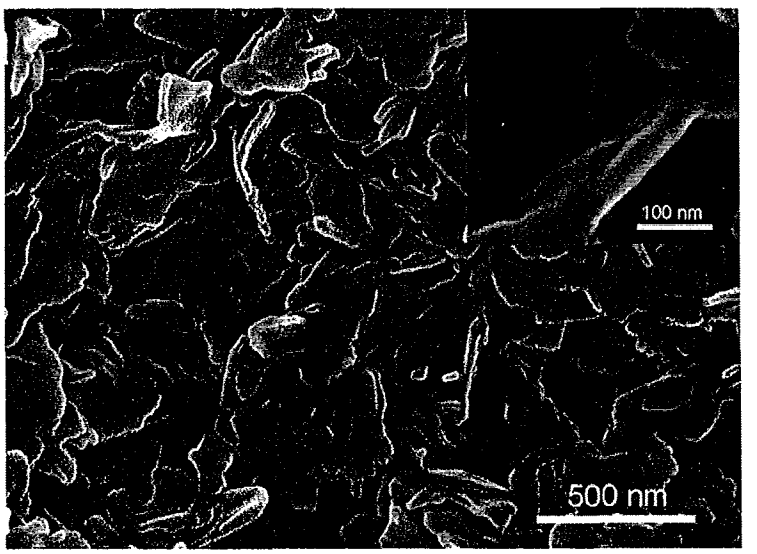

Figure 2-9 PPy/intercalated layered MnO_2 nanocomposite [79]

2.5 Electrolytes

Electrolyte plays an important role in the performance of ES. ES cell voltage is limited by the electrolyte decomposition at high potentials. The resistance or conductivity

of an electrolyte can limit power density, while ion concentration and operating voltage can limit the energy density of ES. Three different types of electrolytes have been currently studied: aqueous, organic and ionic. Properties of various electrolytes are described in Table 2-3 [32].

Table 2-3 Properties of various electrolytes [32]

Electrolyte	Density(g cm^{-3})	Resistivity(Ω-cm)	Cell Voltage (V)
KOH	1.29	1.9	1.0
Sulfuric acid	1.2	1.35	1.0
Propylene carbonate	1.2	52	2.5-3.0
Acetonitrile(AN)	0.78	18	2.5-3.0
Ionic liquids(ILs)	1.3-1.5	125(25°C) /28(100°C)	4.0/3.25

2.5.1 Aqueous Electrolytes

The choice of the aqueous electrolyte for ES cell is obvious. The very low ESR or high electrical conductivity (i.e. 0.8 $S.cm^{-1}$ for H_2SO_4), the low cost and environmental friendliness of aqueous electrolyte and high solubility of the salts are the main reasons for the application of aqueous electrolyte system. In addition, purification and drying processes during production are less stringent compared to organic electrolyte. It is noteworthy that the inner pore size of porous structure and the properties of ions of the respective electrolyte affected the ESR of the cell. For example, Nyquist plots showed a decrease of ESR in the order of Li_2SO_4>Na_2SO_4>K_2SO_4 , mainly because the migration

speeds of the hydrated ions in the bulk electrolyte and within the inner pores of AC electrode increase in the order of $Li^+<Na^+<K^+$ [80]. Further, because depletion of electrolyte occurs during charging of the ES, the high electrolyte concentration is required. Finally, the main drawback of aqueous electrolyte is the unit cell voltage (limited to typically 1 V), thus reducing the available energy significantly compared to organic electrolytes.

2.5.2 Organic Electrolytes

Usually, organic electrolytes such as acetonitrile or propylene carbonate are most commonly used in ES cells, due to their higher dissociation voltage. The latter is preferred because of its low flash point and lower toxicity. Using an organic electrolyte one can usually achieve voltages in the range of 2 – 2.5 V, hence the energy density is improved because the energy density is proportional to the voltage squared. However, the resistivity of organic electrolytes is relatively high (20-60 Ω), compared to a concentrated aqueous electrolyte. The resistance of organic electrolytes is higher than that of aqueous electrolytes by a factor of at least 20. Moreover, the pore size requirements for organic electrolyte are also greater (15-20 Å) due to the large size of organic molecules [17]. The higher electrolyte resistance also affects the equivalent distributed resistance of the porous layer and consequently reduces the maximum power, although part of the reduction in power is compensated by the higher cell voltage achievable with an organic electrolyte [10].

2.5.3 Ionic liquids

Ionic liquids (ILs) are room-temperature liquid solvent-free electrolytes (molten salt); they are entirely composed of cations and anions, their voltage window stability is thus determined by the electrochemical stability of the ions. The ionic conductivity of these liquids at room temperature is low (a few milliSiemens per centimeter), so they are mainly used at higher temperatures. In fact, ILs typically exhibit high thermal stability, high cell voltage window, and good conductivity at temperatures (≥60°C) [5]. A. Balducci et al. [81] reported that activated carbon exhibited high cycling stability (40,000 cycles) as well as a high stable specific capacitance in a voltage window of 3.5 V at 60° C using trifluoromethanesulfonyl imide ($PYR_{14}TFSI$) ionic liquid electrolyte.

2.6 Fabrication of Conducting Polymers Electrodes

The initial discovery of metal like doped polyacetylene by Shirakawa et al. [82] in 1977 led to a group of promising organic polymers-intrinsically conducting polymers. Since then, CPs such as Polyaniline (Pan), PPy, Polythiophene (PTh) and their derivatives have been extensively studied in a wide variety of areas [83-90]. Of particular interest, the low ESR, the high specific energy and power, the ease of processability and the low cost suggest that CPs are promising materials for developing ES electrodes.

2.6.1 Properties of Conducting Polymers

CPs have different forms with respect to the chemical structure, which are aromatic, heterocyclic, benzenoid, or nonbenzenoid. Some common CPs with chemical structure are presented in Figure 2-10 [91].

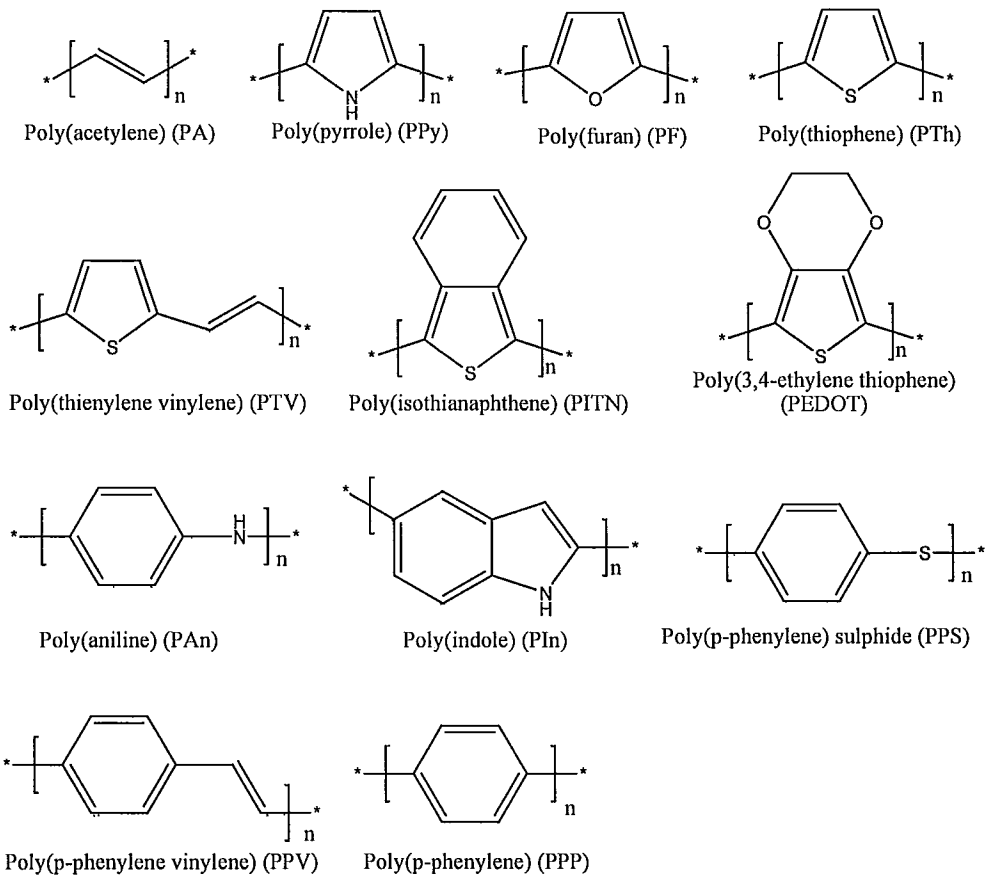

Figure 2-10 Chemical structure of common conducting polymers [91]

The oxidation (or reduction in few case) of these molecules leads to the formation of an electrically conducting organic polymer film at the electrode surface. At present, three groups of polymers have been studied. Polyacetylene (PA) is recognized as linear type polymer with simple structure. PPy and PTh are examples of the polyheterocyclic

polymers. Poly(p-phenylene) (PPP) and Poly (p-phenylene vinylene) (PPV) represent polyaromatic CPs.

Electrical conductivity is the primary property of CPs. CPs are electrically conductive due to their extensively π-conjugated backbone. Table 2-4 [92] gives maximum conductivity and type of doping (n or p) for some common CPs. The degree of conductivity depends on the density and mobility of electrons and/or the nature of charge carriers (solitons, polarons and bipolarons) as well as the conjugation length [93]. Although solitons, polarons and bipolarons are thought to be the main source of the charge carriers in conjugated polymers, mechanisms of electronic conduction as well as the generation of such charge carriers are not fully understood yet.

Table 2-4 Conductivity and doping type of some conducting polymers [92]

Conducting polymer	Conductivity (S cm^{-2})	Doping type
PA	200-1000	n, p
PPy	40-200	p
PT	10-100	p
PITN	1-50	p
PANI	5	n, p
PPP	500	n, p
PPV	1-1000	p
PPS	3-300	p

However, various theoretical models have been proposed based on quantum chemical theory and polymer science [91,94-96]. The main mechanism is the movement of charge carriers between localized sites or between solitons, polaron or bipolaron states. Conductivity is not only the result of charge transfer along the chain or between the different conjugated segments (domains) in the same chain but also the electron hopping between deferent chains. It was stated that the degeneracy (only in PA) or non-degeneracy (i.e. PPy and other CPs) of the ground state produces structural defects in the polymer backbone, causing alternating change in single and double bonds. The possible structure of PPy in non-degenerate configuration ((a) aromatic and (b) quinoid) and charge carrier defects ((c) polaron and (d) bipolaron), as shown in Figure 2-11 [96].

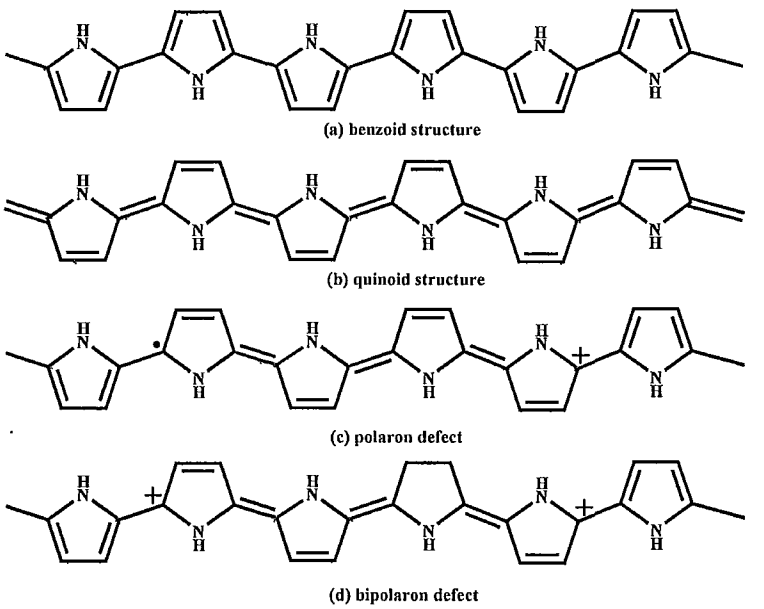

Figure 2-11 Non-degenerate ground state configurations and charge carrier defects of PPy [96]

The conjugated polymers in their undoped, pristine state are semiconductors or insulators. Undoped conjugated polymers, such as, polyacetylenes have a low electrical conductivity of around 10^{-10} - 10^{-8} S cm^{-1} whilst heavily iodine-doped polyacetylene exhibit a conductivity value around 10000 S cm^{-1} [97]. Additionally, the conductivity of doped polymer is dependent of the nature of dopants or oxidants as well the doping temperature and the doping procedure [82,97-99].

The stabilities of CPs vary. Generally, there are two distinct types of stability of CPs: extrinsic stability and intrinsic stability [100]. Extrinsic stability is related to vulnerability to external environmental agents such as oxygen, water which can attack the charged sites of polymers by the nature of nucleophilicity and electrophilicity. In ambient atmosphere, for example, polyheterocyclic polymers, such as PPy and PTh exhibit much higher stability than does PA when exposed to the oxygen whilst PTh is more sensitive to water than is PPy [101]. Intrinsic stability of CPs is thermodynamic in origin. The degradation of CPs is likely due to the irreversible chemical reaction with main chain dopants or counter ions, leading to a break of conjugation and the loss of conductivity. The nature of dopants or counter-ions with respect to different polymers is the key factor affecting the conduction stability [102], under systematically controlled environmental and thermal conditions. The conduction stability of PPy was found to be significantly better than that of the poly(3-alkylthiophenes). PPy doped with arylsulfonates were found to exhibit excellent stability in inert atmospheres but were slightly less stable in the presence of dry or humid air. PPy samples doped with the tosylate anion were found to be

the most stable, while PPy doped with longer side chain substituted benzenesulfonates exhibited poorer stability.

The electrical conductivity of polymers comes from the conjugated polymer backbone in the doped form. As a result, CPs are insoluble, infusible and intractable, and their processing presents difficulties. To overcome the processing problems, the structure of the polymer can be modified by attaching long flexible side groups to some separated monomers along the conjugated back bone. An example is co-polymer poly(3-octythiophene-co-3-methylthephene) (POTMT) [103]. Another way is to deposit the polymer in desired shape and form. For example, PAn/poly (sulfonated styrene) (PSS) nanofiber composites were prepared by the interfacial method [104]. PANI nanofibers in the presence of sulfonated polystyrene allows for the growth of PANI 2-D nanostructures embedded in the polymerized sulfonated host. The mechanism for this growth is believed to involve some alignment of the aniline monomer onto the anionic dopant.

The electroactive behavior of CP films is unique due to its reversible redox reaction switching between an insulating state and conductive state. The process involves electron transitions and mass (ions and solvents) transport which is not involved in other redox systems [105,106]. For example, the oxidation of pyrrole yields a charged polymer film with incorporated anions; the pyrrole units are positively charged and compensated by incorporated anions. When negative potential is applied, the anions are expelled and the film obtains electrons to reduce to its neutral state. Conversely, when positive potential is applied, the anions are inserted into the film and the pyrrole units lose

electrons and transform to an oxidized state. The oxidized state and neutral state of PPy film are shown in the SEM image (Figure 2-12 [105]).

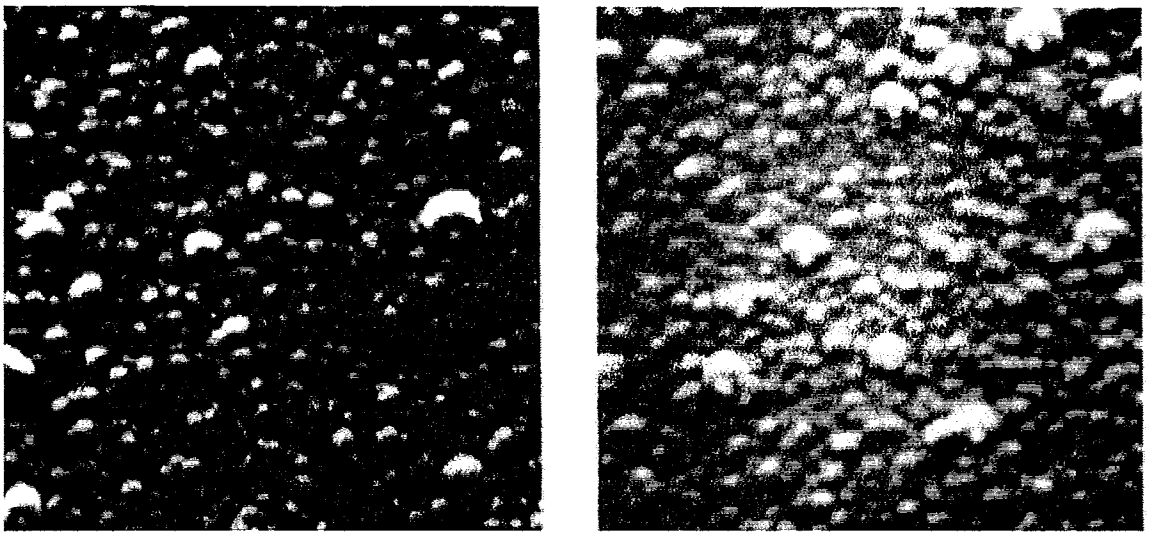

(a) Oxidized state (b) Reduced state

Figure 2-12 SEM of PPy film surface at (a) oxidized and (b) reduced state [105]

It is also noteworthy that the dopant anion (small size) can be exchanged with electrolyte anions during potential sweeping. Further, the immobilized polymeric dopants or large surfactant anions are not released during the reduction of the polymer, and hence, to maintain the charge balance in the film, the electrolyte cations are incprporated into the PPy matrix. Therefore, the electrochemistry of PPy/polyanions film involves cation transport [106,107].

2.6.2 Fabrication methods

Generally, CPs are categorized as the cationic and anionic salts of highly conjugated polymers depending on the n-type and p-type doping process. Most CPs are

cationic polymers, which can be prepared by oxidation and simultaneous polymerization from corresponding monomers.

Various synthetic methods for the fabrication of conducting polymers have been investigated. Among these methods, chemical polymerization [108] and electrochemical polymerization [109] are commonly used. Besides, emulsion polymerization [110], layer-by-layer assembly [111] are employed as well. Particularly, the template and template–free methods for the fabrication of CPs nanomaterials were summarized[90], where anodic aluminum oxide (AAO) membrane [112] and zeolite [113] can be used in the hard template method whilst cyclodextrin [114] and liquid crystal [115] can be used in the soft template method. Template-free methods provide a facile and practical route to produce pure, uniform, and high quality nanofibers. Electrochemical and chemical, template-free synthesis methods include aqueous/organic interfacial polymerization [116], radiolysis synthesis [117], and dispersion polymerization [118].

2.6.3 Synthesis of PPy and PPy Based Composites

In general, films of CPs such as PAn, PPy, and PTh and their derivatives or composites can be synthesized on electrode surfaces by the oxidation of heterocycles like pyrrole (Py), thiophene (TH), aniline (ANI). They can be co-deposited with other active materials (metal oxides and/or carbons) on substrates mostly through chemical or electrochemical routes [113]. The comparison of chemical and electrochemical polymerization is summarized in Table 2-5 [119]. Among these heterocycles prepared to date, PPy was first electrochemically synthesized by Diaz et al. [120]. PPy has attracted

significant attention mainly because its monomer (pyrrole) is easily oxidized, water soluble, and commercially available. Furthermore, PPy presents many advantages including good electrochemical properties (electrical conductivity and electroactivity), high chemical and thermal stability as well as easy processability.

Table 2-5 Comparison of chemical and electrochemical polymerization [119].

Polymerization approach	Advantages	Disadvantages
Chemical polymerization	• Large-sale production possible. • Post-covalent modification of bulk CP possible. • More options to modify CP backbone covalently.	• Synthesis more complicated. • Can not make thin films.
Electrochemical polymerizaation	• Thin film synthesis possible. • Ease and better control of synthesis. • Entrapment of molecules in CP. • Simutaneous polymerization and film formation.	• Hard to separate film from the substrate. • Post-covalent modification of bulk of CP is difficult.

2.6.3.1 Chemical Method

Chemical synthesis is a simple and fast process, by which powdery bulk materials can be obtained. Therefore, this method is suitable for mass production of CPs. In oxidative chemical polymerization, the conductivity, morphologies and other properties

of final product depend on the reaction conditions. The properties are influenced by the nature of oxidants used, concentration of solution components, and the concentration ratio of oxidant to monomer, reaction temperature and the nature of substrate and solution. In the chemical process, oxidants are used for the synthesis of PPy. Many oxidants like ammonium peroxydisulfate (APS), ferric ions, and permanganate anions have been employed to polymerize the pyrrole. Iron(III) chloride is a common reagent used to produce PPy in its oxidized (doped) forms [121]. Thin PPy films are obtained on a non-conducting substrate by dipping the substrate in a pyrrole solution and subsequently in an oxidising solution containing $Fe(ClO4)_3$ and $HClO_4$ [122]. Cerium(IV) sulphate has been used as an oxidant to produce PPy and Pan [123]. The reaction of pyrrole and copper(II) perchlorate in acetonitrile yielded highly conducting PPy which exhibited a conductivity of 60 S cm^{-1} [124]. Montmorillonite/PPy (MMT/PPy) nanocomposites were prepared by the in situ polymerization of pyrrole in the presence of oxidant $K_2S_2O_8$ [125]. These oxidants are able to oxidize the pyrrole in appropriate solutions, i.e., water, acetonitrile, yielding highly active cationic radicals, followed by further reactions between cationic radicals and monomers, forming dimmers, oligomers and the final product PPy polymer.

In addition, the process of polymerization is usually accompanied by visible changes in color. The color change of the film can be observed from initially colorless to blue or dark blue and finally black. However, with chemical polymerizations, control over polymer morphology is extremely limited, purification can be problematic and processing is virtually impossible. In addition, to keep the global environment clean and safe, it is necessary to restrict by-products during the chemical reaction process.

The possible mechanism of oxidative polymerization of pyrrole is shown in Figure 2-13 [113].

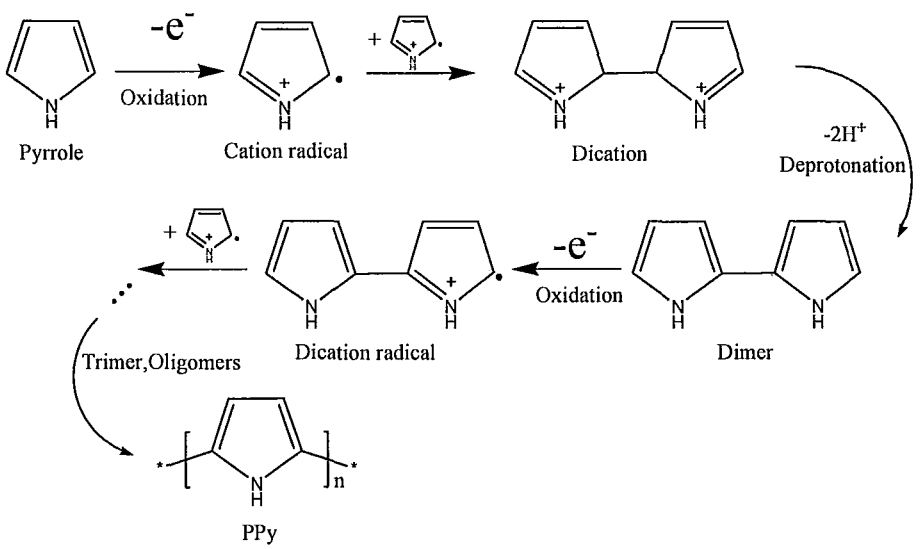

Figure 2-13 Mechanism of chemical oxidative polymerization of pyrrole [113].

2.6.3.2 Electrochemical Method

Electrochemical synthesis of CPs provides many advantages over chemical synthesis, including the in-situ deposition of the polymer at the electrode surface. The process is a facile way by which the film properties, thickness, morphology can be controlled by simply varying the polymerization parameters such as solvent, potential or current density, supporting electrolyte, concentration of monomer and the nature of the substrate, etc. PPy and composites can be prepared by the electrochemical method. The overall polymerization reaction can be simply represented as in Figure 2-14 [126].

In Figure 2-14, A^- is the counter ion (anion) incorporated during the polymerization to maintain the charge balance in the polymer backbone in an oxidized

state. The formation of the PPy film requires anion as well as electrons to transport through the film. The value n was determined to be 2.2-2.4, depending on the type and the charge of the dopant ion. The doping level is usually between 0.2-0.3 for PPy, corresponding to one charge compensated by 3-4 pyrrole units to achieve electro neutrality [127]. The electrochemical polymerization mechanism is similar to that of chemical synthesis which was previously discussed. The difference between them is that there are no chemical oxidants needed in the electrochemical process.

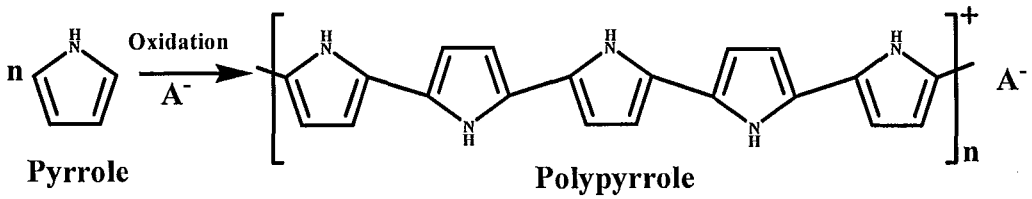

Figure 2-14 Overall electro-polymerization reaction of PPy [126].

The choice of solvent is of particular importance since the solvents have influences on the morphology and conductivity of the film. Solvents should be chemically stable to monomers and electrodes. Aprotic solvents with poor nucleophilic character such as acetonitrile are preferred. The nucleophilic solvents such as dimethyl sulfoxide have to be avoided since they prevent polymer formation. The strong dependence of the conductivity on the nucleophilic properties of the solvent, represented by donor number (DN), has been studied by Quyang et al. [128]. It was found that the conductivity of PPy films increased with the decrease of the DN value of the solvents. PPy can be prepared from organic and aqueous solutions and/or mixed solutions. The conductivity of PPy

films prepared in aqueous solutions were observed larger than in acetonitrile solutions [129]. The conductivity and mechanical properties of PPy films prepared from mixed solutions varied. For example, PPy doped with toluene sufonate (TsO^-) prepared in 99% acetonitrile and 1% water solution showed high conductivity of 100 $Scm^{-1}$and tensile strength of 60 MPa while the PPy film obtained from 75% acetonitrile and 25% water solution showed low conductivity of 0.5 $Scm^{-1}$and tensile strength of 8 MPa[130]. In fact, PPy is one of the few heterocycles that can be prepared in aqueous solutions. Aqueous processing is not possible for PTh. PTh must be prepared from organic solvents whilst PAn is obtained from acidic aqueous solution. Compared to other heterocyclic monomers, the oxidation of pyrrole can be achieved at relatively low potential (0.8V vs. SCE), which is also lower than the decomposition potential of water.

The effect of the counter ions or anion(s) on PPy synthesis has been widely discussed [75,90,106,131]. Some examples of the anions and their electrolyte sources are listed in Table 2-6 [92]. The inorganic and organic anions incorporated into the polymer have a remarkable influence on the redox behavior and morphology as well as electric conductivity of the PPy film during synthesis. A comparative study of the behaviors of anions (Cl^-, Br^-, NO_3^-, ClO_4^-) by Johanson et al. [75] indicated that the redox activity of PPy film is determined by the size and mobility of the anion used Whilst the effect of dopants on the kinetic formation and the electrochemical behavior of PPy film have been studied, the results showed that the dopants had a strong influence on the electropolymerization process(induction time, nucleation and growing) of polymer films, and hence the electrochemical response was remarkably different [131].

Table 2-6 List of dopant anions and their electrolyte sources [92].

Dopant anions	Source(supporting electrolyte)	Note
PF_6^-	R_4NPF_6,MPF_6	R=Alkyl M=Metal(Li^+, Na^+, K^+)
ClO_4-	R_4NClO_4,$MClO_4HCl$,MCl	
Cl^-	R_4NCl, HCl, MCl	
AsF_6^-	$MAsF_6$	
I^-	R_4NI,MI	
HSO_4^-	$MHSO_4$,R_4NHSO_4	
$CF_3SO_3^-$	M CF_3SO_3,R_4N CF_3SO_3	
$CH_3C_6H_4SO_3^-$	M $CH_3C_6H_4SO_3$	
SO_4^-	Na_2SO_4,H_2SO_4	

pH has influence on reactivity, stability, conductivity and electrochemical activity of PPy. A low pH generally favors electropolymerization but the films produced showed low conductivity [132]. A uniform surface morphology of PPy/p-toluenesulfonic acid (p-TSA) with fewer and smaller surface defects was observed when pH value in aqueous solution for the *p*-toluene sulfonate (pTS) dopant anion is approximately [133]. The adhesion strength of PPy deposited on steel substrate was affected by pH of the solution, the film exhibited high adhesion when the pH of the solutions was below 4.1 [134].

Processing temperature plays a role in the quality and morphology as well as conductivity and redox activity of PPy films. The effect of temperature on electropolymerization of pyrrole in oxalic acid solution on a mild steel substrate has been studied [135]. In acidic medium, lower temperatures favored the overall process. At higher temperature and lower current densities, oscillations in electrode potential were observed due to the competition of iron dissolution and pyrrole oxidation reactions. In alkaline medium, higher temperatures favored the process and better quality films were obtained.

PPy can be synthesized by cyclic voltammetry (CV), potentiostatic (constant voltage) and galvanostatic (constant current) deposition methods. In the study of Li [136], PPy thin films have been prepared on glass by these methods. In a cyclic Voltammogram (CV), the higher the redox peaks, the greater the electrochemical reaction activity. The results showed that galvanostatic deposition of PPy film could produce highest electrochemical reactivity in comparison to cyclic voltammetry and potentiostatic deposition methods, as shown in Figure 2-15 [136]. Therefore, the constant current method is preferred to be adopted in the preparation of PPy. However, the electrochemical polymerization process for the preparation of PPy film is very complicated due to the fact that the optimization of various parameters is not easy. Some works have been done to find out the optimized process parameters. For example, Gade et al. [137] reported that the uniform, porous, and micro-globular surface morphology with enhanced electrical conductivity of PPy film can be obtained with optimized process

parameters (0.1:0.1 concentration ratio of pyrrole/sodium nitrate, pH 3.0, current density 1 mA cm^{-2}).

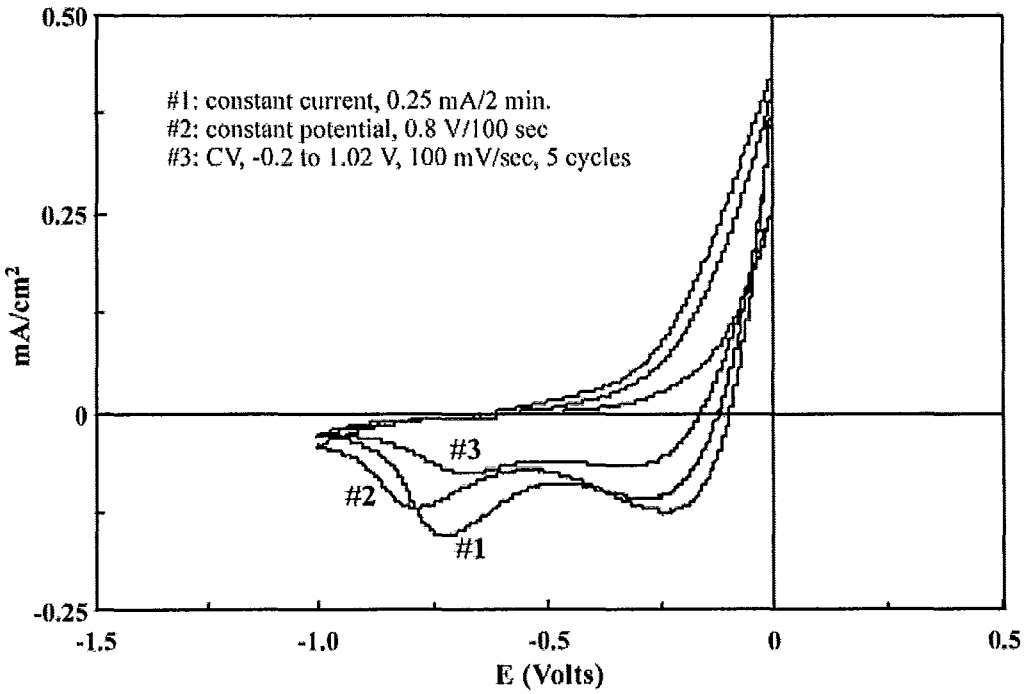

Figure 2-15 CV of PPy films deposited with different methods in 0.1 M phosphate buffered saline (PBS) solution, E vs. Ag/AgCl [136]

3 Objective

The objective of this research is to develop advanced electrodes for electrochemical supercapacitors via following considerations:

- Electrodes: Development of novel electrode materials for ES, including nano-structured conducting polymer PPy and MWCNTs.
- Fabrication techniques: The development of in situ anodic electropolymerization process for fabricating conducting polymer PPy on active stainless steel substrate with novel additives and co-electrodeposition method for the fabrication of advanced PPy/MWCNT composite electrodes on stainless steel substrates.
- Parameters and optimization: capacitance, impedance, microstructure, cycle life, stability, current and voltage, corrosion protection, as well as power density and energy density.
- Design factors: development of electrodes via low cost novel active materials, facile electrochemical deposition procedure, novel additives, and current collectors.

4 Approach and methodology

4.1 Approach

PPy films were deposited by anodic electropolymerization on stainless steel substrate from aqueous solutions containing pyrrole monomers and additives (tiron and sodium salicylate). The deposition yield was studied at galvanostatic conditions.

PPy with MWCNTs composite were deposited by anodic co-electrodeposition on stainless steel from aqueous solutions containing pyrrole monomers, MWCNTs suspension and tiron additives. The composite yield was studied at galvanostatic conditions.

4.2 Methodology

4.2.1 Dissolution and Passivation

The electropolymerization of PPy on oxidizable metals such as stainless steel is challenging, since the active metal as an anode tends to dissolve before the electropolymerization potential of the pyrrole monomer is reached. The oxidation potential of metal is much more negative than that of pyrrole. Therefore, the dissolution of metal in the electrodeposition prevents the oxidation of pyrrole and impedes the formation of PPy. Thus, to achieve the deposition of PPy on stainless steel, it requires a partial passivation of the metal and reduces the dissolution rate without preventing the formation of PPy. On the other hand, the passivation layer formed during the

electrodeposition may impede the electron transfer and result in over-oxidation of PPy initiated by the anodic potential shift.

4.2.2 Novel Additives

In order to overcome problems discussed above, the electron transfer mediation may be useful in reducing the over potential required for electropolymerization and help to form a passivation layer which can stabilize the interface between the substrate and PPy as well as promote electron transfer without hindering the formation of PPy film on the passivation layer.

The passivation layer formed between a stainless steel substrate and PPy film is attributed to the complexation of metal ions by chelating ligands. Chelating properties can be found in tiron and sodium salicylate additives. The chemical structure of tiron and sodium salicylate is presented in Figure 4-1.

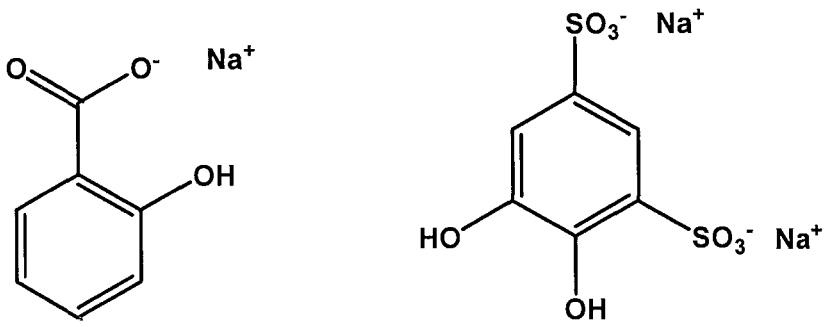

Figure 4-1 Chemical structure of (a) sodium salicylate and (b) tiron

The chelating ability of tiron and sodium salicylate to complex metal ions is attributed to their function groups, such as the catechol group in tiron or hydroxylic and

carboxylic groups in sodium salicylate, as shown in the chemical structure. Figure 4-2 (a) shows how the ferrous ion coordinates with the deprotonated oxygen of the carboxylate and the phenolic donor groups of the sodium salicylate molecule. Similarly, Figure 4-2 (b) shows how ferrous ion coordinates with the catechol group of the tiron molecule. In both cases, the chelate complexes form five-membered or six-membered rings, which are thought to be the most stable for chelates containing one or more double bonds [138, 139].

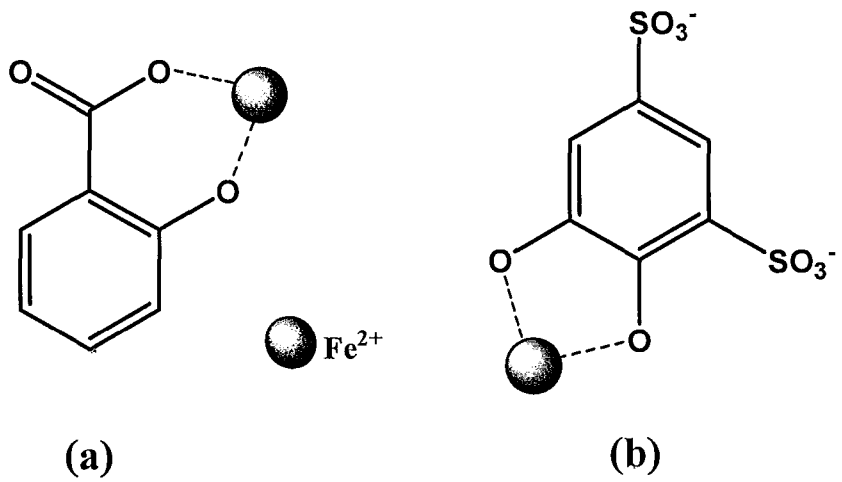

Figure 4-2 Chelate complexes formed with Fe^{2+} by (a) sodium salicylate and (b) tiron

Tiron and sodium salicylate are also found to be the effective electron transfer mediators. Adhesive uniform PPy films were successfully deposited on aluminum alloy using tiron [140] and adherent homogenous PPy films were obtained on zinc or zinc-electroplated steel using sodium salicylate [141, 142]. The passivation layer formed in the presence of tiron and sodium salicylate is non-blocking and stable. The electron transfer or improved conductivity of the layer promoted was possible due to the surface complexation of the metal ions at the metal surface.

Obviously, tiron and sodium salicylate are anionic dopants which are required for the PPy polymerization. They are both soluble in aqueous solution. In particular, tiron can be used as a surfactant in the preparation of PPy/MWCNT composite. Tiron can stabilize the solution containing a MWCNT suspension and pyrrole due to its two sulfonate groups [143].

5 Experimental Procedures

5.1 Materials Preparation

Sodium salicylate and tiron were purchased from Aldrich. Pyrrole (98^{+}%) and commercial purity multiwall carbon nanotubes were purchased from Arkema. 302/304 annealed stainless steel foil (50 x 30 x 0.05 mm) and Nickel wafer (ϕ1.2 cm^{-2}) were purchased from McMaster Carr.

5.2 Equipment Set-up

The electrodeposition was performed in the electrochemical cell, which included an anodic stainless steel substrate and a platinum counter-electrode. The distance between the anode and cathode was set 20 mm. The cell (beaker) volume was 200 mL. Power supply (EPS 2A200, Amersham Biosciences) provided constant voltage or constant current for electrodeposition. Potentiostat (PARSTAT 2273. Princeton Applied Research) provided cyclic voltammetry and galvanic static and potential static techniques for electrodeposition and testing.

5.3 Electropolymerization of PPy Film

Pyrrole (0.05 M-0.5 M) was dissolved in deionized water. Electropolymerization was performed from solutions containing tiron (0.003 M-0.01 M) or sodium salicylate (0.1 M-1 M) and appropriate concentration of pyrrole. The aqueous solutions were stirred 15 minutes before deposition. Anodic deposits were obtained on stainless steel foils (2.5

cm x 4 cm), stainless steel wires (ϕ 0.01 mm) and silicon wafers. The electrodeposition was carried out either potentiostatically (constant voltage 1-5 V) or galvanostatically (constant current 0.5-2 mA cm^{-2}). The deposition time was varied in the range of 1 to 20 minutes. The pH value was adjusted by adding hydrochloric acid in the range of 2-7. The PPy films were dried at room temperature at least 2 hours. The salient feature of PPy electrodeposition is that polymerization, doping and film processing take place simultaneously. The electropolymerization procedure is shown in Figure 5-1.

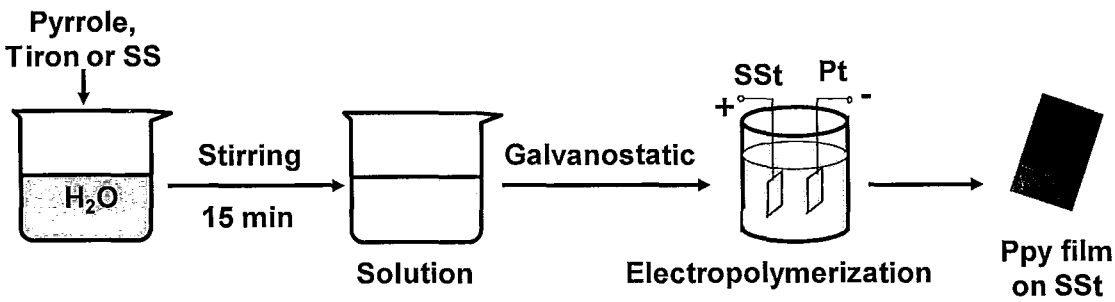

Figure 5-1 Scheme of PPy film preparation on SSt

5.4 Co-Deposition of PPy/MWCNT Composite

Co-electrodeposition of PPy/MWCNT composites was performed from aqueous suspensions containing 0.2 - 1 g L^{-1} MWCNTs, 0.05 M pyrrole and 0.005 M tiron. The MWCNTs was pretreated by strong acid (mixture of sulfuric acid and nitric acid, in a ratio of 3:1). The MWCNTs suspension first was sonicated for 30 minutes in the presence of tiron in water bath, then pyrrole was added into the solution. The mixed solution was stirred 15 minutes before electrodeposition. Composites were obtained on stainless steel

at a constant current (1 mA cm^{-2}) condition. The deposition time was varied in the range of 1-24 minutes. No acid was added, the pH value was kept at 7. The procedure was also presented in Figure 5-2.

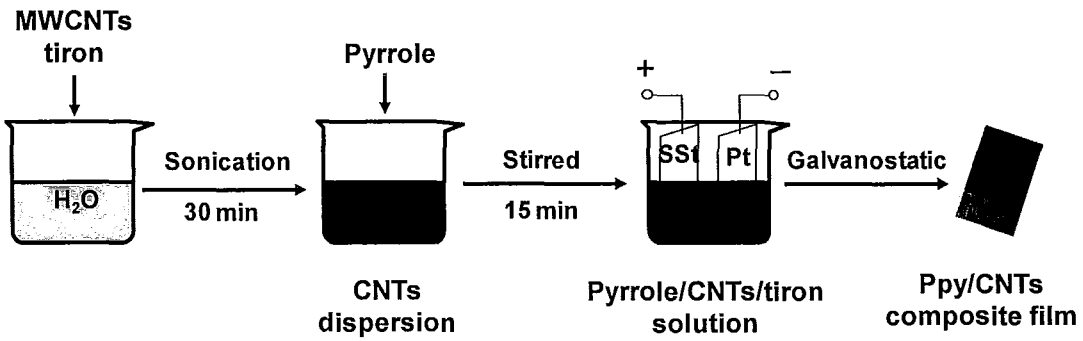

Figure 5-2 Scheme of PPy/MWCNT composite fabrication process

5.5 Characterization

5.5.1 Morphology Characterization

The microstructure and morphology of electrodeposited films were studied using a JEOL JSM-700F Scanning Electron Microscope (SEM). Surface and cross-section images were observed at high magnification (up to 50000X). Deposits were platinum-sputtered or non-sputtered depending on the nature of films before observation.

5.5.2 Electrochemical Characterization

The deposited films were studied using Potentiostat (PARSTAT 2273, Princeton Applied Research) controlled by computer program by a PowerSuite electrochemical software. The films were tested using a standard three electrode electrochemical cell.

0.5M Na_2SO_4 aqueous solution was used as a test electrolyte. The electrolyte solution was deaerated by purging purified nitrogen gas before electrochemical measurements. The working electrode area was 1 cm^2. The counter electrode was platinum gauze and the reference electrode was a standard calomel reference electrode (SCE in saturated KCl solution). Cyclic Voltammetry (CV) studies were performed within a voltage range of -0.5-0.4 V versus SCE at scan rates of 2-500 mV s^{-1}.

The specific capacitance (SC) was calculated by integrating half the area of the CV curve to obtain the charge (Q), and subsequently dividing the charge by the mass (m) of the electrode and the potential window ΔV:

$$C = \frac{Q}{m\Delta V} \qquad (5\text{-}1)$$

In CV, a time –and potential- dependent current I can be described as:

$$\mathrm{I} = \mathrm{C}\frac{dV}{dt} \qquad (5\text{-}2)$$

The specific power density (S_P) and the specific energy density (S_E) were calculated from the chronopotentiograms using following equations.

$$S_P = \frac{\mathrm{I}\Delta E}{2m} \qquad (5\text{-}3)$$

$$S_E = \frac{\mathrm{I}\Delta E\Delta t}{2m} \qquad (5\text{-}4)$$

where, ΔE is voltage windows in the galvanostatic discharge. I is the current.

Electrochemical impedance spectroscopy (EIS) was applied to measure the a.c. Impedance of the films in the frequency range of 0.05 Hz to 100 kHz at an applied a.c.

signal of 5 mV r.m.s. A 1 cm^2 stainless steel foil with deposits was used as the working electrode, while platinum gauze was used as a counter electrode. A saturated calomel electrode was used as a reference electrode. The solution consisted of sodium sulfate at a concentration of 0.5 M that served as electrolyte, dissolved in water. A Randle equivalent circuit shown in Figure 5-3, was used for the a.c. impedance analysis of PPy-electrolyte system.

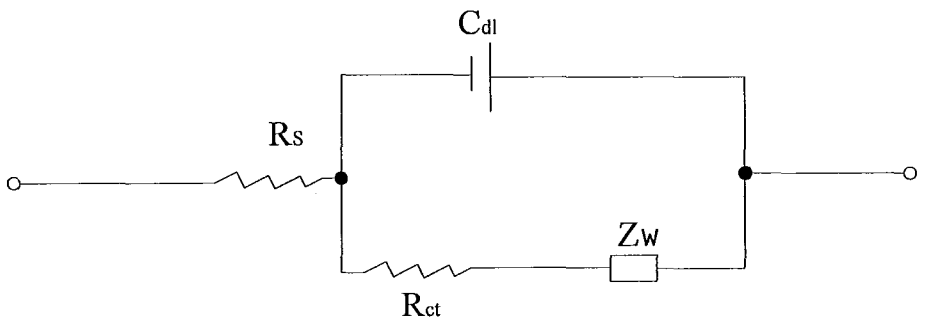

Figure 5-3 Equivalent circuit of the PPy-electrolyte system [144]

R_s is the uncompensated ohmic resistance of the electrode and electrolyte, C_{dl} is the double-layer capacitance of the electrode/electrolyte interface, R_{ct} is the charge transfer resistance. Z_w is Warburg impedance arising from the diffusion of anions in PPy corresponding to the pseudocapacitance [144].

The total a.c. impedance Z_t of a circuit is a function of frequency, which is expressed as:

$$Z_t = Z_{re} + Z_{im} \qquad (5\text{-}5)$$

and the imaginary part Z_{im} is:

$$Z_{im} = -\frac{j}{2\pi fC} \qquad (5\text{-}6)$$

where, $j=\sqrt{-1}$, Z_{re} is the real part and Z_{im} is the imaginary part of Z_t. f is the frequency, C is the capacitance.

6 Results and Discussion

6.1 Electropolymerization of PPy from Aqueous Salicylate Solutions

6.1.1 Electrochemical Behavior of Stainless Steel in Aqueous Salicylate Medium

In order to understand the different processes occurring at the electrode surface, the 304 stainless steel was polarized in 0.15 M sodium salicylate and 0.15 M sodium nitrate solution by cycling continuously the electrode potential between -1.0 and 1.2 V at a potential scan rate of 20 mV s^{-1}. The electrochemical testing experiments were performed in oxygen-free electrolytes.

Stainless steel was first polarized in the solution containing 0.15 M sodium salicylate without pyrrole as shown in

Figure 6-1. The scans was characterized by an anodic peak A at ~0.9 V, which decreased with increasing scan number. The decreases of the electrode potential revealed the reduction peaks $C_1$and C_2 at ~0.27 V and ~-0.26 V, respectively. It is suggested that the small peak A may result from the salicylate species oxidation. The onset of the anodic current increase was at ~0.43 V, the sharp increase in the range of ~-0.5 V – 1 V suggests the dissolution of substrate. The decrease in anodic peak A can be attributed to the passivation of substrate. Considering the published studies [141,145] on the chelate complexes formed by the salicylate ion and metal ion, a decrease of current for peak A with increasing sweeps can be attributed to the passivation effect related to the complexation of salicylate ion with Fe^{2+} or Fe^{3+}. The formed passive layer may contain the iron oxide since the current wave was observed during the negative potential scans.

The cathodic peak C_1 and C_2 represent the reduction of salicylate ions and reduction of ions, respectively. Therefore, the complexation behavior of salicylate and metal ions play a significant role since it provides a non–block barrier that partially inhibited the metal dissolution process.

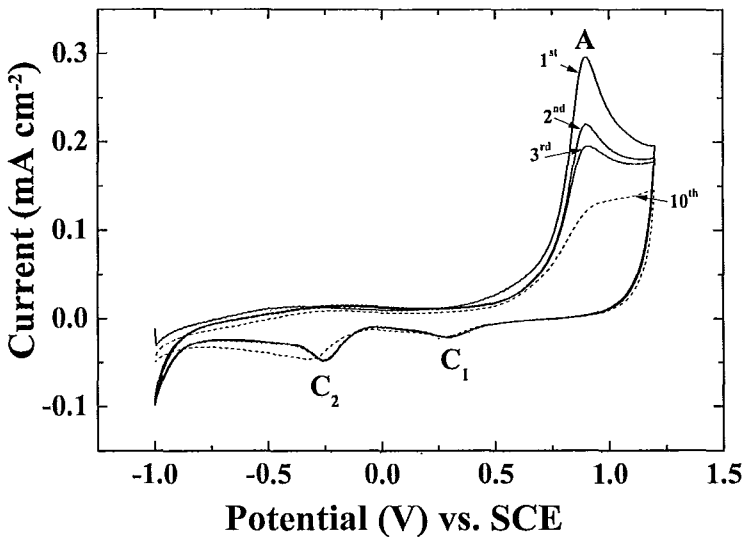

Figure 6-1 Cyclic voltammogram of the stainless steel recorded in 0.15 M sodium salicylate aqueous neutral solution at a scan rate of 20 mV s^{-1}

For the purpose of comparison, sodium nitrate was also polarized in the same potential range and scan rate. The CV was presented in Figure 6-2. The CV depicted in Figure 6-2 had a different shape in contrast to the behavior shown in

Figure 6-1. The CV was characterized by (a) A broad anodic shoulder A which centered at ~0.21 V and (b) a broad cathodic wave C was at ~-0.43 V. The shoulder A observed in the first cycle may be attributed to formation of non-compact thin passive

layer of Fe_2O_3 and/or Cr_2O_3 The subsequent increase of current at ~0.65 V represented the oxidation of Cr^{3+} oxide to soluble Cr^{6+} [146]. It is suggested that the strong metal dissolution occurring on the anode surface may prevent the formation and precipitation of PPy in the presence of sodium nitrate.

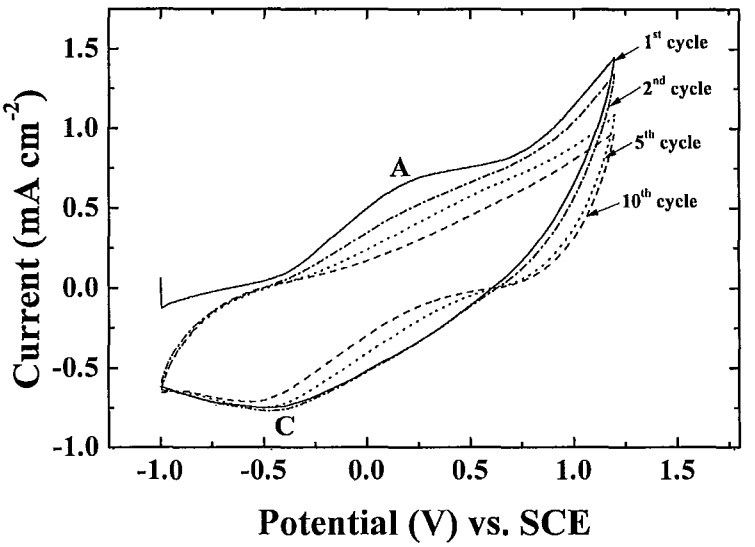

Figure 6-2 Cyclic voltammogram of the stainless steel surface recorded in 0.15 M sodium nitrate aqueous neutral solution at a scan rate of 20 mV s^{-1}

6.1.2 Electropolymerization of PPy from Aqueous Salicylate Solutions

6.1.2.1 Cyclic Voltammogram Electropolymerization of PPy

The cyclic voltammogram of the sweeps recorded during the electrodeposition of PPy film on the stainless steel electrode from aqueous solution containing 0.15 M sodium salicylate and 0.2 M pyrrole is shown in Figure 6-3.

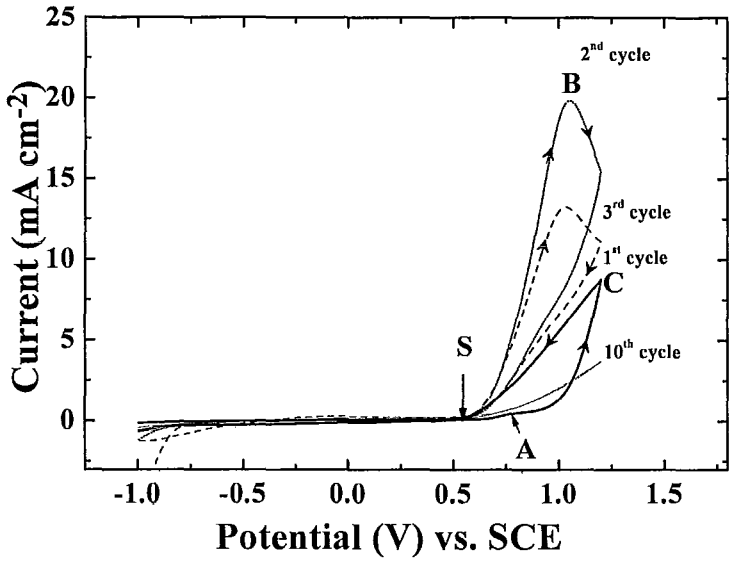

Figure 6-3 Cyclic voltammogram of 1st, 2nd, 3rd and 10th scans during the electropolymerization on stainless steel from solution containing 0.2 M pyrrole and 0.15 M sodium salicylate. Scan rate: 20 mV s^{-1}.

The first positive cycle was characterized by an oxidation wave A at ~0.78 V following by a sharp increase in the anodic current at ~0.85 V. A rapid decrease of current was shown in the negative sweep beyond peak C at 1.2 V, and a small current was observed above ~0.53 V (S). The oxidation peak A was attributed to the passivation layer formation due to the complexation of salicylate and iron ions, and subsequently pyrrole oxidation corresponding to conversion of pyrrole monomers into cation radicals. The sharp increase of current after peak A to C indicated that the PPy generated on the substrate since a black uniform film was observed on the electrode surface. The deposit was formed as a result to the chain reaction of pyrrole units with cation radicals, and the polymerization on the metal surface. During the next scan, peak A disappeared and a high

current peak B was observed which indicated that no chelating reaction occurred since the metal surface was covered by the PPy film formed in the first scan. It was noted that the electrode potential corresponding to the initial oxidation of pyrrole in the second and following scans was ~0.2 V lower than that of in the first cycle. The PPy film grew continuously on the repetitive sweep, the third scan was similar to that of second scan. However, the current corresponding to the anodic peaks B decreased gradually with the number of scans. In the 10^{th} scan, the CV did not show well–defined redox peaks.

6.1.2.2 Galvanostatic Electropolymerization of PPy

The PPy films were obtained on the anode at a constant current of 1 mA cm^{-2} from solutions containing 0.15 M sodium salicylate and 0.15M sodium nitrate. The galvanostatic behavior is shown in Figure 6-4. The potential–time curve is characterized by a induction peak curve followed by a plateau wave which represents the electropolymerization potential of PPy. Within the same deposition time of 600 s, the black shiny and strong adherent deposit is achieved in the presence of sodium salicylate whilst the patchy deposit with numerous exposed bare substrate spots were observed in the presence of sodium nitrate. Additional observations are noteworthy (Figure 6-4), which indicated that sodium salicylate substantially reduces the oxidation potential by nearly 400 mV from ca. 1.05 V at induction peak to ca. 0.65 V in the plateau region (electropolymerization) whilst in curve b (dashed line), the oxidation potential increases from ca. 0.84 V to ca. 1.13 V in the plateau region. The polymerization potential in the

presence of sodium salicylate is ca. 480 mV lower than that in the presence of sodium nitrate.

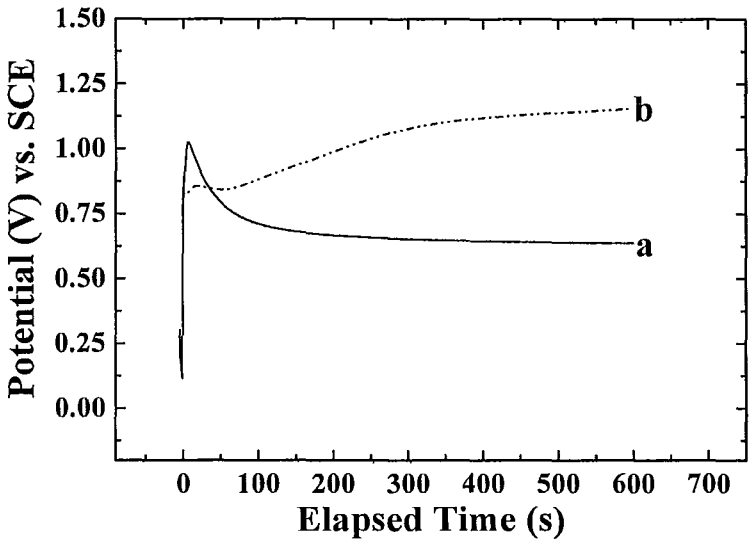

Figure 6-4 Galvanostatic behavior for deposition of 0.1 M pyrrole on stainless steel at a current density of 1 mA cm^{-2} in the presence of 0.15 M (a) sodium salicylate and (b) sodium nitrate.

Since the less positive polymerization potential was beneficial to the formation of PPy, it was clear that sodium salicylate can be used to deposit PPy by minimizing the substrate corrosion and polymer overoxidation without preventing the formation of PPy due to the non-blocking passive layer formed from complexation with metal on the substrate surface. On the other hand, due to the strong dissolution of metal, it was difficult to obtain PPy film using sodium nitrate as supporting electrolyte. These results are in a good agreement with the electrochemical behavior of stainless steel in the presence of the same electrolytes discussed previously.

6.1.3 Characterization of PPy Film Deposited Using Sodium Salicylate

6.1.3.1 Deposit Mass and Morphology Characterization

Anodic polymerization from aqueous 0.1 M pyrrole solutions containing 0.15 M sodium salicylate resulted in the formation of strongly adherent films on the stainless steel substrate. Sodium salicylate (the chemical structure shown in Figure 4-1a) was negatively charged in the aqueous solutions due to the dissociation of –COONa groups which were served as anionic dopants. The anions were incorporated into the PPy matrix to ensure the electrical neutrality of the growing film during the anodic polymerization.

The film mass increased with increasing deposition time at a constant current of 1 mA cm^{-2} condition (Figure 6-5), indicating the formation of films of different thickness.

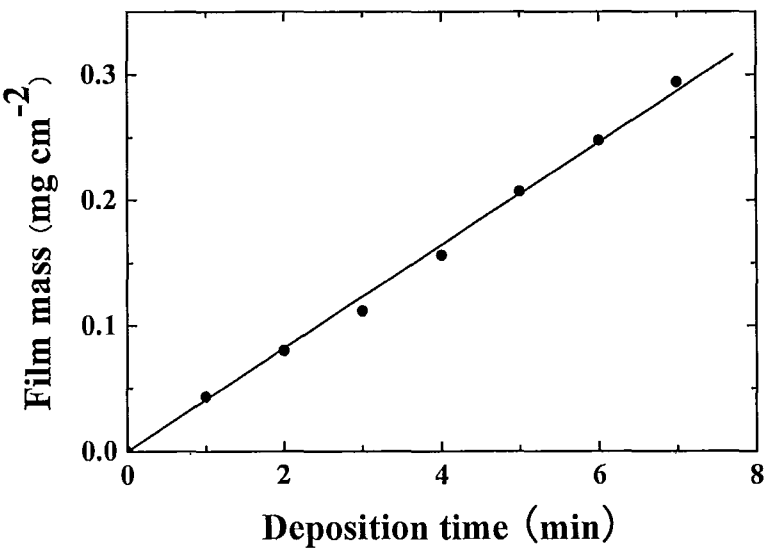

Figure 6-5 PPy/sodium salicylate film mass versus deposition time at 1 mA cm^{-2}

Nearly linear dependences was observed. Therefore, the amount of deposited material can be controlled by the variation of deposition time at a constant current density. This approach can be used for film formation on other conductive substrates, such as nickel and platinized silicon wafers. SEM (Figure 6-6) investigations of the cross section of the PPy/sodium salicylate films on silicon wafers shows that the films exhibite surface roughness due to the formation of PPy particles.

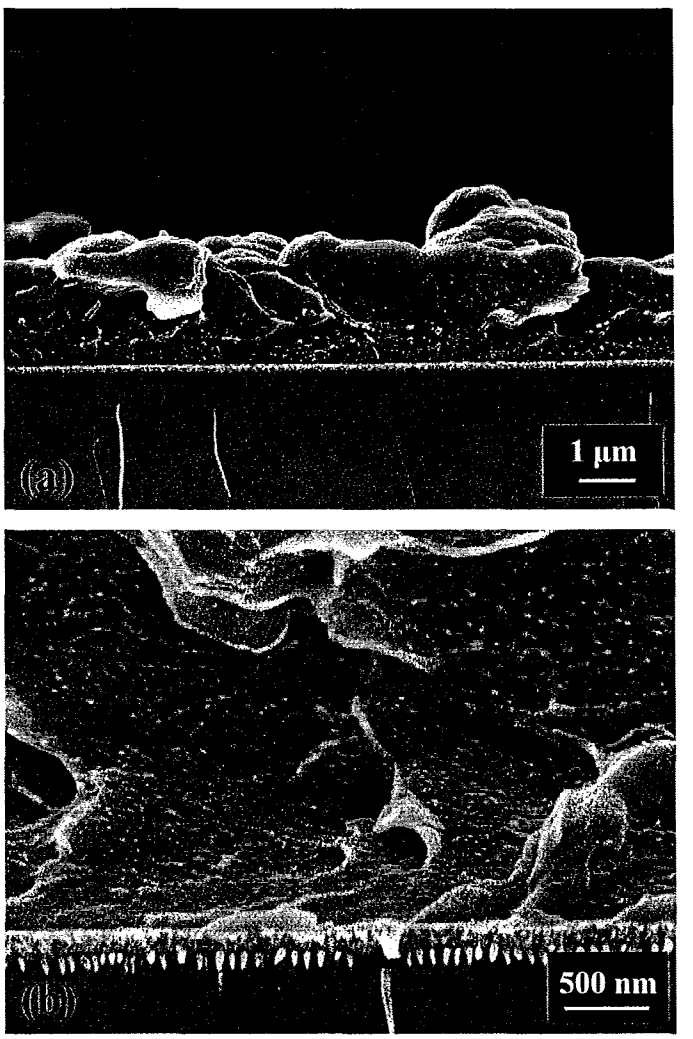

Figure 6-6 SEM images of cross section for the PPy/sodium salicylate film shown at (a) low magnification and (b) high magnification.

The thickness of films was varied in the range of 0-5 μm depending on the deposition time and current density. Microporous structure was clearly observed, the films showed the porosity which is beneficial for application in ES, as it improves the electrolyte access to the electrochemically active electrode material. Figure 6-7 shows surface of the PPy/sodium salicylate film deposited on a stainless steel foil.

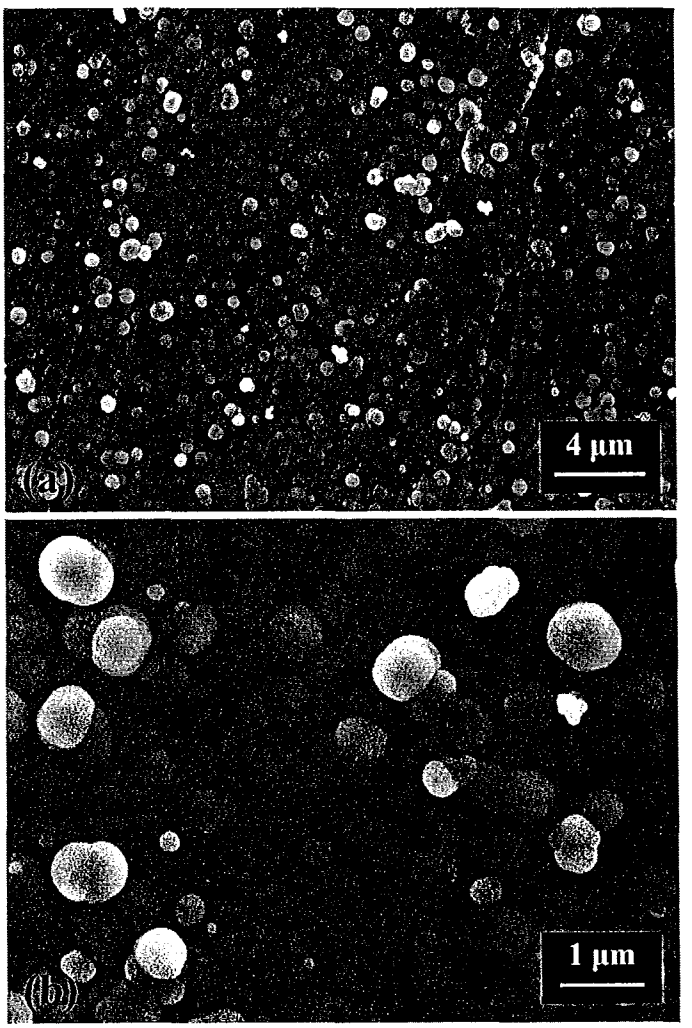

Figure 6-7 SEM image of surface for PPy/sodium salicylate on stainless steel shown at a (a) low magnification and (b) high magnification.

In Figure 6-7 (a) at low–magnification showed that the films were crack free. Figure 6-7 (b) at high magnification showed the film morphology is cauliflower like. The PPy particles sizes are in the range of 0.1 - 0.5 μm.

Anodic electropolymerization has been utilized for the film formation on substrate of complex shapes. As an example, Figure 6-8 shows PPy film coated stainless steel wire (ϕ 0.1 mm).

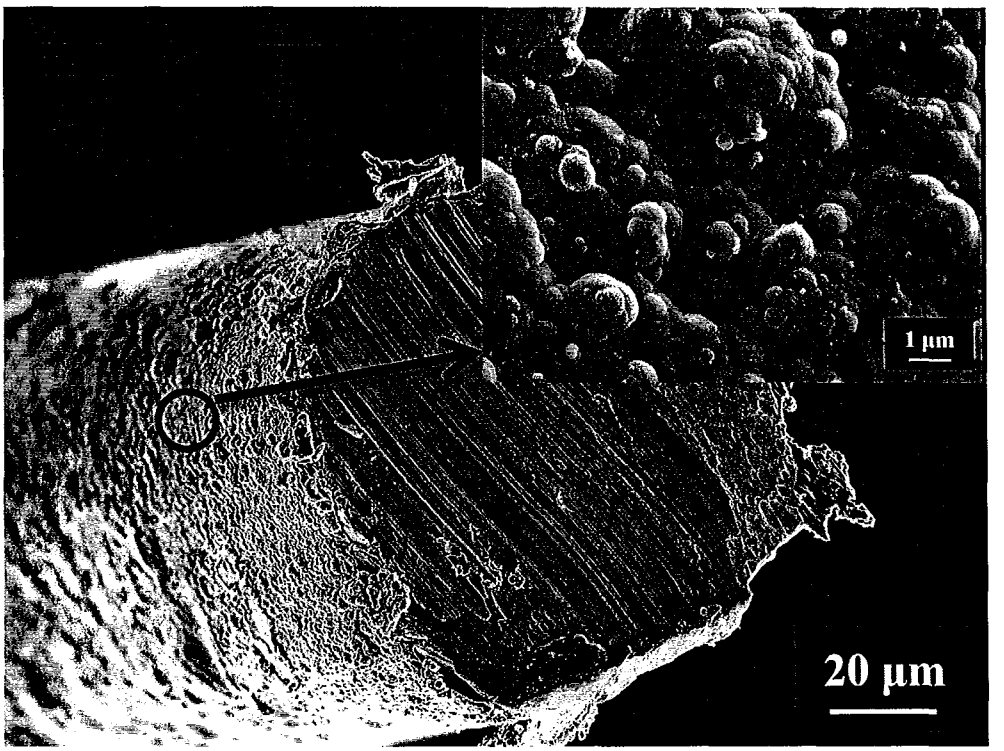

Figure 6-8 SEM images for the PPy/sodium salicylate film on a stainless steel wire. Inset is the surface image in the circle area at high magnification.

The SEM image of the cross-section indicated a significant surface roughness. The high magnification image (inset) of the wire surface shows that the PPy film consisted of relatively large particles with a particle size of about 1 μm in diameter. Therefore, the

surface roughness of the film can be attributed to the relatively large particle size, which is comparable to the film thickness.

6.1.3.2 Redox Reaction Properties

The electrochemical properties of the films were studied in a 0.5 M Na_2SO_4 solution using cyclic voltammograms (CV) as shown in Figure 6-9.

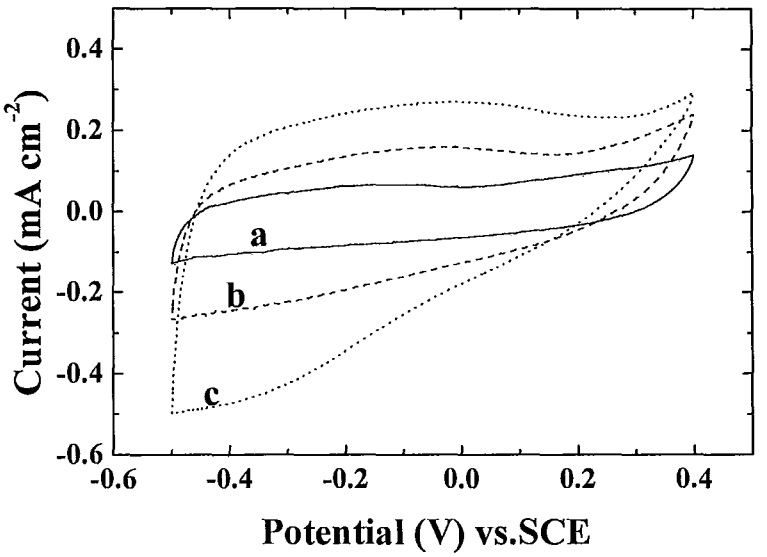

Figure 6-9 CV for the film deposited from the 0.1 M pyrrole solution containing 0.15 M sodium salicylate on a stainless steel foil at scan rate of (a) 2, (b) 5 and (c) 10 mV s^{-1}. Film Mass: 207 μg cm^{-2}

The films shows capacitive behavior in the voltage window of 0.9 V. The area of CV increases with increasing scan rate. The CVs show that PPy film exhibits better capacitive behavior in the range of negative potentials, as indicated by the larger area of the CVs. The sodium salicylate ions participated in the electroactive behavior by

insertion and de-insertion from the matrix during the oxidation and reduction process The redox reactions of polymer can be expressed as follows:

$$PPy^{+}(A^{-}) + e^{-} \underset{\text{oxidation}}{\overset{\text{reduction}}{\rightleftharpoons}} PPy^{0} + A^{-} \qquad (6\text{-}1)$$

where A^- is the counter anion.

6.1.3.3 Capacitance of PPy Doped with Sodium Salicylate

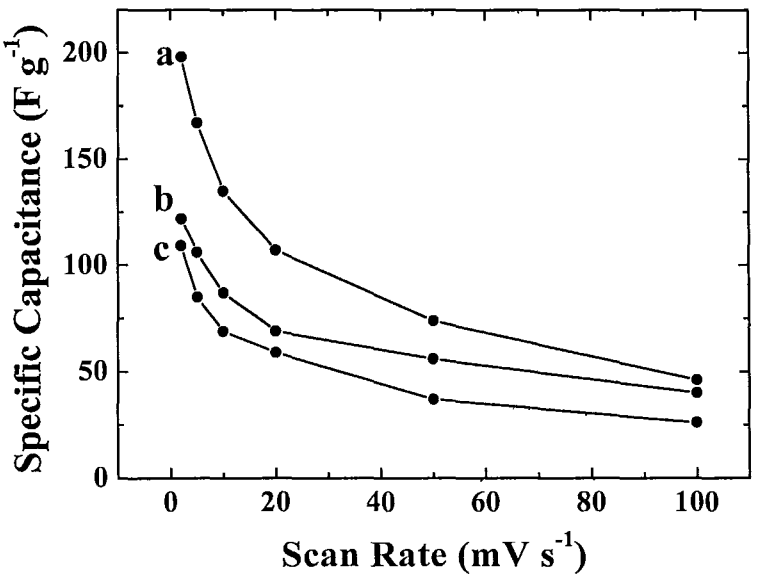

Figure 6-10 SC versus scan rates for the films deposited from the solution containing sodium salicylate on a stainless steel foil with a film mass of (a) 165, (b) 373, (c) 658 μg cm^{-2}

Figure 6-10 shows specific capacitance (SC) versus scan rate for the films of different thickness prepared from the pyrrole solutions containing sodium salicylate. The films show SC in the range of 100 - 200 F g^{-1} at a scan rate of 2 mV s^{-1}. The SC decrease

with increasing film thickness and increasing scan rate in the range of 2 - 100 mV s^{-1}. Such decrease is attributed to the penetration of electrolyte in to the pores of PPy matrix and ions mobility within the pores.

6.1.4 Corrosion Performance of PPy Coated Stainless Steel

6.1.4.1 Open Circuit Potential Measurement

The OCP of PPy coated stainless steel substrate and bare stainless steel immersed in aqueous 0.5 M NaCl was measured separately as a function of time and the corresponding plot is presented in Figure 6-11.

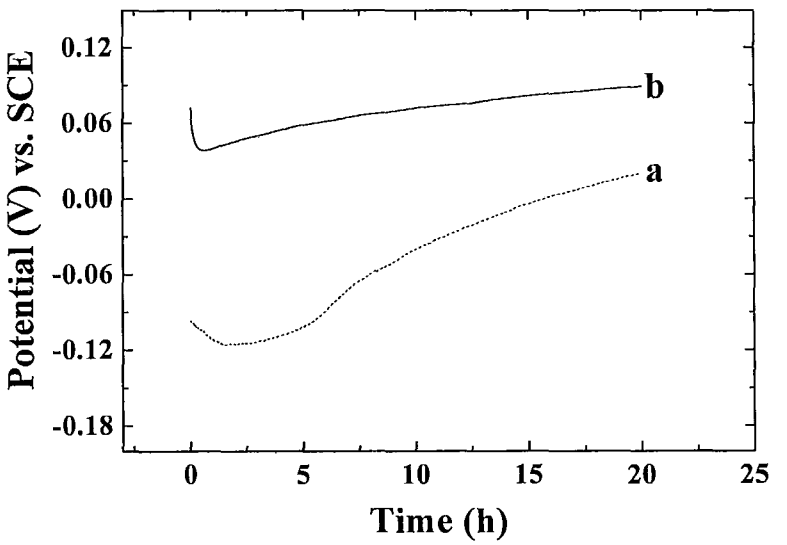

Figure 6-11 Open circuit potential–time curve recorded for (a) bare stainless steel and (b) PPy coated stainless steel in aqueous 0.5 M NaCl solution.

In this figure, curve a (dashed line) represents the OCP of bare stainless steel while curve b (solid line) represents the OCP of PPy coated stainless steel. The initial values of

the OCP of PPy coated stainless steel and bare stainless steel in 0.5 M NaCl were 0.08 V and -0.09 V, respectively. Initial E_{ocp} value of PPy coated stainless steel was more positive in contrast to the bare stainless steel, indicating the positive potential shift from PPy film. In the early stages, the OCP of both lines decreased, it may be the initiation of the water uptake process in the film for curve b whilst the dissolution of metal for curve a. An increase of open circuit potential for both curves was observed. This is attributed to the formation of oxide at the substrate surface, which behaved like a barrier against the aggressive medium attack.

6.1.4.2 Potentiodynamic Polarization

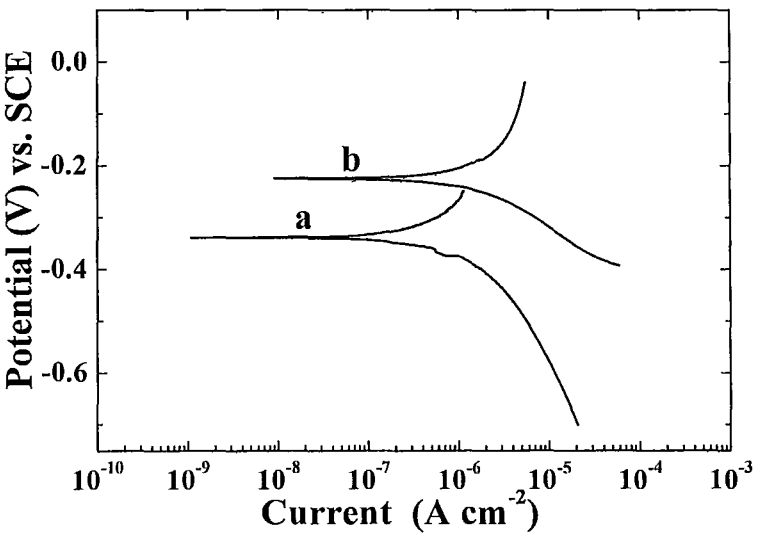

Figure 6-12 Potentiodynamic polarization curves for (a) bare stainless steel and (b) PPy coated stainless steel recorded in a 0.5 M Na_2SO_4 solution

The potentiodynamic polarization curves for bare stainless steel and PPy doped with sodium salicylate coated on stainless steel were carried out in a 0.5 M Na_2SO_4 solution as shown in Figure 6-12.

The Tafel extrapolations shows that the PPy caused a remarkable potential shift of ~ 0.167 V in the corrosion potential (E_{corr}), relative to the value of the uncoated stainless steel (~-0.353 V). The positive shift in E_{corr} confirmed the PPy barrier effect for corrosion protection of steel, and the Tafel result was in a good agreement with OCP measurements.

6.2 Electropolymerization of PPy from Aqueous Tiron Solution

6.2.1 Electrochemical behavior of stainless steel in aqueous tiron medium

The 304 stainless steel substrate were polarized in 0.15 M tiron and 0.15 M sodium sulfate solutions, by cycling continuously the electrode potential between -1.0 and 1.2 V at a potential scan rate of 20 mV s^{-1}. The recorded CV for stainless steel in 0.05M tiron solution is shown in Figure 6-13.

In the first cycle, an anodic shoulder B was observed at ~ 0.75 V, which can be attributed to the dissolution of iron and the formation of oxide layer. The anodic peak A at ~ 0.95 V represents the oxidation of tiron and complexation of tiron with iron ions. In the following cycles (2^{nd} to 10^{th} cycle), the CV shapes were very similar to that of the first cycle except that peak A shifted to lower current values and the reduction peak C at ~ -0.01 V increased in the negative direction with increasing cycle indicating the reduction of tiron and other anodically formed species.

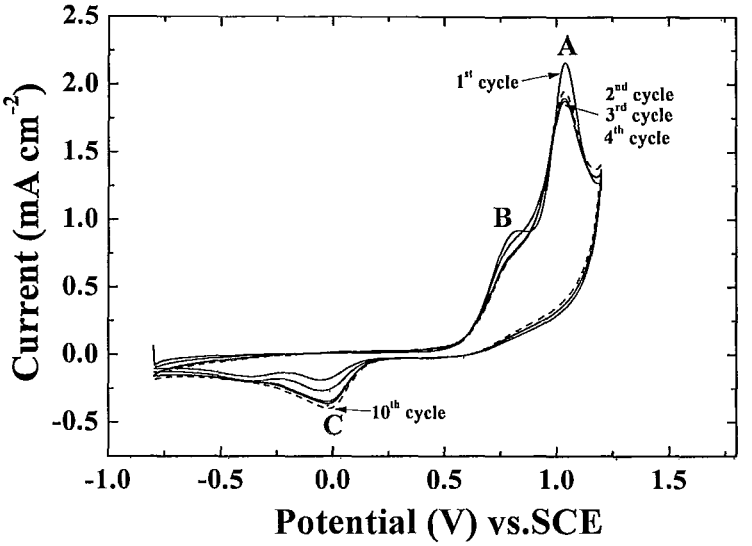

Figure 6-13 Cyclic voltammogram of the stainless steel surface recorded in 0.15 M tiron aqueous neutral solution at a scan rate of 20 mV s^{-1}

The CV of stainless steel versus concentration of tiron is shown in Figure 6-14. The increase of tiron concentration from 5 mM to 15 mM did not hinder the oxidation and complexation process but had a clear influence in the potential domain previously attributed to the formation of a passive layer. In other words, the oxidation shoulder B and the oxidation peak A decreased in the current value with decreasing concentration of tiron. The comparison of CV response recorded in a 0.005 M tiron condition but at different scan rates is shown in Figure 6-15.

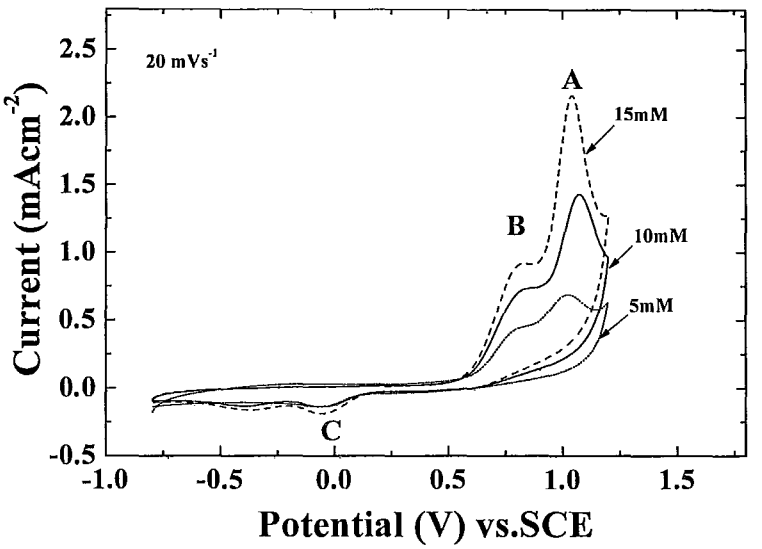

Figure 6-14 Cyclic voltammogram of the stainless steel surface recorded at a scan rate of 20 mVs^{-1}in a 0.15 M, 0.01M and 0.005M tiron aqueous neutral solution

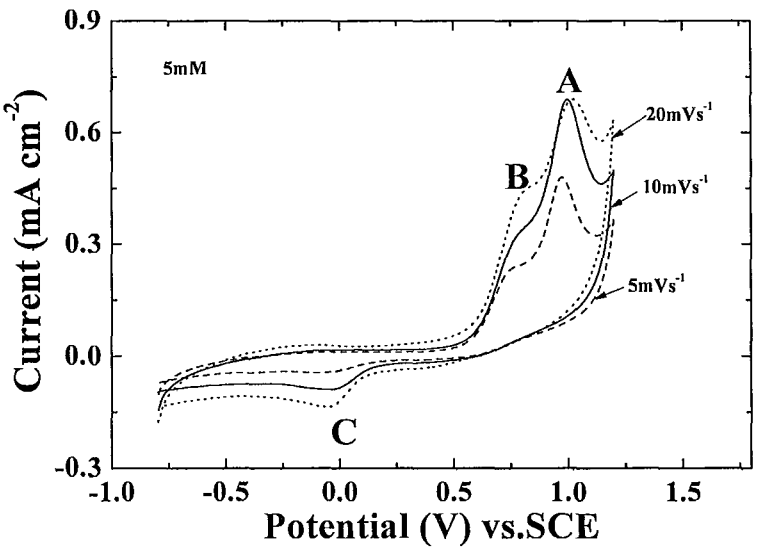

Figure 6-15 Cyclic voltammogram of the stainless steel surface recorded at a scan rate of 20 mV s^{-1},10 mV s^{-1} and 5 mV s^{-1} in a 0.005 M tiron aqueous neutral solution

The CVs recorded at different scan rates were similar. It also can be concluded that the oxidation shoulder B and the oxidation peak A decreased in the current value with decreasing scan rate without affecting the iron –tiron complexation formation.

In contrast, when the stainless steel electrode was polarized in a sodium sulfate solution, strong dissolution of metal occurred as shown in Figure 6-16.

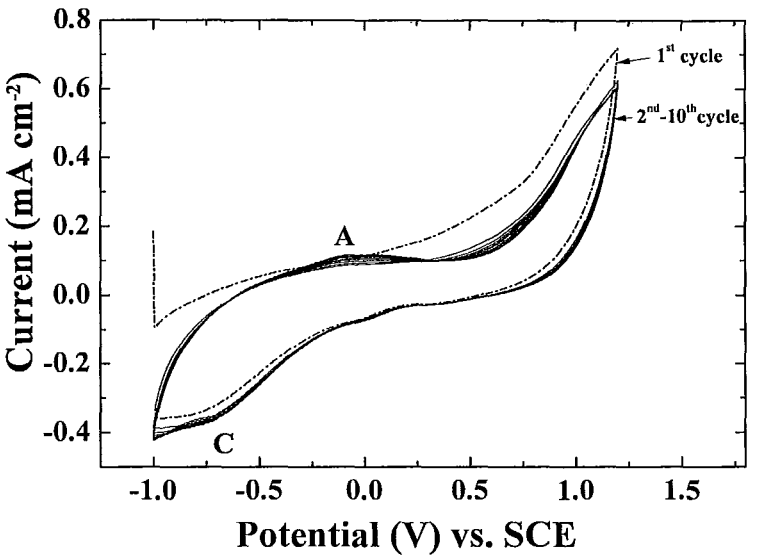

Figure 6-16 Cyclic voltammogram of the stainless steel surface recorded in a 0.15 M Na_2SO_4 aqueous neutral solution at a scan rate of 20 mV s^{-1}

The CV recorded in the first sweep (dashed line) displayed a strong metal dissolution of iron. The following 2 to 10 sweeps (solid lines) showed a broad anodic peak A at about -0.09 V followed by a sharply increasing anodic shoulder at the onset of potential around 0.3 V and a broad cathodic peak C at about -0.7V in the reverse polarization sweep. The anodic hump A was related to the formation of a thin and non-compact Fe^{2+}/Fe^{3+} layer (i.e., Fe_2O_3), and the cathodic peak C was related to the reductive

decomposition of the passive layer to Fe^{2+} species. It was also suggested that the passive layer of Fe_2O_3 was unstable[147] since the repetitive sweeps of 2 to 10 were observed indicating that the passive layer formed in the positive scans decomposed completely in the following negative scans. Therefore, the dissolution of metal cannot be prevented by a passive layer in the sodium sulfate solution.

6.2.2 Electropolymerization of PPy from aqueous tiron solution

6.2.2.1 Galvanostatic Electropolymerization of PPy

The PPy films were obtained on the steel substrate at a constant current of 1 mA cm^{-2} from 0.05 M pyrrole solutions containing 0.005 M tiron. On the other hand, for the purpose of comparison, the deposition was also performed at the same condition in the presence of 0.005 M *p*-toluene sulfonic acid sodium salt (pTS-Na) within the same deposition time of 600 s. The galvanostatic behavior is shown in Figure 6-17.

The black thicker uniform and strongly adherent deposit was achieved in the presence of tiron whilst the very thin and non-adherent film was observed in the presence of pTS-Na, indicating that tiron facilitated a two-stage nucleation and growth process during the electropolymerization of PPy as an electron transfer mediator. It was observed that in the nucleation stage, the oxidation potential value (peak 2) of curve b (in the presence of tiron) was 350 mV lower than that of peak 1 of curve a (in the presence of pTS-Na). This indicated that the oxidation of pyrrole units to radical cations is facilitated in the presence of tiron. This can be attributed to the conductive passive layer formed due to the tiron complexation with iron on the substrate surface. pTS-Na, however, cannot

complex with iron on the stainless steel surface. The comparison of the chemical structures of pTS-Na and tiron Figure 6-17 (inset) and the experimental data shown in Figure 6-17 indicated that OH groups of tiron were beneficial for the application of this material as an additive for PPy electropolymerization on stainless steel substrates. As discussed previously, tiron is a phenolic compound, belonging to the catechol family. The adsorption mechanism was attributed to the deprotonation of phenolic OH groups and surface complexation of metal ions on the material surface. The adsorption of tiron was favored by the presence of the two OH groups.

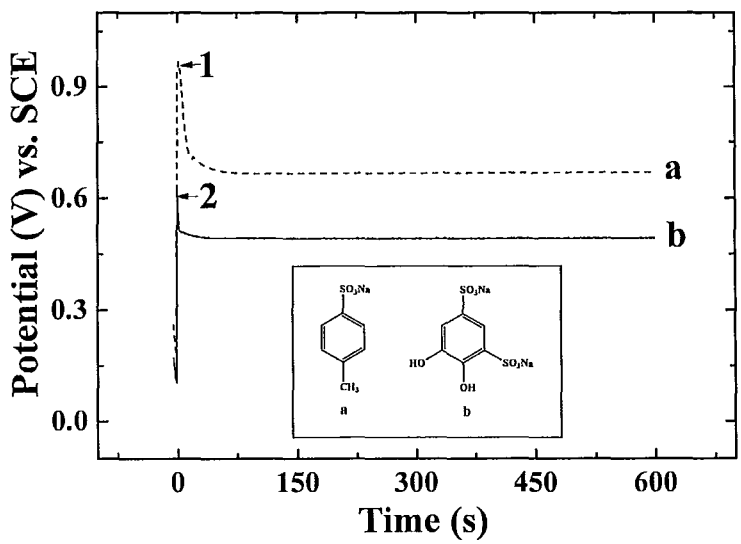

Figure 6-17 Galvanostatic behavior of PPy deposit on stainless steel from a 0.05 M pyrrole solution in the presence of 0.005 M (1) pTS-Na and (2) tiron at a current density of 1 mA cm^{-2}. Inset shows the chemical structure of (a) pTS-Na and (b) tiron.

In the electrodeposition process, namely, growth stage of PPy, the potential difference between the working and reference electrode after the peak decreased to a steady value. The deposition potential (plateau region) of curve a from the solution containing tiron was 200 mV lower than that for pTS-Na. The reduced deposition potential is beneficial for suppressing the substrate dissolution. It was suggested that the adsorbed tiron provided wiring between the substrate and the growing PPy film, promoted charge transfer during electropolymerization, and reduced the deposition potential. Moreover, the anionic tiron was incorporated into the PPy to ensure the electrical neutrality of the film.

6.2.3 Characterizations of PPy Film Prepared Using Tiron

6.2.3.1 Deposit Mass and Morphology Characterization

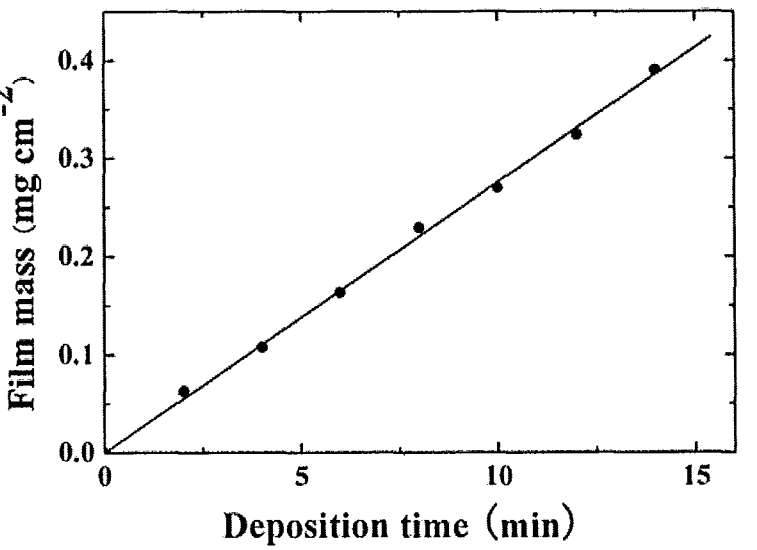

Figure 6-18 PPy/tiron film mass versus deposition time at 1 mA cm^{-2}

Strongly adherent PPy films were obtained on the stainless steel substrate by anodic polymerization from a 0.05M pyrrole aqueous solution containing 0.005 M tiron. Almost linear dependences were obtained as shown in Figure 6-18, which was similar to PPy film prepared from a pyrrole solution containing sodium salicylate

The film mass increased with increasing deposition time at a constant current density of 1 mA cm^{-2} condition. Therefore, the amount of the deposited materials can be controlled by the variation of deposition time at a constant current density. Accordingly, given an identical substrate surface area for PPy deposition, the film thickness increased with increasing deposition time as shown in Figure 6-19.

The SEM investigations of the cross-section of the PPy/tiron films on silicon wafers clearly show that PPy films prepared from tiron exhibite a greater uniformity and more porous structure compared to those prepared from sodium salicylate (see Figure 6-6). It also can be seen that when the deposition time tripled, the film thickness increased from ~ 1 μm to ~ 3 μm.

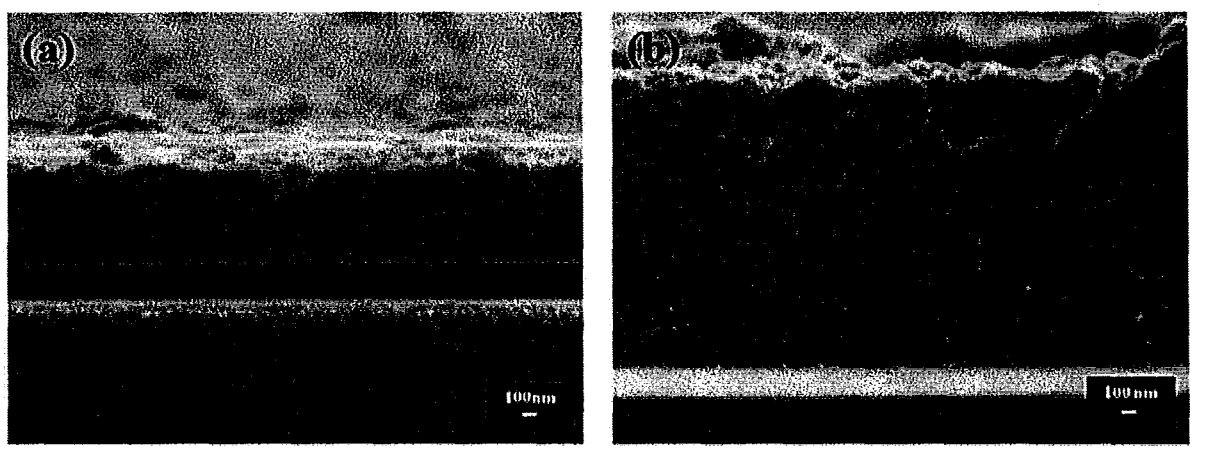

Figure 6-19 PPy/tiron film obtained at a constant current of 1 mA cm^{-2} with deposition time (a) 6 min and (b) 18 min on silicon wafer

Since tiron can promote electron transfer during the electropolymerization process, nearly 100% current efficiency can be achieved, therefore, the film thickness can be calculated by the following expression [140]:

$$\delta = \frac{jt}{F} \times EW \times \frac{1}{\rho} \qquad (6\text{-}2)$$

Where j is the current density (A cm^{-2}), t is the deposition time (s), F is the Faraday constant (C mol^{-1}), ρ is the film density (g cm^{-3}), and EW is the equivalent weight of PPy (g mol^{-1}).

Strongly adherent films were obtained from pyrrole solutions containing tiron on a stainless steel foil. The SEM surface images at low and high magnification are shown in Figure 6-20. Figure a at low–magnification shows that the film is crack free. Figure b at high magnification showes a much finer particle size compared to the PPy/sodium salicylate film (Figure 6-7).

According to the nucleation and growth (NG) theory [148], it is suggested that the lower roughness surface can be attributed to the addition of tiron which can mediate the PPy film deposition by generating additional nucleation sites (progressive nucleation) and growing new polymer particles on the existing layer, resulting in a relatively smooth uniform surface structure.

Figure 6-21 shows a PPy film coated on a stainless steel wire (ϕ 0.1mm) in the presence of tiron additive. The SEM image of the film on the wire surface indicated a better uniformity morphology with the film thickness in the avcrage range of 1.5 μm. The high magnification image (inset) of the cross-section showed that the PPy film consisted

of relatively small PPy particles in the size range of 0.1 ~ 0.3 μm in diameter. Therefore, the lower surface roughness of the film on steel wire can be attributed to the smaller PPy particle size due to the tiron mediation.

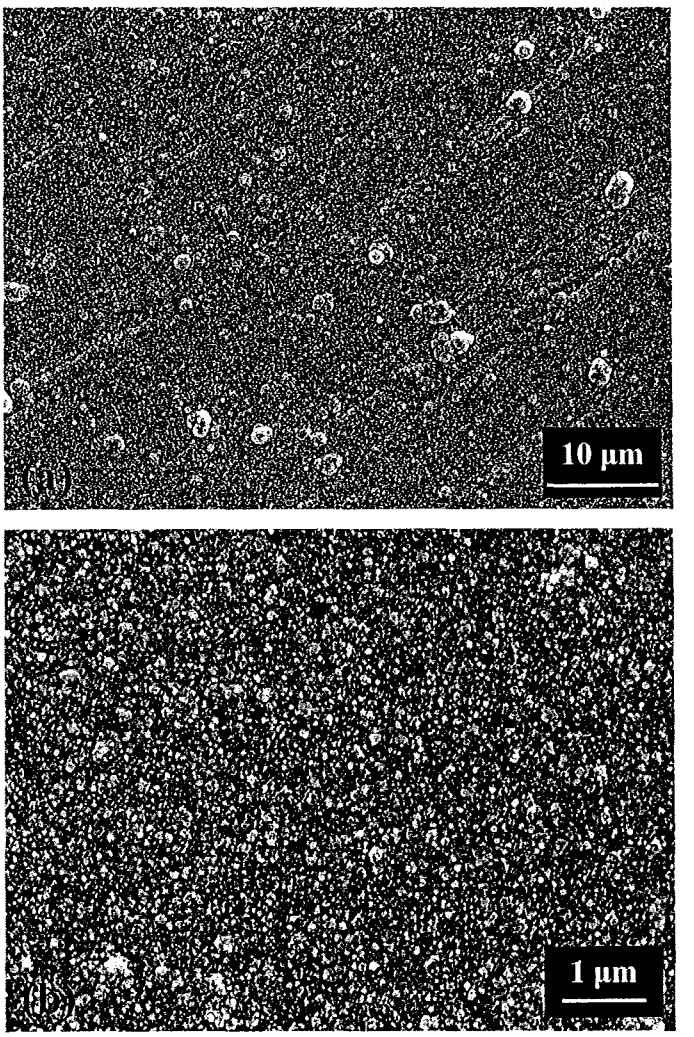

Figure 6-20 SEM image of surface of PPy/tiron on stainless steel shown at a (a) low magnification and (b) high magnification

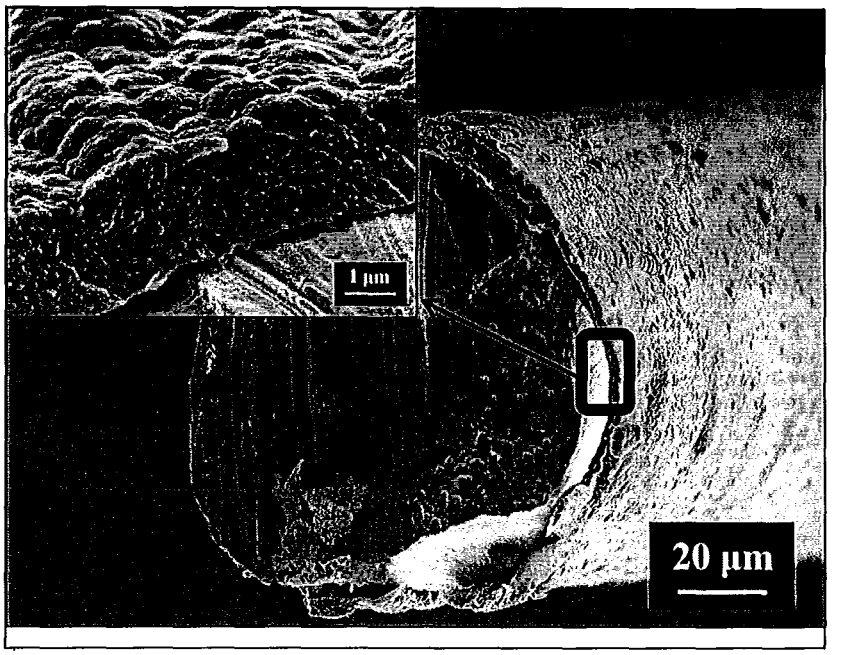

Figure 6-21 SEM images for the PPy/tiron film on a stainless steel wire. Inset is the cross-section image in a rectangle frame at a high magnification

6.2.3.2 Redox Reaction Properties

The electrochemical properties of the PPy/tiron films were studied in 0.5 M Na_2SO_4 solutions using cyclic voltammograms (CV) as shown in Figure 6-22. Compared to PPy/sodium salicylate films, the PPy/tiron films show better capacitive behavior and box shape in a voltage window of 0.9 V between -0.5 - 0.4 V at low scan rates. The CVs show that PPy film exhibits improved capacitive behavior in the negative potential window range. The area of CVs increased with increasing scan rate. A broad anodic peak A which centered at ~ -0 2 V and a cathodic peak C at ~ -0.25 V were observed. It is proposed that the majority of tiron ions doped during PPy synthesis still exist in the inner

layer of film due to its relatively large size, leading to poor mobility of tiron anions within the polymer matrix.

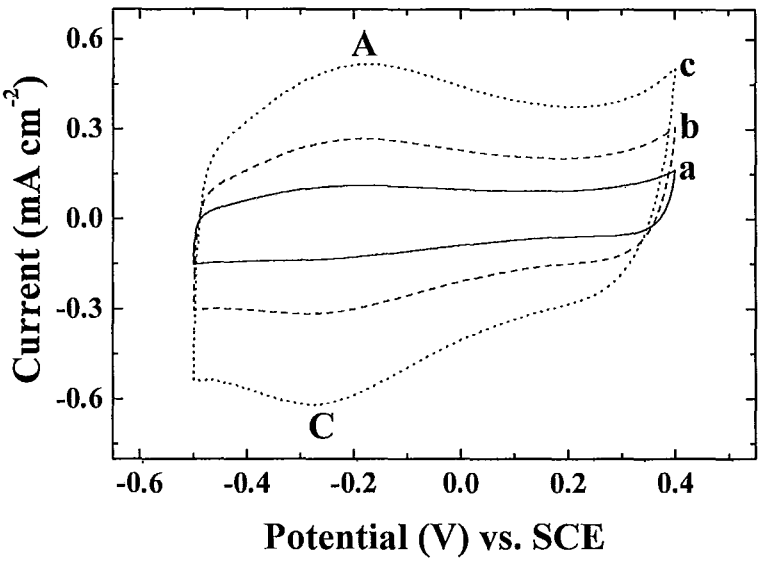

Figure 6-22 CV for the film deposited from the 0.1 M pyrrole solution containing 0.005 M tiron on a stainless steel foil in 0.5 M Na_2SO_4 electrolyte at scan rate of (a) 2, (b) 5 and (c) 10 mV s-1. Film mass: 213 μg cm^{-2}

It is also suggested that strong charge-discharge behavior is related to cation transport properties. The supporting electrolyte cations (in this case, ion Na^+) readily diffuse in and out of the polymer during the redox process, in order to neutralize the immobilized charge of PPy/tiron by the insertion of sodium cations (Na^+) [126,149]. The peak A and C indicate release and insertion of Na^+ during the positive and negative scan, respectively. However, tiron anions incorporation and release were also involved during redox process. The CVs show that PPy/tiron film exhibits both anion and cation-exchange properties. The redox reactions of film matrix can be expressed as follows:

$$PPy^{+}\left(A^{-}\right)+e^{-}\underset{\text{oxidation}}{\overset{\text{reduction}}{\rightleftharpoons}}PPy^{0}+A^{-} \quad (6\text{-}3)$$

(dopant release)

$$PPy^{+}\left(A^{-}\right)+M^{+}+e^{-}\underset{\text{oxidation}}{\overset{\text{reduction}}{\rightleftharpoons}}PPy^{0}\left(A^{-}M^{+}\right) \quad (6\text{-}4)$$

(cation transport)

Where A^{-} is the counter anion and M^{+} is the cation.

6.2.3.3 Capacitance of PPy Doped with Tiron

6.2.3.3.1 Effect of Scan Rates on Capacitance of PPy/tiron Film

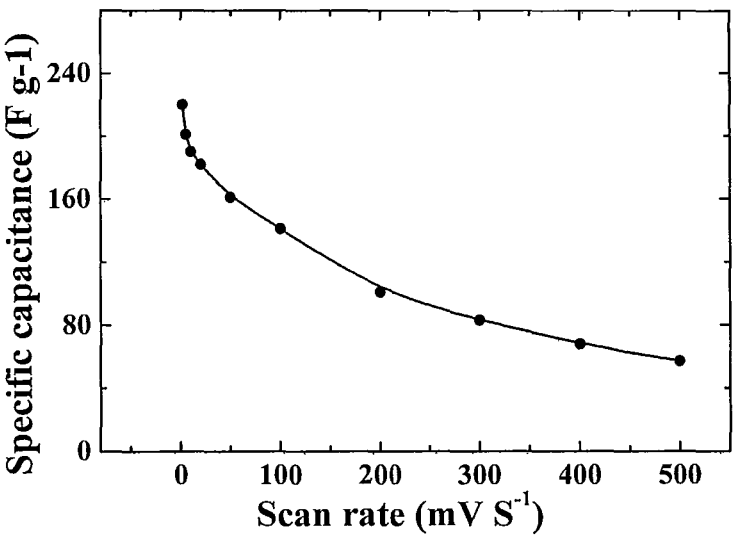

Figure 6-23 SC versus scan rate for the films deposited from the 0.1 M pyrrole solution containing 0.005 M tiron on a stainless steel foil in 0.5 M Na_2SO_4 electrolyte with the film mass of 213 μg cm^{-2}

Figure 6-23 shows the specific capacitance of PPy/tiron film as a function of scan rate. The SC decreased with increasing scan rate. A maximum value of 220 F g^{-1} was obtained at scan rate of 2 mV s^{-1}. The SC value of PPy/tiron at high scan rates, for example, at a san rate of 100 mV s^{-1}, was almost two orders of magnitude higher than that of PPy/sodium salicylate. This relatively high capacitance of PPy/tiron can be attributed to the uniform porous structure and small polymer particle size which determined the ability of electrolyte ions to enter and to enable local ion transfer process.

6.2.3.3.2 Effect of Concentration of Tiron on Capacitance of PPy/tiron Film

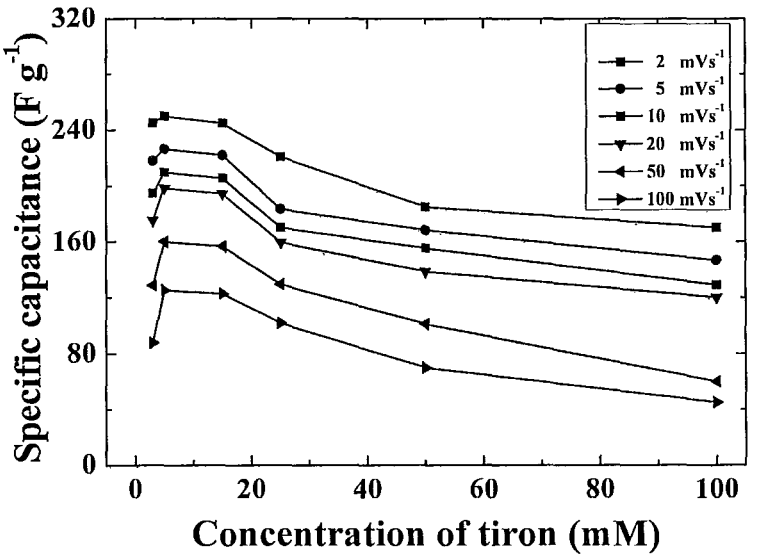

Figure 6-24 Plot of SC versus concentration of tiron at different scan rates. PPy films were obtained on stainless steel from 0.05M solutions containing tiron. Film mass: 140 μ g cm^{-2}.

To examine the relationship between SC and concentration of tiron, PPy films were deposited at a constant current on stainless steel from a 0.05 M pyrrole solution containing tiron whose concentration varied from 3 mM to 100 mM. Figure 6-24 shows that the SC decreased with increasing concentration of tiron in the concentration range of 5 mM to 100 mM. This can be attributed to the more compact films formed as electropolymerization proceeded at higher concentration of tiron. However, in the low concentration range of 3 mM to 5 mM, the SC increased with increasing concentration indicating that tiron catalyzed the formation of polymer film with porous microstructure and finer polymer particle size.

6.2.3.3.3 Effect of pH on Capacitance of PPy/tiron Film

PPy films were prepared at a constant current from 0.05 M pyrrole solutions containing 0.005 M tiron at different pH values and were tested using CV in 0.5 M Na_2SO_4 electrolyte. The plot of SC versus pH is depicted in Figure 6-25.

The result shows that PPy/tiron film prepared in neutral solution (pH=7) exhibits higher SC than that prepared in acidic solutions (pH=1, 3, 5). Although a low pH or acidic solution generally favored polymerization, it was suggested that acid catalyzed formation of non-conjugated trimers, which further react to form a partly conjugated PPy or were incorporated in the film resulting in weak conductivity [132,150] and the lower SC of the films prepared in acidic solutions.

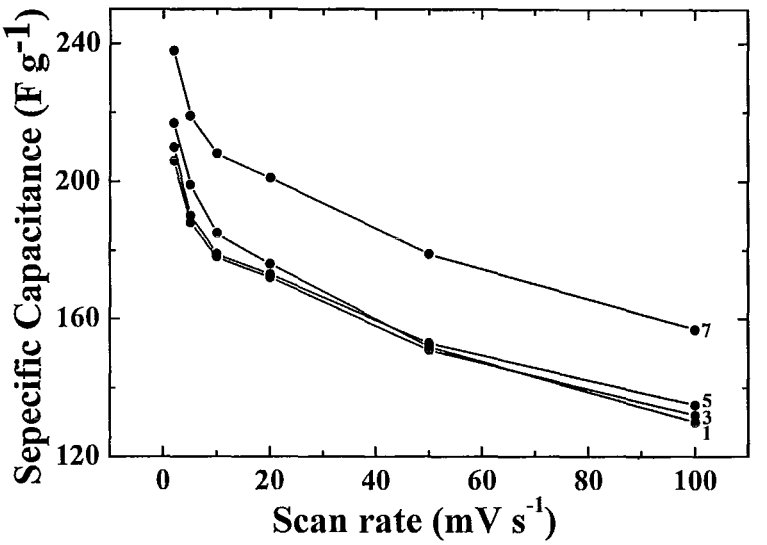

Figure 6-25 Plot of SC versus scan rate for the films deposited from 0.05M pyrrole solutions containing 0.005M tiron on a stainless steel at the pH values of 1, 3, 5, 7. Film mass: 145 μg cm^{-2}

6.2.3.3.4 Effect of Specific Mass on Capacitance of PPy/tiron Film

Figure 6-26 shows SC versus film mass for PPy/tiron films prepared at a constant current from the 0.05 M pyrrole solutions containing 0.005 M tiron at different scan rates. It is interesting to notice that the SC increased with increasing specific mass of PPy films at lower scan rates i.e. 2, 5, 10, 20 mV s^{-1} whilst the SC first increases with an increasing mass then decreased after a maximum value of 150 μg cm^{-2} has been reached at relatively high scan rates of 50 and 100 mV s^{-1}. the reason for decrease of SC with increase of mass at low scan rates can be explained that the electrolyte diffusion in the pores becoming harder due to the long distance. The reason for increase of SC with increase of mass

under 150 μg cm^{-2} at high scan rate may be attributed to the very thin film thickness (less than 1 μm), such that the entire polymer particles were involved in the redox reaction.

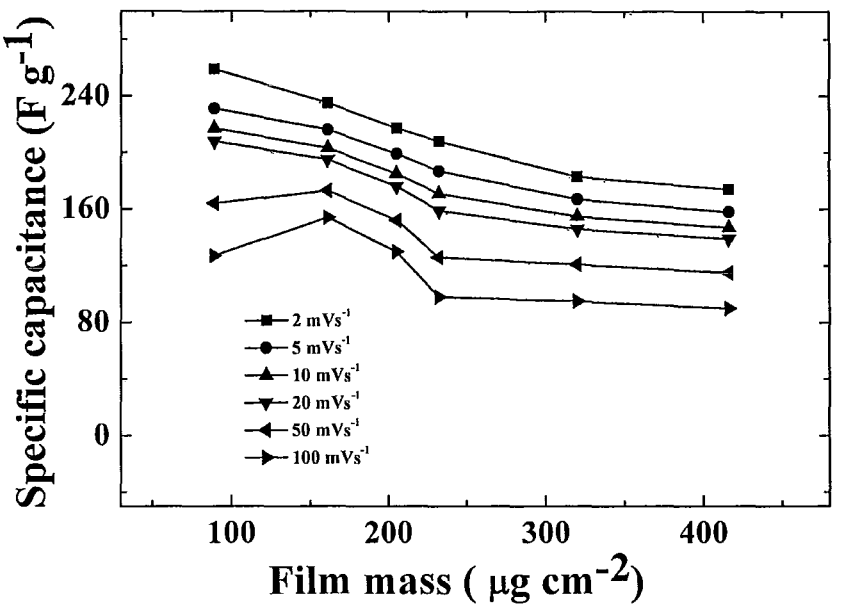

Figure 6-26 Plot of SC versus specific mass on a stainless steel at different scan rates. PPy films were obtained from 0.05 M pyrrole solutions containing 0.005 M tiron

6.3 PPy/MWCNT Composite

6.3.1 Electro-Co-Deposition of PPy/MWCNT in The Presence of Tiron.

6.3.1.1 The Role of Tiron in Electro-Co-Deposition

Tiron is a phenolic compound, belonging to the catechol family. It was mentioned previously that tiron can be used as chelating agent and anionic dopants in the electropolymerization of PPy on stainless steel. The tiron cheating complexation with

metals was due to the deprotonation of OH groups, whereas the anionic properties of the molecules are related to the SO_3^- groups bonded to the aromatic ring.

It should be noted that phenolic compounds exhibit remarkable adsorption properties. Recent studies showed strong adsorption of catechol and tiron on various inorganic materials. The adsorption of tiron was favored by the presence of the two OH groups. Recent studies showed strong adsorption of phenolic molecules on CNTs. The adsorption mechanism was mainly attributed to π-π interactions. It was demonstrated that the adsorption affinity of the phenolic molecules to CNTs increased with the increasing number of OH groups. It is in this regard that tiron can be used as a surfactant to provide efficient dispersion of CNTs in aqueous solutions. It was suggested that the charged phenolic compounds can be used for the dispersion and charging of CNTs and for the fabrication of novel composites by electrodeposition. With this in mind, anionic tiron has been further explored in an effort to obtain stable suspensions of negatively charged MWCNTs and to fabricate composite PPy/MWCNT films by electrodeposition.

It was observed that suspensions of MWCNTs were unstable and showed rapid sedimentation when ultrasonic agitation was interrupted. In contrast, the addition of tiron to the suspensions resulted in improved suspension stability. It was found that tiron can provide dispersion of MWCNTs. It was suggested that similar to other phenolic compounds, tiron was adsorbed on the surfaces of the MWCNTs via π-π interactions. The electrical charge of the SO_3^- groups resulted in electrostatic repulsion and dispersion of the MWCNTs. Sedimentation experiments showed that suspensions of 0.3 – 0.5 g L^{-1} MWCNTs containing 5 – 10 mM tiron were stable during 1 – 2 days after ultrasonic

agitation as shown in a photo below. These results were further utilized for the fabrication of PPy/MWCNT composite films.

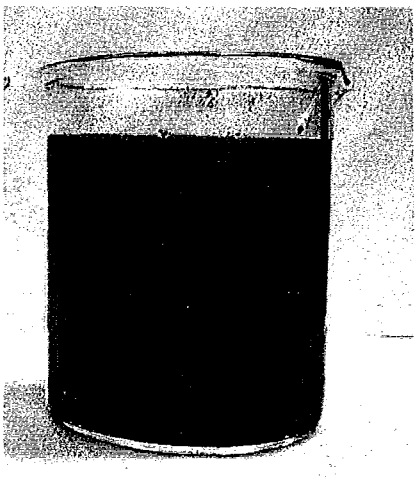

Figure 6-27 Photo of 0.4 g L^{-1} MWCNT suspension in the presence of 5 mM tiron

6.3.1.2 Deposition Mass

The deposition of PPy/MWCNT composite films was performed from pyrrole solutions, containing tiron and MWCNTs. The MWCNTs were acid treated before co-deposition. It was suggested that the electrophoretic motion of the negatively charged MWCNTs, containing adsorbed tiron resulted in the electrochemical incorporation of the MWCNTs into the PPy matrix formed by electropolymerization. Figure 6-28 shows the deposit mass versus deposition time for the deposits prepared galvanostatically at a current density of 1 mA cm^{-2}. The deposit mass increased with an increasing deposition time. Nearly linear dependence was observed. This result indicates that the film mass can be varied and controlled, and therefore, the film thickness also can be predicted according to the varying deposition times.

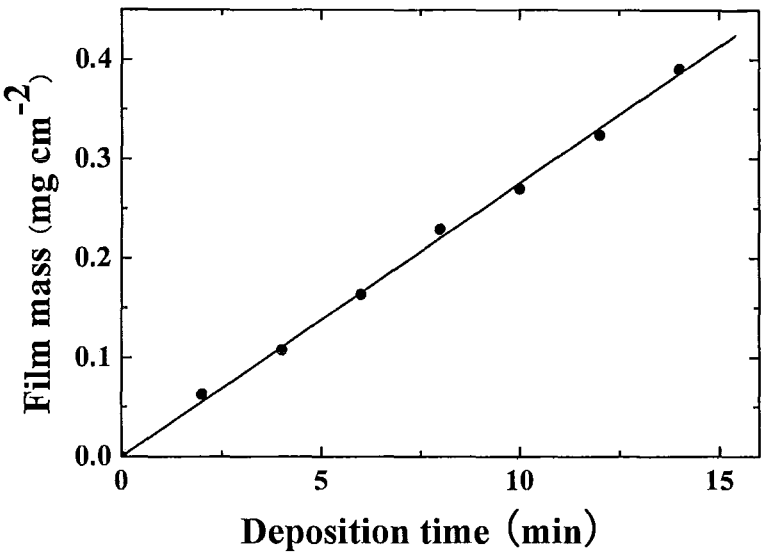

Figure 6-28 Deposit mass versus deposition time at a current of 1 mA cm^{-2} for the composite from 0.1 M pyrrole solution containing 5 mM tiron and 0.4 g L^{-1} MWCNTs

6.3.1.3 Morphology Characterization of PPy/MWCNT Composite.

The SEM surface image of the film prepared from pyrrole solutions containing tiron and MWCNTs is shown in Figure 6-29. Compared to the pure PPy films prepared from the pyrrole/tiron or sodium salicylate solution (Figure 6-20 and Figure 6-7) which are relatively smooth and dense, the PPy/MWCNT composite formed under similar conditions shows very different features. The inset picture at low magnification shows the film surface is porous and indicates that the incorporation of the MWCNTs resulted in an increased roughness of the composite films. It can be seen that MWCNTs are relatively uniformly incorporated in the PPy matrix

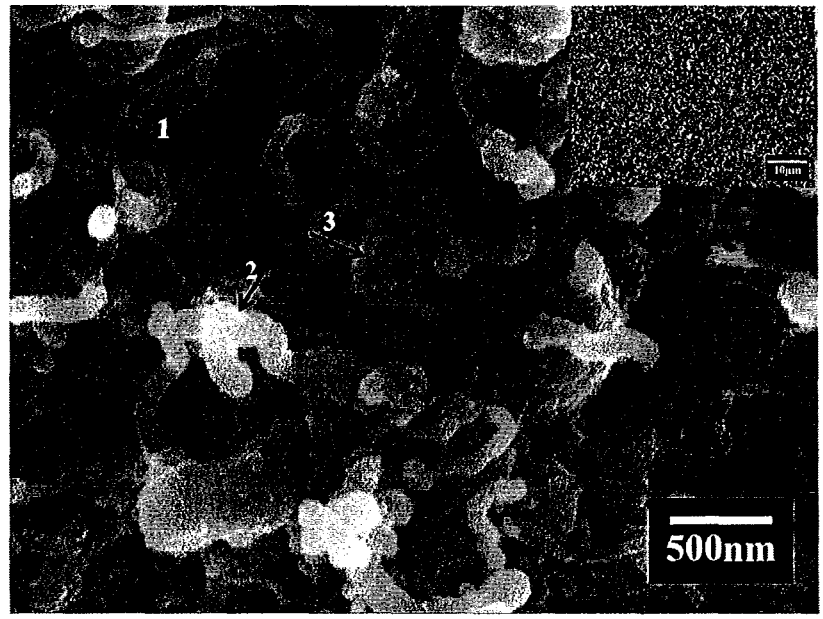

Figure 6-29 SEM image of the films prepared on stainless steel foil at a current of 1 mA cm^{-2} from 0.1M pyrrole solution containing 5mM tiron and 0.4g L^{-1} MWCNTs. Inset is the surface at low magnification. The dashed circle is the area shown at higher magnification

Figure 6-29 further indicates that MWCNTs incorporated into the PPy film matrix construct a network which provide micro- and macro- pores for the movement of ions within the matrix. Moreover, the MWCNTs embedded in the composite served to enhance the mechanical properties of the film matrix. Further, some microscopic features in this figure are observed: (I), A nanotube (denoted as 1) that have not been coated by PPy is due to the end of the deposition. The diameter of MWCNTs was ~ 10-30 nm. (II), the majority of carbon nanotubes are coated by PPy particles. A fully coated nanotube (denoted as 2) shows the size was ~ 50-100 nm in diameter which indicates that the polymers formed a uniform coating on the surface of individual MWCNTs. (III), the

nodular PPy particle (denoted as 3) is connected to other particles by means of coated nanotubes. It can be assumed that the electrochemical properties of the PPy film will be enhanced due to the incorporated MWCNTs.

6.3.2 Electrochemical behavior of PPy/MWCNT composite

6.3.2.1 Electroactivity of PPy/MWCNT Composite

The films prepared by the electrochemical polymerization from the pyrrole solutions are investigated for application in ES and the results obtained for the pure PPy and PPy/MWCNT composite films are compared. The CV data shown in Figure 6-30 indicates the capacitive behavior of the two films in the mild Na_2SO_4 electrolyte.

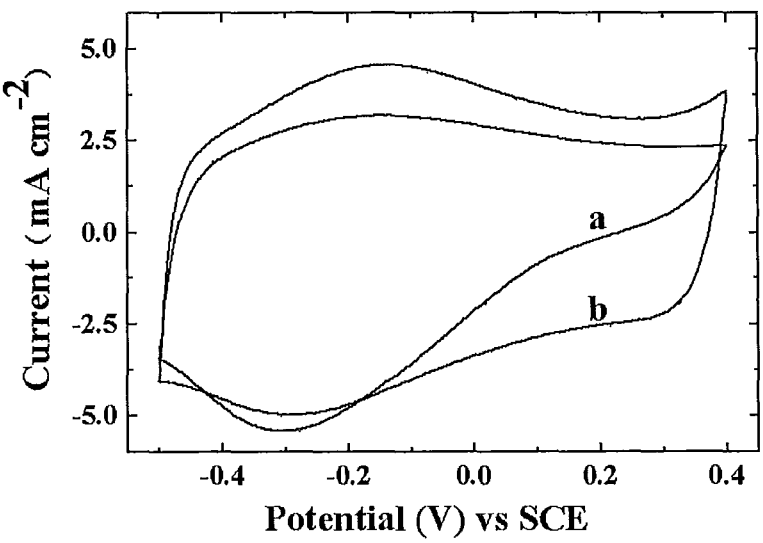

Figure 6-30 CV data at a scan rate of 100 mV s^{-1} for the 160 μg cm^{-2} films prepared at a current density of 1 mA cm^{-2} from 0.1 M pyrrole solution containing 5 mM tiron(a) without MWCNTs and (b) containing 0.4 g L^{-1} MWCNTs

The comparison of the CV data for the pure PPy and PPy/MWCNT composite electrodes of the same mass shows improved capacitive behavior of the composite electrode, as indicated by the larger area of the corresponding CV curve. Although it was discussed that the CV shapes for the pure PPy were box-like at low scanning rates, the CV curve of pure PPy tended to be non-box shape when the scanning rates become larger than 50 mV s^{-1}. The area of the CV for the pure PPy film tended to be smaller with increasing scan rates in the positive potential range of 0 – 0.4 V, indicating a poor capacitive behavior in this range at high scanning rates, because pure PPy polymers becomes more resistive at more positive potentials.

In contrast, the PPy/MWCNT composite films shows good capacitive behaviors. It can be seen at both negative and positive ends of the potential scan. The CVs of the composite exhibits almost straight and vertical current variations at the end potentials, which suggest that a fast charge /discharge switching occurs, which results from high electronic and ionic conductivity in the potential range of 0-0.4V. The box shape is observed at scanning rate of 100 mV s^{-1} indicating an excellent electrical conductivity of film enhanced by incorporated MWCNTs into the PPy matrix. This can be further evidenced by CV curves at relatively high scan rates in the range of 200 – 500 mV s^{-1}, as shown in Figure 6-31. The area of the CVs curve increased significantly with the increasing scan rate. The curves were still rectangle-like even at high scanning rate of 500 mV s^{-1} indicating a very quick charging /discharging process in the composite films. This was because the PPy/MWCNT films were very porous and enabled the counterions entering into/ejection from the composites at a fast rate. The redox reaction processes of

PPy/MWCNT were similar to those of pure PPy films as depicted previously in equations (6-3) and (6-4). However, the redox reaction rate and electrolyte ion diffusion rate are different, apparently, because the reaction and diffusion rates in composites are much larger than that in pure PPy films.

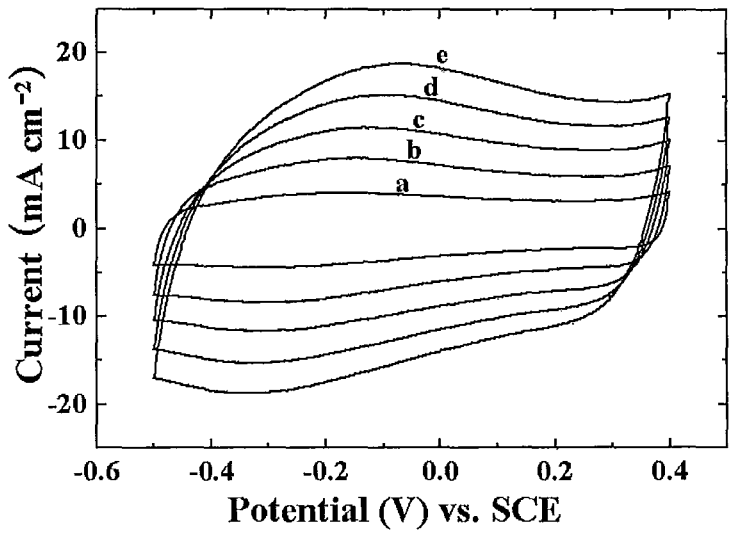

Figure 6-31 CV data at a scan rate of (a) 200, (b) 300, (c) 400, (d) 500 mV s^{-1} for the 160 μg cm^{-2} films prepared at a current density of 1 mA cm^{-2} from 0.1 M pyrrole solution containing 5 mM tiron and 0.4 g L^{-1} MWCNTs

6.3.2.2 Specific Capacitance of PPy/MWCNT

Conductive additives, such as MWCNTs, are usually used to achieve a high electronic conductivity in the composite materials. The advantages of CNTs include their good conductivity and high aspect ratio (>1000), which provides percolation effect at very low volume fractions. Moreover, MWCNTs mechanically reinforce the composite

matrix and prevent cracking. However, MWCNTs possess a rather low SC, typically in the range of 10 – 40 F g^{-1}. Therefore, the amount of MWCNTs in the composite materials must be minimized and the MWCNTs must be well dispersed in the polymer matrix. However, the MWCNTs showed a strong tendency to agglomeration and their dispersion in the polymer matrix presents difficulties. It was suggested that the method, developed in this investigation, offers processing advantages for the fabrication of composite materials containing MWCNTs. As pointed out above, tiron provided good dispersion of MWCNTs in the solutions, containing pyrrole monomer. The MWCNTs were incorporated in-situ in the polymer matrix formed at the electrode surface. Therefore, the problems of the MWCNT agglomeration related to mixing with polymer were diminished.

The SCs calculated from the CV data at different scan rates (2 - 500 mV s^{-1}) for the PPy and PPy/ MWCNT films are shown in Figure 6-32. As expected, the SC of PPy films, presented by curve a in Figure 6-32, decreased from 236 to 60 F g^{-1} with an increasing scan rate from 2 to 500 mV s^{-1}. The PPy/MWCNT composite films show higher capacitances (curve b) compared to the pure PPy films. The highest SC of 310 F g^{-1} was obtained at a scan rate of 2 mV s^{-1}. The improvement in the capacitive behavior of the composite films, compared to the PPy films was especially evident at high scan rates. For example, the SC of the PPy/MWCNT composite film at a scan rate of 500 mV s^{-1} was found to be 150 F g^{-1} which was almost three times larger than that of PPy films. According to the equation (2-1), the PPy/MWCNT composite can store much more energy compared to pure PPy films, especially at high scan rates, indicating that the embedded MWCNTs can improve the electrode properties in energy storage of ES.

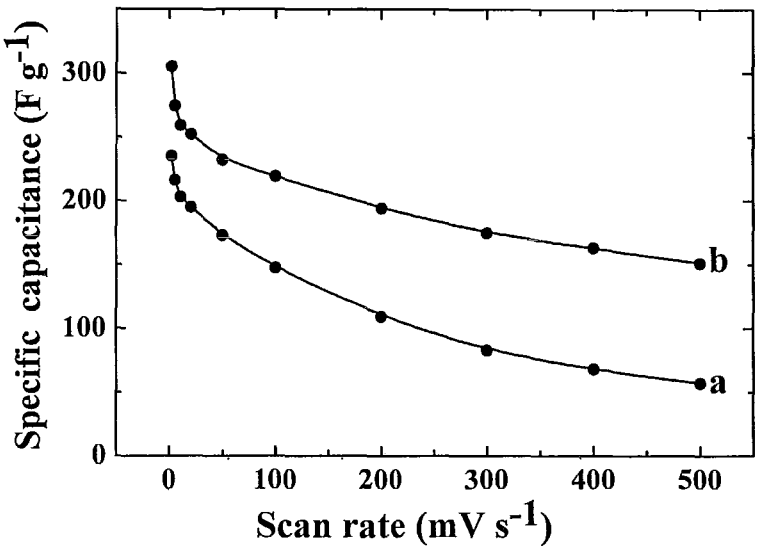

Figure 6-32 SC versus scan rate for the 160 μg cm^{-2} films prepared at a current density of 1 mA cm^{-2} from 0.1 M pyrrole solutions containing 5 mM tiron: (a) without MWCNTs and (b) containing 0.4 g L^{-1} MWCNTs

The difference in the capacitive behavior became more evident with an increasing film mass as shown in Figure 6-33 which shows the SC versus film mass dependences at a scan rate of 5 mV s^{-1} for pure PPy and PPy/MWCNT composite films. The SC decreased with the increasing film thickness by ~ 30% and ~ 10% for the pure PPy and PPy/MWCNT films, respectively. The decrease in SC is attributed to the increase in electrode resistance, resulting from the increased film thickness and diffusion limitations in pores. The higher porosity of the PPy/MWCNT composite films and higher conductivity result in higher SCs.

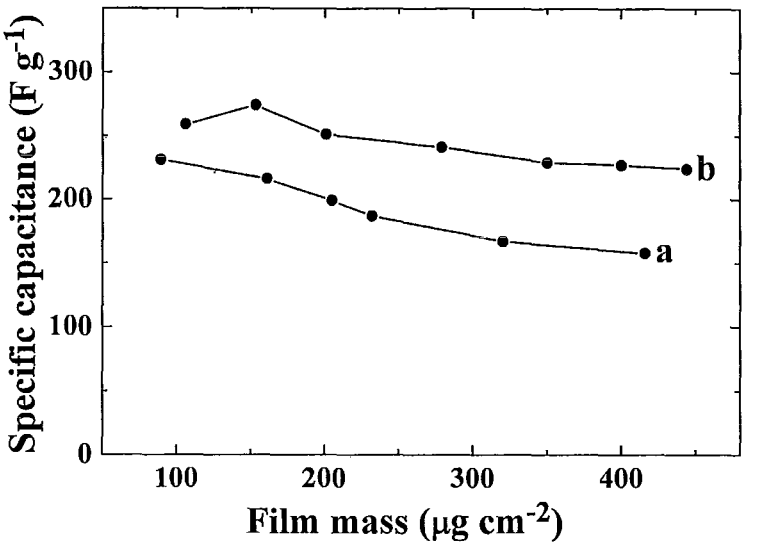

Figure 6-33 SCs measured at a scan rate of 5 mV s^{-1} versus film mass for the films prepared at a current density of 1 mA cm^{-2} from 0.1 M pyrrole solution s containing 5 mM tiron: (a) without MWCNTs and (b) containing 0.4 g L^{-1} MWCNTs

6.3.2.3 Electrochemical Impedance Spectra

The improvement in the capacitive behavior of the PPy/MWCNT composite films compared to the PPy films is attributed to the changes in film morphology and incorporation of MWCNTs into the composite films. It is known that charge-discharge behavior of electrodes of ES is influenced by ionic conductivity and electronic conductivity of the electrode material. SEM investigations shown above (Figure 6-29 and Figure 6-20) exhibit a higher porosity of the PPy/MWCNT composite films compared to the pure PPy films. It is suggested that the higher porosity of the PPy/MWCNT films result in a better electrolyte access to the active materials, whereas the incorporation of

MWCNTs into the composite films result in an improved electronic conductivity. This is in a good agreement with the further results of electrochemical impedance spectra (EIS) studies.

EIS provides the information on charge transfer and mass transport process occurring at the electrolyte/electrode interface and in active electrode materials [146]. The series resistance (R) can be measured from the Nyquist plot to evaluate electronic and ionic conductivities of the electrochemical system. The R is the sum of two major parts, an ohmic resistance R_e of the electrolyte and/or electrode and a charge transfer resistance R_{ct} [151]. The EIS curves for PPy and PPy/MWCNT composite were obtained at open circuit potential (OCP) as shown in Figure 6-34.

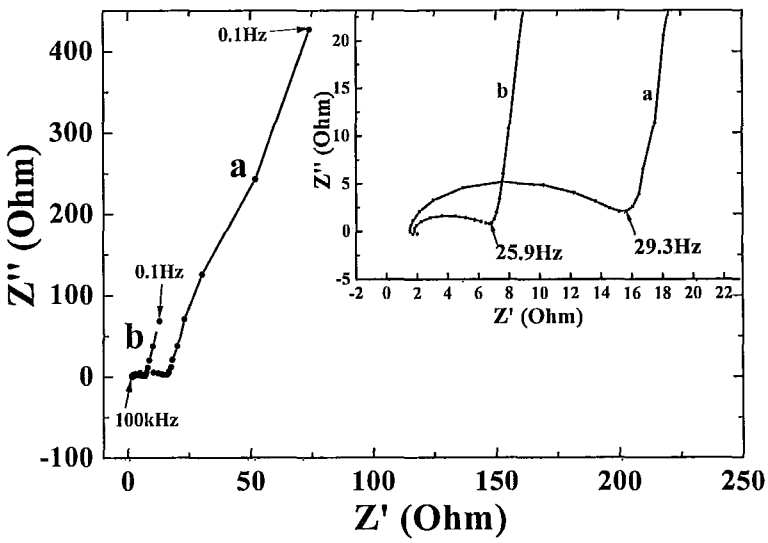

Figure 6-34 Nyquist plots for the 160 μg cm^{-2} films prepared at a current density of 1 mA cm^{-2} from 0.1 M pyrrole solution s containing 5 mM tiron: (a) without MWCNTs and (b) containing 0.4 g L^{-1} MWCNTs. Inset is the enlarged region at high-frequency

As can be seen from the inset of the figure, two well-separated patterns are observed: a semi-circle region represents impedance at high frequencies (100 k Hz - 25.9 Hz and 100 k Hz - 29.3 Hz for PPy film and PPy/MWCNT composite, respectively.) and a linear region at lower frequencies. The arc is related to the interfacial processes, and can be used to evaluate the value of electrochemical charge transfer resistance (R_{ct}), which is thought to be the main part of the resistance of ES [152]. The regions for both curves at low frequencies (from the knee frequency to 0.1 Hz) are relatively linear, indicating a capacitive behavior related to the film charging mechanism discussed above. In Figure 6-34, the impedance curve for the composite film at low frequencies is almost parallel to the imaginary axis, a better capacitive behavior than that of the pure PPy film. The capacitance could also be calculated from the low-frequency data of the EIS plot by the equation:

$$C=-1/(2\pi f Z_{img}) \qquad (6\text{-}5)$$

Therefore, the comparison of the EIS data for the PPy/MWCNT composite and pure PPy films, in the Nyquist plots presented in Figure 6-34 indicate that the composite films have a much lower electrical resistance (Z') than that of pure PPy films. The R_{ct} value of PPy films is ~ 14.5 Ω at open circuit potential whilst in PPy/MWCNT composite films, the R_{ct} value was ~ 5.7 Ω. The lower electrical resistance resulted in a higher SC of the PPy/MWCNT composite films. However, it was reported that the capacitance evaluated from EIS was smaller than that calculated from the CV curve at low scanning rate due to the redox switching hysteresis of conducting polymer [152,153]. It should be

noted that CV data give a capacitance in the voltage window of 0.9 V, whereas the EIS data give a capacitance measured at a low voltage range.

In order to analyze quantitatively the electrochemical behavior of pure PPy and PPy/MWCNT composite electrodes, the experimental EIS data could be simulated by using an appropriate electrical equivalent circuit (EEC) as shown in Figure 6-35. In this equivalent circuit model, R_s is so-called a electrolyte solution resistance; R_{ct} is related to ionic charge transfer resistance at the polymer/electrolyte interface and/or electron transfer resistance at the metal/polymer interface; The capacitance C_{dl} presented in the equivalent circuit discussed previously in literature (see Figure 5-3) is replaced with the constant phase element CPE1, whilst Z_w was replaced by a parallel combination of CPE2 (Faradaic pseudocapacitance) and R_f which is the low-frequency electron transfer resistance of the redox reactions [154]. Due to the huge value of R_f, the EEC model can be modified by eliminating the R_f element in the circuit as shown in Figure 6-36.

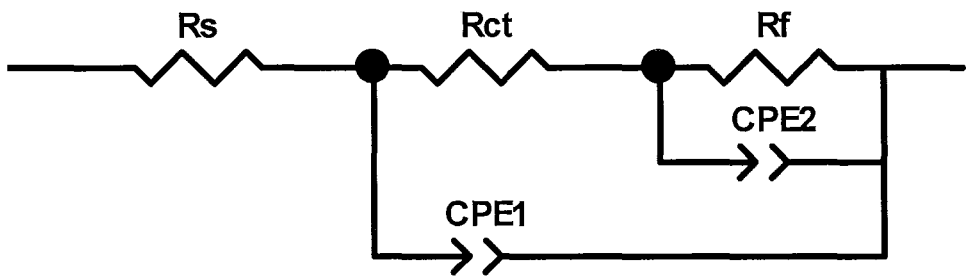

Figure 6-35 Equivalent circuit model for pure PPy and PPy/MWCNT composite electrode in a 0.5 M Na_2SO_4 electrolyte

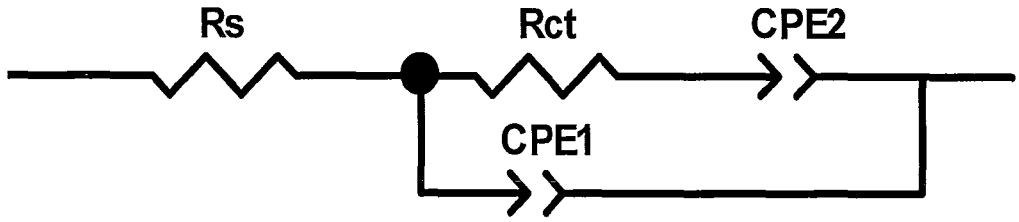

Figure 6-36 Modified equivalent circuit model for pure PPy and PPy/MWCNT electrode in a 0.5 M Na_2SO_4 electrolyte

The use of CPE in place of a capacitor in this model is to compensate for non-homogeneity such as surface roughness/porosity, adsorption, or diffusion in the system [146,155]. The CPE is defined by the constants Q and n, and the impedance of CPE defined as Z(w) is given according to:

$$Z(w)=\frac{1}{Q}(j\omega)^{-n} \qquad (6\text{-}6)$$

Where, n is the factor describing deviation from ideal capacitance ($0\leq n\leq 1$). For n=1, the CPE exhibits an ideal capacitor; for n=0, it describes an ideal resistor. Q is the CPE constant which is frequency independent, and resembles a capacitor when n=1; ω is the angular frequency (rad s^{-1}); j is the imaginary number ($j=\sqrt{-1}$)

Hence, the electrochemical behavior of the system could be simulated and quantified based on the equivalent circuit presented in Figure 6-35. The Faraday impedance might arise from the electroactive species and could be represented in EIS spectra by finite length Warburg element, which was related to the diffusion of counter-

anions [156]. At low frequencies range, the diffusion interpretation can be described with the time constant T:

$$T=\frac{L^2}{D} \qquad (6\text{-}7)$$

Where, L is the effective diffusion thickness and D is the effective diffusion coefficient of the particle.

An excellent agreement between the experimental and calculated EIS data for PPy and PPy/MWCNT composite (inset) was observed as shown in Figure 6-37. This fitting process verified that the proposed EEC model can be used to simulate the electrochemical system for both PPy and PPy/MWCNT composite films in a 0.5 M Na_2SO_4 electrolyte solution in the frequency range of 100k Hz - 0.1 Hz.

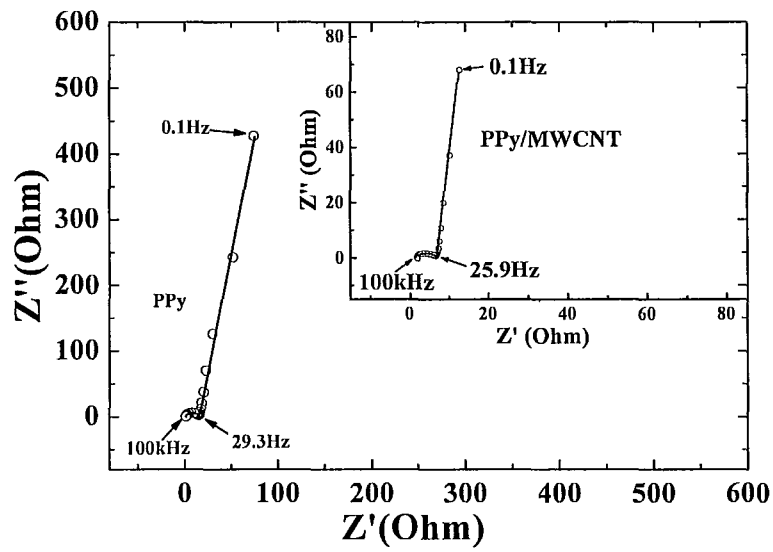

Figure 6-37 Nyquist plot of PPy and PPy/MWCNT composite recorded at OCP. Experimental (circle) and theoretical (solid line). EIS data fitting results according to the EEC model

6.3.2.4 Cycle Life Test

The charge-discharge stability of the composite films was studied by continuous sweeping the potential for 1000 cycles between -0.5 - 0.4V at a scan rate of 50 mV s^{-1}. The CV of 1st and 1000th cycle is plotted as shown in Figure 6-38.

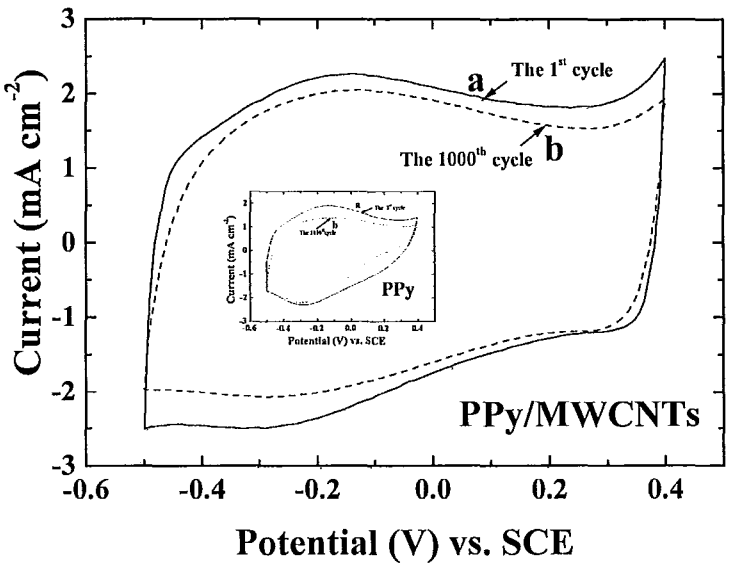

Figure 6-38 CV of the PPy/MWCNT film recorded in the (a)1st and (b)1000th potential cycle at a scan rate of 50 mV s^{-1} in 0.5M Na_2SO_4 electrolyte solution. Inset is CV of the PPy film in the 1st and 1000th potential cycle under same test condition. Film mass:183μg cm^{-2}

This figure compares the cycling behavior of PPy film with and without MWCNTs between the first cycle and the last cycle. PPy/MWCNT composite shows similarity of CVs in shape after 1000 cycles, indicating that the stabilized porous structure kept the excellent conductivity of composite due to the incorporated MWCNTs. In contrast, the PPy film (inset) shows significant changes in CV shape as well as area. The CV shape

shifted inward in the potential range of -0.2 V - 0.3 V during the 1000th negative scan, and the capacitive area become smaller after 1000th cycle indicating that the pure PPy film exhibits much more degradation compared to PPy/MWCNT composite after 1000-cycle aging.

The SC versus cycle number for the PPy and the PPy/MWCNT composite films is further shown in Figure 6-39. The SC decreased with an increasing cycle number. The decrease in SC values may be due to PPy degradation on swelling and shrinking in aqueous media and the PPy nanostructure may also change. A 24% and 15% lose of SC for PPy and PPy/MWCNT are observed after 1000 cycles aging, respectively. The data demonstrates that the PPy/MWCNT composites have higher cycling stability than that of PPy films, indicating that this improvement may result from the relatively rigid incorporated MWCNTs which support and stabilize the porous structure of the composite against the influence of the repeated intercalation and removal of the charge balance ions.

The results of this investigation indicate that the PPy/MWCNT composite films prepared on the stainless steel substrates are promising materials for application in electrodes of ES. The SC of the PPy/MWCNT composite prepared by electrodeposition is higher than that of the PPy-single-walled CNTs (SWCNTs) prepared by chemical methods. The SC was comparable with that reported for the PPy and PPy/SWCNTs films deposited on Ti, Ta and other chemically inert substrates with a similar film mass. The method developed in this investigation offers the advantages of using low-cost stainless steel substrates and a mild electrolyte.

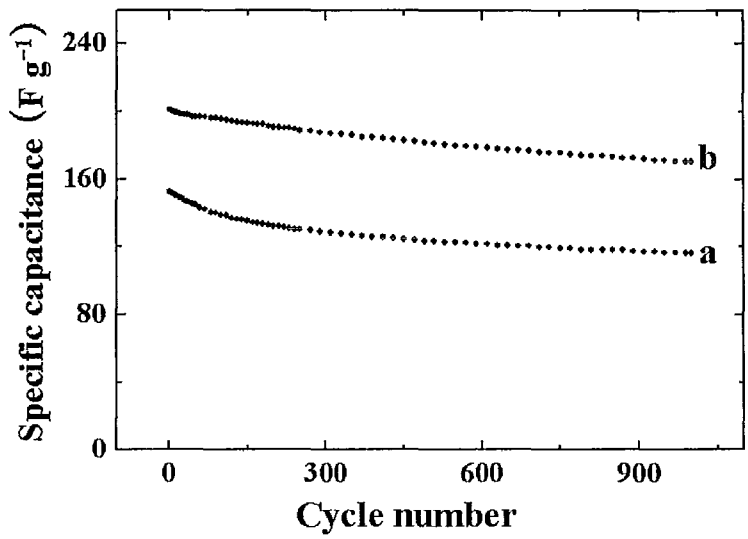

Figure 6-39 SC at a scan rate of 50 mV s^{-1} versus cycle number for the 220 μg cm^{-2} films prepared at a current density of 1 mA cm^{-2} from 0.1 M pyrrole solutions containing 5 mM Tiron (a) without MWCNTs and (b) containing 0.4 g L^{-1} MWCNTs

7 Conclusions

PPy films were deposited by anodic electropolymerization on stainless steel substrates from aqueous pyrrole solutions containing sodium salicylate and tiron as anionic charge compensating additives. The electrochemical behavior of stainless steel in the presence of additives in salt solution was tested and analyzed. Adherent and uniform films were successfully obtained from the pyrrole solutions containing tiron and sodium salicylate additives. The anode dissolution during the electropolymerization process reduced in the presence of sodium salicylate and tiron without preventing the formation and precipitation of PPy on the substrate surface. It was suggested that the passivation layer formed on the stainless steel surface was due to the complexation of tiron and salicylate with metal ions. It was also found that tiron can be used for the dispersion of MWCNTs and fabrication of composite PPy/MWCNT films. The results indicated that the OH groups of tiron promoted its adsorption on the stainless steel surface. The deposition yields can be varied and controlled by a variation of deposition time at a constant current density. The OCP and Tafel test of stainless steel coated with PPy showed corrosion protection in a salt electrolyte solution. SEM studies showed that the incorporation of MWCNTs into the PPy during electropolymerization resulted in the formation of porous films. Cyclic voltammetry data for the films tested in the 0.5 M Na_2SO_4 solutions showed a capacitive behavior and high SC in a voltage window of -0.5 – +0.4 V versus SCE. The incorporation of MWCNTs into the PPy films and film porosity were beneficial for the application of the PPy/MWCNT composite films in electrodes of ES. The PPy/MWCNT composite films showed improved capacitive

behavior and lower electrical resistance compared to pure PPy films. A highest SC of 310 F g^{-1} was obtained at a scan rate of 2 mV s^{-1} for the composite films. The SC decreased with an increasing film thickness and scan rate. The cycling stability of the films was investigated. EIS analysis further verified that high capacitance and low resistance of PPy matrix were due to the incorporation of MWCNTs. The EIS data fitting process were tested by an EEC model. The results indicated that the PPy/MWCNT films deposited on the stainless steel substrates by anodic electropolymerization are promising electrode materials for ES.

References

[1] J. Sheffield, "Forecasts for the 21st century" *Journal of Fusion Energy, vol. 18, pp. 23-26, 2001.*

[2] B. Viswanathan, "Energy sources," *in An introduction to energy sources, 2006.*

[3] H. Ibrahim, A. Ilinca, J. Perron, "Energy storage systems - characteristics and comparisons" *Renewable and Sustainable Energy Reviews, vol. 12, pp. 1221-1250, 2008.*

[4] C. Liu, F. Li, M. Lai-Peng, H.-M. Cheng, "Advanced materials for energy storage" *Advanced Materials, vol. 22, pp. E28-E62, 2010.*

[5] P. Simon, Y. Gogotsi, "Materials for electrochemical capacitors" *in Nature Materials, vol. 7, pp. 845-854, 2008.*

[6] S. S. A. K. Shukla*, K. Vijayamohana, "Electrochemical supercapacitors: Energy storage beyond batteries" Current Science, vol. 79, pp. 1656-1661, 2000.

[7] V. Ramani, "Fuel cells" *The Electrochemical Society Interface, vol. 15, pp. 41-44, 2006.*

[8] B.E.Conway, *Electrochemical Supercapacitors: Scientific Fundamentals and Technological Applications. New York, N.Y.: Kluwer Academic, 1999.*

[9] J. R. Miller, "Capacitors | Overview Encyclopedia of Electrochemical Power Sources," *J. x. F. r. Garche, Ed. Amsterdam: Elsevier, pp. 587-599, 2009.*

[10] R. Kötz, Carlen, M., "Principles and applications of electrochemical capacitors" *Electrochimica Acta, vol. 45, pp. 2483-2498, 2000.*

[11] S. M. Lukic, J. Cao, R. C. Bansal, F. Rodriguez, A. Emadi, "Energy storage systems for automotive applications," *IEEE Transactions on Industrial Electronics, vol. 55, pp. 2258-2267, 2008.*

[12] Y. Zhang, H. Feng, X. Wu, L. Wang, A. Zhang, T. Xia, H. Dong, X. Li, L. Zhang, "Progress of electrochemical capacitor electrode materials: a review" *International Journal of Hydrogen Energy, vol. 34, pp. 4889-99, 2009.*

[13] A. Lewandowski, M. Galinski, "Practical and theoretical limits for electrochemical double-layer capacitors" *Journal of Power Sources, vol. 173, pp. 822-828, 2007.*

[14] L. T. Lam, R. Louey, "Development of ultra-battery for hybrid-electric vehicle applications" *Journal of Power Sources, vol. 158, pp. 1140-1148, 2006.*

[15] F. S. Garcia, A. A. Ferreira, J. A. Pomilio, "Control strategy for battery-ultracapacitor hybrid energy storage system" p*resented at 2009 Twenty-Fourth Annual IEEE Applied Power Electronics Conference and Exposition (APEC), 15-19 Feb. 2009, Piscataway, NJ, USA, 2009.*

[16] P. Thounthong, V. Chunkag, P. Sethakul, B. Davat, M. Hinaje, "Comparative study of fuel-cell vehicle hybridization with battery or supercapacitor storage device" *IEEE Transactions on Vehicular Technology, vol. 58, pp. 3892-3904, 2009.*

[17] A. Burke, "Ultracapacitors: why, how, and where is the technology" *Journal of Power Sources, vol. 91, pp. 37-50, 2000.*

[18] E. Serrano, G. Rus, J. Garcia-Martinez, "Nanotechnology for sustainable energy" *Renewable and Sustainable Energy Reviews, vol. 13, pp. 2373-2384, 2009.*

[19] W. Sun, X. Chen, "Preparation and characterization of polypyrrole films for three-dimensional micro supercapacitor" *Journal of Power Sources, vol. 193, pp. 924-929, 2009.*

[20] P. P. Barker, "Ultracapacitors for use in power quality and distributed resource applications," *presented at IEEE PES Summer Meeting, 21-25 July 2002, Piscataway, NJ, USA, 2002.*

[21] K. I. Akihiko Yoshida, Hajime Yoneda, and Atsushi Nishino, "An electric double-layer capacitor with high capacitance and low resistance" *Microelectronics and Reliability, vol. 32, pp. 1784-1785, 1992.*

[22] M. V. Fedorov , A. A. Kornyshev, "Towards understanding the structure and capacitance of electrical double layer in ionic liquids" *Electrochimica Acta, vol. 53, pp. 6835-6840, 2008.*

[23] A. K. Shukla, S. Sampath, K. Vijayamohanan, "Electrochemical supercapacitors: energy storage beyond batteries" *Current Science,* vol. 79, pp. 1656-61, 2000.

[24] B. E. Conway, V. Birss, J. Wojtowicz, "The role and utilization of pseudocapacitance for energy storage by supercapacitors" *Journal of Power Sources, vol. 66, pp. 1-14, 1997.*

[25] C. Peng, S. Zhang, D. Jewell, G. Z. Chen, "Carbon nanotube and conducting polymer composites for supercapacitors" *Progress in Natural Science, vol. 18, pp. 777-788, 2008.*

[26] B. E. Conway, W. G. Pell, "Double-layer and pseudocapacitance types of electrochemical capacitors and their applications to the development of hybrid devices" *Journal of Solid State Electrochemistry, vol. 7, pp. 637-644, 2003.*

[27] T. Aida, K. Yamada, M. Morita, "An advanced hybrid electrochemical capacitor that uses a wide potential range at the positive electrode" *Electrochemical and Solid-State Letters, vol. 9, pp. A534-A536, 2006.*

[28] K. Karthikeyan, V. Aravindan, S. B. Lee, I. C. Jang, H. H. Lim, G. J. Park, M. Yoshio, Y. S. Lee, "Electrochemical performance of carbon-coated lithium manganese silicate for asymmetric hybrid supercapacitors" *Journal of Power Sources, vol. 195, pp. 3761-3764, 2010.*

[29] A. Balducci, U. Bardi, S. Caporali, M. Mastragostino, F. Soavi, "Ionic liquids for hybrid supercapacitors" *Electrochemistry Communications, vol. 6, pp. 566-570, 2004.*

[30] A. G. Pandolfo, A. F. Hollenkamp, "Carbon properties and their role in supercapacitors" *Journal of Power Sources, vol. 157, pp. 11-27, 2006.*

[31] C. Largeot, C. Portet, J. Chmiola, P.-L. Taberna, Y. Gogotsi, P. Simon, "Relation between the ion size and pore size for an electric double-layer capacitor" *Journal of the American Chemical Society, vol. 130, pp. 2730-2731, 2008.*

[32] A. B. Patrice Simon, "Nanostructured carbons: double-layer capacitance and more" *The Electrochemical Society Interface, vol. 17, pp. 38-43, 2008.*

[33] Z. Shao-yun, L. Xin-hai, W. Zhi-xing, G. Hua-jun, P. Wen-jie, "Effect of activated carbon and electrolyte on properties of supercapacitor" *Transactions of the Nonferrous Metals Society of China, vol. 17, pp. 1328-33, 2007.*

[34] A. Y. Rychagov, N. A. Urisson, Y. M. Vol'fkovich, "Electrochemical characteristics and properties of the surface of activated carbon electrodes in a double-layer capacitor" *Russian Journal of Electrochemistry, vol. 37, pp. 1172-1179, 2001.*

[35] S. M. Lipka, "Electrochemical capacitors utilizing low surface area carbon fiber" *Aerospace and Electronic Systems Magazine, vol. 12, pp. 27-30, 1997.*

[36] H. Shi, "Activated carbons and double layer capacitance" *Electrochimica Acta, vol. 41, pp. 1633-1639, 1996.*

[37] Bleda-Martínez, "Role of surface chemistry on electric double layer capacitance of carbon materials" *Carbon, vol. 43, pp. 2677-2684, 2005.*

[38] D. Qu, H. Shi, "Studies of activated carbons used in double-layer capacitors" *Journal of Power Sources, vol. 74, pp. 99-107, 1998.*

[39] C.x. Zhang, "Effect of pore structure on the electrochemical performance of coal-based activated carbons in non-aqueous electrolyte" *New Carbon Materials, vol. 25, pp. 129-133, 2010.*

[40] G. Gryglewicz, J. Machnikowski, E. Lorenc-Grabowska, G. Lota, E. Frackowiak, "Effect of pore size distribution of coal-based activated carbons on double layer capacitance" *Electrochimica Acta, vol. 50, pp. 1197-1206, 2005.*

[41] L.-h. WANG, M. Toyoda, M. Inagaki, "Dependence of electric double layer capacitance of activated carbons on the types of pores and their surface areas" *New Carbon Materials, vol. 23, pp. 111-115, 2008.*

[42] S. T. Mayer, R. W. Pekala, J. L. Kaschmitter, "The Aerocapacitor: An Electrochemical Double-Layer Energy-Storage Device" *Journal of The Electrochemical Society, vol. 140, pp. 446-451, 1993.*

[43] R. W. Pekala, J. C. Farmer, C. T. Alviso, T. D. Tran, S. T. Mayer, J. M. Miller, B. Dunn, "Carbon aerogels for electrochemical applications" *Journal of Non-Crystalline Solids, vol. 225, pp. 74-80, 1998.*

[44] R. Saliger, U. Fischer, C. Herta, J. Fricke, "High surface area carbon aerogels for supercapacitors" *Journal of Non-Crystalline Solids, vol. 225, pp. 81-85, 1998.*

[45] E. Frackowiak, F. Béguin, "Carbon materials for the electrochemical storage of energy in capacitors" *Carbon, vol. 39, pp. 937-950, 2001.*

[46] H. Tamon, H. Ishizaka, M. Mikami, M. Okazaki, "Porous structure of organic and carbon aerogels synthesized by sol-gel polycondensation of resorcinol with formaldehyde" *Carbon, vol. 35, pp. 791-796, 1997.*

[47] J. Li, X. Wang, Y. Wang, Q. Huang, C. Dai, S. Gamboa, P. J. Sebastian, "Structure and electrochemical properties of carbon aerogels synthesized at ambient temperatures as supercapacitors" *Journal of Non-Crystalline Solids, vol. 354, pp. 19-24, 2008.*

[48] W. Li, G. Reichenauer, J. Fricke, "Carbon aerogels derived from cresol-resorcinol-formaldehyde for supercapacitors" *Carbon, vol. 40, pp. 2955-2959, 2002.*

[49] J. Wang, X. Yang, D. Wu, R. Fu, M. S. Dresselhaus, G. Dresselhaus, "The porous structures of activated carbon aerogels and their effects on electrochemical performance" *Journal of Power Sources, vol. 185, pp. 589-594, 2008.*

[50] A. Braun, "Exponential growth of electrochemical double layer capacitance in glassy carbon during thermal oxidation" *Carbon, vol. 41, pp. 759-765, 2003.*

[51] A. Braun, "X-ray scattering and adsorption studies of thermally oxidized glassy carbon" *Journal of Non-Crystalline Solids, vol. 260, pp. 1-14, 1999.*

[52] Y. Y. Fan, A. Kaufmann, A. Mukasyan, A. Varma, "Single- and multi-wall carbon nanotubes produced using the floating catalyst method: Synthesis, purification and hydrogen up-take" *Carbon, vol. 44, pp. 2160-2170, 2006.*

[53] W. K. Maser, A. M. Benito, "Production of carbon nanotubes: the light approach" *Carbon, vol. 40, pp. 1685-1695, 2002.*

[54] R. M. Reilly, "Carbon nanotubes: potential benefits and risks of nanotechnology in nuclear medicine" *Journal of Nuclear Medicine, vol. 48, pp. 1039-1042, 2007.*

[55] E. Frackowiak, "Nanotubular materials as electrodes for supercapacitors" *Fuel Processing Technology, vol. 77-78, pp. 213-219, 2002.*

[56] E. Frackowiak, "Enhanced capacitance of carbon nanotubes through chemical activation" *Chemical Physics Letters, vol. 361, pp. 35-41, 2002.*

[57] Q. Jiang, "A study of activated carbon nanotubes as electrochemical super capacitors electrode materials" *Materials Letters, vol. 57, pp. 988-991, 2002.*

[58] H. Zhang, G. Cao, Y. Yang, Z. Gu, "Comparison between electrochemical properties of aligned carbon nanotube array and entangled carbon nanotube electrodes" *Journal of The Electrochemical Society, vol. 155, pp. K19-K22, 2008.*

[59] H. Zhang, G. Cao, Y. Yang, "Electrochemical properties of ultra-long, aligned, carbon nanotube array electrode in organic electrolyte" *Journal of Power Sources, vol. 172, pp. 476-480, 2007.*

[60] C.C. Hu, M.J. Liu, K.H. Chang, "Anodic deposition of hydrous ruthenium oxide for supercapacitors" *Journal of Power Source, vol. 163, pp. 1126-1131, 2007.*

[61] J.J. Jow, H.J. Lee, H.R. Chen, M.S. Wu, T.Y. Wei, "Anodic, cathodic and cyclic voltammetric deposition of ruthenium oxides from aqueous RuCl3 solutions" *Electrochimica Acta, vol. 52, pp. 2625-2633, 2007.*

[62] B. J. Lee, "Carbon nanofibre/hydrous RuO2 nanocomposite electrodes for supercapacitors" *Journal of Power Sources, vol. 168, pp. 546-552, 2007.*

[63] S.H. Lee, P. Liu, H. M. Cheong, C. E. Tracy, S. K. Deb, "Electrochromism of amorphous ruthenium oxide thin films," *Solid State Ionics, vol. 165, pp. 217-221, 2003.*

[64] X. Qin, "Electrochemical characterization on $R_uO_2 \cdot xH_2O$/carbon nanotubes composite electrodes for high energy density supercapacitors" *Carbon, vol. 42, pp. 451-453, 2004.*

[65] I.H. Kim , K.B. Kim, "Electrochemical Characterization of Hydrous Ruthenium Oxide Thin-Film Electrodes for Electrochemical Capacitor Applications" *Journal of The Electrochemical Society, vol. 153, pp. A383-A389, 2006.*

[66] S. W. Z. a. G. Z. Chen, "Manganese oxide based materials for supercapacitors," *Energy Materials :materials science and engineering for energy systems, vol. 3, pp. 186*-200, 2008.

[67] J. Wei, I. Zhitomirsky, "Manganese oxide films for electrochemical supercapacitors" *Journal of Materials Processing Technology, vol. 186, pp. 356-361, 2007.*

[68] P. Staiti, F. Lufrano, "Study and optimization of manganese oxide-based electrodes for electrochemical supercapacitors" *Journal of Power Sources, vol. 187, pp. 284-289, 2009.*

[69] C.Y. Chen, "Hybrid manganese oxide films for supercapacitor application prepared by sol-gel technique" *Thin Solid Films, vol. 518, pp. 1*557-1560, 2009.

[70] W. Wei, X. Cui, W. Chen, D. G. Ivey, "Electrochemical cyclability mechanism for MnO2 electrodes utilized as electrochemical supercapacitors" *Journal of Power Sources, vol. 186, pp. 543-550, 2009.*

[71] C. Yuan, B. Gao, L. Su, X. Zhang, "Interface synthesis of mesoporous MnO2 and its electrochemical capacitive behaviors" *Journal of Colloid and Interface Science, vol. 322, pp. 545-550, 2008.*

[72] S.Y. Wang, "Investigation on capacitance mechanisms of Fe_3O_4 electrochemical capacitors" *Journal of the Electrochemical Society, vol. 153,pp.A75-A80, 2006.*

[73] K. S. Ryu, X. Wu, Y.G. Lee, S. H. Chang, "Electrochemical capacitor composed of doped polyaniline and polymer electrolyte membrane" *Journal of Applied Polymer Science, vol. 89, pp. 1300-1304, 2003.*

[74] S. K. Mondal, K. Barai, N. Munichandraiah, "High capacitance properties of polyaniline by electrochemical deposition on a porous carbon substrate" *Electrochimica Acta, vol. 52, pp. 3258-3264, 2007.*

[75] U. Johanson, M. Marandi, T. Tamm, J. Tamm, "Comparative study of the behavior of anions in polypyrrole films" *Electrochimica Acta, vol. 50, pp. 1523-1528, 2005.*

[76] E.L. Kupila, J. Kankare, "Influence of electrode pretreatment, counter anions and additives on the electropolymerization of pyrrole in aqueous solutions" *Synthetic Metals, vol. 74, pp. 241-249, 1995.*

[77] N. G. Sahoo, S. Rana, J. W. Cho, L. Li, S. H. Chan, "Polymer nanocomposites based on functionalized carbon nanotubes" *Progress in Polymer Science, vol. In Press, Corrected Proof, 2010.*

[78] B. Du, Q. Jiang, X. F. Zhao, B. Huang, Y. Zhao, "Preparation of PPy/CNT composite applications for supercapacitor electrode material" *Materials Science Forum, pp. 502-5, 2009.*

[79] X. Zhang, W. Yang, Y. Ma, "Synthesis of polypyrrole-intercalated layered manganese oxide nanocomposite by a delaminationreassembling method and its electrochemical capacitance performance" *Electrochemical and Solid-State Letters, vol. 12, pp. A95*-A98, 2009.

[80] Q. T. Qu, B. Wang, L. C. Yang, Y. Shi, S. Tian, Y. P. Wu, "Study on electrochemical performance of activated carbon in aqueous Li_2SO_4, Na_2SO_4 and

K_2SO_4 electrolytes" *Electrochemistry Communications, vol. 10, pp. 1652-1655, 2008.*

[81] A. Balducci, R. Dugas, P. L. Taberna, P. Simon, D. Plée, M. Mastragostino, S. Passerini, "High temperature carbon-carbon supercapacitor using ionic liquid as electrolyte" *Journal of Power Sources, vol. 165, pp. 922-927, 2007.*

[82] E. J. L. Hideki Shirakawa, Alan G. MacDiarmid, Chwan K. Chiang Alan J. Heeger, "Synthesis of electrically conducting organic polymers: halogen derivatives of polyacetylene, (CH)x" *Journal of the Chemical Society, Chemical Communications, pp. 578-580, 1977.*

[83] E. M. Genies, J. M. Pernaut, "Spectroelectrochemical studies of the redox and kinetic behavior of polypyrrole film" *Synthetic Metals, vol. 10, pp. 117-129, 1984.*

[84] A. Rudge, J. Davey, I. Raistrick, S. Gottesfeld, J. P. Ferraris, "Conducting polymers as active materials in electrochemical capacitors" *Journal of Power Sources, vol. 47, pp. 89-107, 1994.*

[85] S. Ghosh, O. Inganäs, "Conducting Polymer Hydrogels as 3D Electrodes: Applications for Supercapacitors" *Advanced Materials, vol. 11, pp. 1214-1218, 1999.*

[86] G. M. Spinks, A. J. Dominis, G. G. Wallace, D. E. Tallman, "Electroactive conducting polymers for corrosion control. Part 2. Ferrous metals" *Journal of Solid State Electrochemistry, vol. 6, pp. 85-100, 2002.*

[87] Y.T. Kim, W.S. Kim, H.W. Rhee, M.K. Song, "Iron corrosion protection by ultra-thin conductive films based on polypyrrole/poly(methyl methacrylate) composite" *Molecular Crystals and Liquid Crystals, vol. 445, pp. 193/[483]-200/[490], 2006.*

[88] E. Sezer, "Conducting nanocomposite systems" *The New Frontiers of Organic and Composite Nanotechnology, Elsevier, pp. 143-235,2008.*

[89] Rajesh, T. Ahuja, D. Kumar, "Recent progress in the development of nano-structured conducting polymers/nanocomposites for sensor applications" *Sensors and Actuators B: Chemical, vol. 136, pp. 275-286, 2009.*

[90] D. Svirskis, J. Travas-Sejdic, A. Rodgers, S. Garg, "Electrochemically controlled drug delivery based on intrinsically conducting polymers" *Journal of Controlled Release, vol. In Press, Corrected Proof, 2010.*

[91] S. A. Campbell, Y. Li, S. Breakspear, F. C. Walsh, J. R. Smith, "Conducting polymer coatings in electrochemical technology. Part 1 - synthesis and fundamental aspects" *Transactions of the Institute of Metal Finishing, vol. 85, pp. 237-44, 2007.*

[92] K. Gurunathan, A. V. Murugan, R. Marimuthu, U. P. Mulik, D. P. Amalnerkar, "Electrochemically synthesised conducting polymeric materials for applications towards technology in electronics, optoelectronics and energy storage devices" *Materials Chemistry and Physics, vol. 61, pp. 173-91, 1999.*

[93] K. Meerholz, J. Heinze, "Influence of chain length and defects on the electrical conductivity of conducting polymers" *Synthetic Metals, vol. 57, pp. 5040-5045, 1993.*

[94] S. Stafström, J. L. Brédass, "Electronic structure of highly conducting conjugated polymers: evolution upon doping of polyacetylene, polythiophene, and polyemeraldine" *Journal of Molecular Structure: THEOCHEM, vol. 188, pp. 393-427, 1989.*

[95] R. Erlandsson, W. R. Salaneck, I. Lundström, "Electrically conducting organic polymer materials: Defects make them better" *Materials & Design, vol. 7, pp. 246-251, 1986.*

[96] B. Malhotra, "Defects in conducting polymers" Bulletin of Materials Science, vol. 10, pp. 85-96, 1988.

[97] H. Kaneko, Y. Nogami, T. Ishiguro, H. Nishiyama, H. Ishimoto, A. Takahashi, J. Tsukamoto, "Low temperature electrical conductivity of highly conducting iodine doped polyacetylene" *Synthetic Metals, vol. 57, pp. 4888-4893, 1993.*

[98] C. K. Chiang, C. R. Fincher, Y. W. Park, A. J. Heeger, H. Shirakawa, E. J. Louis, S. C. Gau, A. G. MacDiarmid, "Electrical conductivity in doped polyacetylene" *Physical Review Letters, vol. 39, pp. 1098 LP - 1101, 1977.*

[99] Y. W. Park, C. Park, Y. S. Lee, C. O. Yoon, H. Shirakawa, Y. Suezaki, K. Akagi, "Electrical conductivity of highly-oriented-polyacetylene" *Solid State Communications, vol. 65, pp. 147-150, 1988.*

[100] C. Pratt, "Conducting polymers" *in Chemistry. London: Kingston University, , pp. 7, 1996.*

[101] N. C. Billingham, P. D. Calvert, P. J. S. Foot, F. Mohammad, "Stability and degradation of some electrically conducting polymers" *Polymer Degradation and Stability, vol. 19, pp. 323-341, 1987.*

[102] Y. Wang, M. F. Rubner, L. J. Buckley, "Stability studies of electrically conducting polyheterocycles," *Synthetic Metals, vol. 41, pp. 1103-1108, 1991.*

[103] Q. Pei, O. Inganäs, J.-E. Österholm, J. Laakso, "Electrically conducting copolymers from 3-octylthiophene and 3-methylthiophene" *Polymer, vol. 34, pp. 247-252, 1993.*

[104] A. R. Hopkins, D. D. Sawall, R. M. Villahermosa, R. A. Lipeles, "Interfacial synthesis of electrically conducting polyaniline nanofiber composites" *Thin Solid Films, vol. 469-470, pp. 304-308, 2004.*

[105] A. F. Diaz, J. I. Castillo, J. A. Logan, W.-Y. Lee, "Electrochemistry of conducting polypyrrole films" *Journal of Electroanalytical Chemistry, vol. 129, pp. 115-132, 1981.*

[106] R. Ansari, "polypyrrole conducting electroactive polymers:synthesis and stability studies" *E-Journal of Chemistry, vol. 3, pp. 186-201, 2006.*

[107] G. Bidan, B. Ehui, M. Lapkowski, "Conductive polymers with immobilised dopants: ionomer composites and auto-doped polymers-a review and recent advances" *Journal of Physics D (Applied Physics), vol. 21, pp. 1043-54, 1988.*

[108] J. M. Pringle, O. Ngamna, J. Chen, G. G. Wallace, M. Forsyth, D. R. MacFarlane, "Conducting polymer nanoparticles synthesized in an ionic liquid by chemical polymerisation" *Synthetic Metals, vol. 156, pp. 979-983, 2006.*

[109] D. D. Borole, U. R. Kapadi, P. P. Mahulikar, D. G. Hundiwale, "Electrochemical synthesis and characterization of conducting copolymer: Poly(o-aniline-co-o-toluidine)" *Materials Letters, vol. 60, pp. 2447-2452, 2006.*

[110] J. Duchet, S. Demoustier-Champagne, "Study of polystyrene microstructures and nanostructures synthesised in particle track-etched membranes used as templates" *Polymer, vol. 41, pp. 1-8, 2000.*

[111] Q. Tang, J. Wu, X. Sun, Q. Li, J. Lin, "Layer-by-layer self-assembly of conducting multilayer film from poly(sodium styrenesulfonate) and polyaniline" *Journal of Colloid and Interface Science, vol. 337, pp. 155-161, 2009.*

[112] J. P. Cannon, S. D. Bearden, S. A. Gold, "Characterization of conjugated polymer/anodic aluminum oxide nanocomposites fabricated via template wetting" *Composites Part A: Applied Science and Manufacturing, vol. 41, pp. 836-841, 2010.*

[113] A. Malinauskas, "Chemical deposition of conducting polymers" *Polymer*, vol. 42, pp. 3957-3972, *2001.*

[114] J. Arjomandi, R. Holze, "In situ characterization of N-methylpyrrole and (N-methylpyrrole-cyclodextrin) polymers on gold electrodes in aqueous and nonaqueous solution" *Synthetic Metals,* vol. 157, *pp. 1021-1028, 2007.*

[115] K. Kobayashi, X. H. Yin, M. Ozaki, T. Kawai, K. Yoshino, "Novel properties of conducting polymer-liquid crystal system and their doping effect" *Synthetic Metals, vol. 69, pp. 597-598, 1995.*

[116] X. B. Yan, Z. J. Han, Y. Yang, B. K. Tay, "NO_2 gas sensing with polyaniline nanofibers synthesized by a facile aqueous/organic interfacial polymerization" *Sensors and Actuators B: Chemical, vol. 123, pp. 107-113, 2007.*

[117] M. R. Karim, C. J. Lee, M. S. Lee, "Synthesis of conducting polypyrrole by radiolysis polymerization method" *Polymers for Advanced Technologies, vol. 18, pp. 916-920, 2007.*

[118] J. Bhadra, D. Sarkar, "Self-assembled polyaniline nanorods synthesized by facile route of dispersion polymerization" *Materials Letters,* vol. *63, pp. 69-71, 2009.*

[119] N. K. Guimard, N. Gomez, C. E. Schmidt, "Conducting polymers in biomedical engineering" *Progress in Polymer Science,Polymers in Biomedical Applications, vol. 32, pp. 876-921, 2007.*

[120] K. K. K. a. G. P. G. A. F. Diaz, "Electrochemical Polymerization of Pyrrole" *Journal of the Chemical Society, Chemical Communications, pp. 635-636, 1979.*

[121] C. He, C. Yang, Y. Li, "Chemical synthesis of coral-like nanowires and nanowire networks of conducting polypyrrole" *Synthetic Metals*, vol. 139, *pp. 539-545, 2003.*

[122] R. C. G. M. van den Schoor, R. H. M. van de Leur, J. H. W. de Wit, "Synthesis of a polypyrrole film on a non-conducting substrate; the influence of the oxidant and acid concentration" *Synthetic Metals, vol. 99, pp. 17-20, 1999.*

[123] M. Omastová, K. Mosnáckova, M. Trchová, E. N. Konyushenko, J. Stejskal, P. Fedorko, J. Prokes, "Polypyrrole and polyaniline prepared with cerium(IV) sulfate oxidant," *Synthetic Metals,* vol. 160, *pp. 701-707, 2010.*

[124] M. M. Castillo-Ortega, M. B. Inoue, M. Inoue, "Chemical synthesis of highly conducting polypyrrole by the use of copper(II) perchlorate as an oxidant," *Synthetic Metals, vol. 28, pp. 65-70, 1989.*

[125] K. Boukerma, J.-Y. Piquemal, M. M. Chehimi, M. Mravcáková, M. Omastová, P. Beaunier, "Synthesis and interfacial properties of montmorillonite/polypyrrole nanocomposites" *Polymer,* vol. 47, pp. 569-576, *2006.*

[126] R. Ansari Khalkhali, "Electrochemical Synthesis and Characterization of Electroactive Conducting Polypyrrole Polymers" *Russian Journal of Electrochemistry, vol. 41, pp. 950-955, 2005.*

[127] J. L. Bredas, "Bipolarons in doped conjugated polymers: a critical comparison between theoretical results and experimental data" *Molecular Crystals and Liquid Crystals, vol. 118, pp. 49-56, 1985.*

[128] J. Ouyang, Y. Li, "Effect of electrolyte solvent on the conductivity and structure of as-prepared polypyrrole films," *Polymer*, vol. 38, pp. 1971-1976, *1997.*

[129] L. F. Warren, D. P. Anderson, "Polypyrrole Films from Aqueous Electrolytes" *Journal of The Electrochemical Society, vol. 134, pp. 101-105, 1987.*

[130] A. F. Diaz, B. Hall, "Mechanical properties of electrochemically prepared polypyrrole films " *IBM Journal of Research and Development, vol. 27, pp. 342-347, 1983.*

[131] A. A. A. Almario, R. L. T. Cáceres, "Study of kinetic formation and the electrochemical behavior of polypyrrole films" J*ournal of the Chilean Chemical Society, vol. 54, pp. 14-19, 2009.*

[132] G. Sabouraud, S. Sadki, N. Brodie, "The mechanisms of pyrrole electropolymerization " *Chemical Society Reviews*, vol. *29, pp. 283-293, 2000.*

[133] J. Unsworth, P. C. Innis, B. A. Lunn, Z. Jin, G. P. Norton, "The influence of electrolyte pH on the surface morphology of polypyrrole" *Synthetic Metals,* vol. 53, pp. *59-69, 1992.*

[134] W. Su, J. O. Iroh, "Electrodeposition mechanism, adhesion and corrosion performance of polypyrrole and poly(N-methylpyrrole) coatings on steel substrates" *Synthetic Metals,* vol. 114, pp. *225-234, 2000.*

[135] S. U. Rahman, M. S. Ba-Shammakh, "Thermal effects on the process of electropolymerization of pyrrole on mild steel" *Synthetic Metals,* vol. 140, pp. *207-223, 2004.*

[136] C. M. Li, C. Q. Sun, W. Chen, L. Pan, "Electrochemical thin film deposition of polypyrrole on different substrates" *Surface and Coatings Technology, vol. 198, pp. 474-477, 2005.*

[137] V. K. Gade, D. J. Shirale, P. D. Gaikwad, P. A. Savale, K. P. Kakde, H. J. Kharat, M. D. Shirsat, "Influence of process parameters on the conductivity and surface morphology of polypyrrole films" *International Journal of Polymeric Materials, vol. 56, pp. 167-176, 2007.*

[138] A. P. E. Junquera, E. Aicart, "Electrochemical study of the chelation of Cu2+ cation by 18-crown-6-ether and hydroxybenzoic acids in aqueous solution" *Journal of Solution Chemistry, vol. 30, 2001.*

[139] *Z. Zhang,* R. B. Jordan, "Kinetics of dissociation of iron(III) complexes of tiron in aqueous acid," *Inorganic Chemistry, vol. 35, pp. 1571-1576, 1996.*

[140] D. E. Tallman, C. Vang, G. G. Wallace, G. P. Bierwagen, "Direct electrodeposition of polypyrrole on aluminum and aluminum alloy by electron transfer mediation" *Journal of the Electrochemical Society, vol. 149, pp. C173-C179, 2002.*

[141] J. Petitjean, S. Aeiyach, J. C. Lacroix, P. C. Lacaze, "Ultra-fast electropolymerization of pyrrole in aqueous media on oxidizable metals in a one-step process" *Journal of Electroanalytical Chemistry, vol. 478, pp. 92-100, 1999.*

[142] E. Hermelin, J. Petitjean, S. Aeiyach, J. C. Lacroix, P. C. Lacaze, "Industrial polypyrrole electrodeposition on zinc-electroplated steel" *Journal of Applied Electrochemistry, vol. 31, pp. 905-911, 2001.*

[143] S. K. Sadrnezhaad, M. R. Vaezi, "The effect of addition of tiron as a surfactant on the microstructure of chemically deposited zinc oxide" *Materials Science and Engineering: B, vol. 128, pp. 53-57, 2006.*

[144] T. F. Otero, E. Angulo, "Impedance studies of electrogenerated polypyrrole films" *Synthetic Metals*, vol. 51, pp. *87-94, 1992.*

[145] J. Petitjean, J. Tanguy, J. C. Lacroix, K. I. Chane-Ching, S. Aeiyach, M. Delamar, P. C. Lacaze, "Interpretation of the ultra-fast electropolymerization of pyrrole in aqueous media on zinc in a one-step process: The specific role of the salicylate salt investigated by X-ray photoelectron spectroscopy (XPS) and by electrochemical quartz crystal microbalance (EQCM)" *Journal of Electroanalytical Chemistry, vol. 581, pp. 111-121, 2005.*

[146] S. O. Arash Shahryar, Jerzy A. Szpunar, "Enhancement of biocompatibility of 316LVM stainless steel by cyclic potentiodynamic passivation" *Journal of Biomedical Materials Research Part A, vol. 89A, pp. 1049-1062, 2009.*

[147] a. J. L. L. W. S. Li, "Electrochemical investigations on formation and pitting susceptibility of passive films on iron and iron-based alloys" *Int. J. Electrochem. Sci., vol. 2, pp. 627-665, 2007.*

[148] D. O. N. Yan Wang, "An investigation into the nucleation and growth of an electropolymerized polypyrrole coating on a 316L stainless steel surface" *Thin Solid Films, vol. 516, pp. 7427-7432, 2008.*

[149] R. Zhu, G. Li, G. Huang, "Two-step electrosynthesis of polypyrrole for corrosion protection of stainless steel" *Materials and Corrosion, vol. 60, pp. 34-39, 2009.*

[150] T. F. Otero, J. Rodríguez, "Parallel kinetic studies of the electrogeneration of conducting polymers: mixed materials, composition and properties control" *Electrochimica Acta, vol. 39, pp. 245-253, 1994.*

[151] Y. a. Q. Li, Renyuan, "Studies on the electrode kinetics of polypyrrole in aqueous solution by a.c. impedance measurement" *Synthetic Metals, vol. 64, pp. 241-245, 1994.*

[152] J. Wang, Y. Xu, X. Chen, X. Sun, "Capacitance properties of single wall carbon nanotube/polypyrrole composite films" *Composites Science and Technology, Polymer Nanocomposites - Modeling, Mechanical and Functional Properties - Polymer Nanocomposites, vol. 67, pp. 2981-2985, 2007.*

[153] R. Hass, J. García-Cañadas, G. Garcia-Belmonte, "Electrochemical impedance analysis of the redox switching hysteresis of poly(3,4-ethylenedioxythiophene) films" *Journal of Electroanalytical Chemistry, vol. 577, pp. 99-105, 2005.*

[154] A. Hallik, A. Alumaa, J. Tamm, V. Sammelselg, M. *Väärtnõu, A. Väärtnõu,* E. Lust, "Analysis of electrochemical impedance of polypyrrolesulfate and polypyrroleperchlorate films" *Synthetic Metals, vol. 156, pp. 488-494, 2006.*

[155] *T.* T. N. Lien, T. D. Lam, V. T. H. An, T. V. Hoang, D. T. Quang, D. Q. Khieu, T. Tsukahara, Y. H. Lee, J. S. Kim, "Multi-wall carbon nanotubes (MWCNTs)-doped polypyrrole DNA biosensor for label-free detection of genetically modified organisms by QCM and EIS" *Talanta, vol. 80, pp. 1164-1169, 2010.*

[156] A. Ramanavicius, A. Finkelsteinas, H. Cesiulis, and A. Ramanaviciene, "Electrochemical impedance spectroscopy of polypyrrole based electrochemical immunosensor" *Bioelectrochemistry, vol. 79, pp. 11-16, 2010.*